On the seasonal hydrological and thermal regimes of Arctic hillslopes: Field and modeling investigations in the context of climate change.

by

Caitlin Rushlow

A dissertation submitted in partial fulfillment

of the requirements for the degree of

Doctor of Philosophy in the Department of Geosciences

Idaho State University

Summer 2018

To the Graduate Faculty:

The members of the committee appointed to examine the thesis of CAITLIN RUSHLOW find it satisfactory and recommend that it be accepted.

Dr. Sarah E. Godsey,
Major Advisor

Dr. Benjamin T. Crosby,
Committee Member

Dr. Kathleen A. Lohse,
Committee Member

Dr. James P. McNamara,
Committee Member

Dr. Colden V. Baxter,
Graduate Faculty Representative

Dedication

To my sister and eternal light, Kristen Marie. Te amo.

Acknowledgements

My gratitude flows first and foremost to my advisor, Dr. Sarah Godsey, for being my trusting collaborator, mentor, and guide throughout the entire experience represented by this dissertation. My committee members Benjamin Crosby, Colden Baxter, Kathleen Lohse, and James McNamara generously contributed their time and perspectives to evaluating my progress in this endeavor. Tamara Harms, Emily Voytek, Kamini Singha, Audrey Sawyer, Cliff Voss, Benjamin Soderquist, and Arwen Bird shaped the stories herein with their collaborative voices, both directly and through the development of my own thinking and writing. Emily and Ben, along with Margit Jaeger, Becca Risser, Chris Cook, and Ludda Ludwig made the work both deeper and lighter as close friends and co-workers. Karla Eitel, Teresa Cohn, Melissa Barker-Tamplin, and Annesofie Norn challenged me to consider more deeply what it means to be a scientist and communicate science. Water tracks team volunteers and the scientists and staff of Toolik Field Station provided additional emotional and logistical support in the field. Chris Tennant led the way through the ISU Geosciences PhD program. George Allen continued sharing the experience of becoming a scientist with me as he has for eight years. John Whiting and Amy Staley were true friends through joy and sorrow. Shane Vatland invited me Wallowa County and introduced me to Beth Gibans, who supported and inspired me through my first non-academic job in over ten years. Kyle Anderson, my best friend, grounded me through the best and most challenging times and kept me connected to the world outside this work. Adopting Jasper was the best decision I made in the last six years. My parents, Terri and Mike, endured it all with me and shared their infinite love.

TABLE OF CONTENTS

On the seasonal hydrological and thermal regimes of Arctic hillslopes: Field and modeling investigations in the context of climate change

Dissertation Abstract—Idaho State University (2018)

In upland Arctic watersheds, features called water tracks commonly drain the precipitation received by hillslopes through the shallow soils of the seasonally thawed active layer to downslope aquatic ecosystems. Little is known about the seasonal extent and controls on this hydrologic connection, and how it may be affected by the rapid changes occurring in the regional climate. I measured the runoff generated by water tracks in response to rainfall during the thaw season and found that the response was often delayed relative to the stream network due to storage within the hillslope watershed. Runoff was proportional to rainfall once it exceeded the water storage capacity near the water track outlet. Runoff generation thresholds varied by site, emphasizing the role of spatially distributed water storage and exceedance patterns in controlling the emergent response at each water track. While it is generally assumed that hydrological and ecological processes are relatively quiescent in the cold season, I found that the active layer of water tracks remained thawed or only partially frozen for months longer than the surrounding hillslope. Water tracks also thawed later than hillslopes in the spring, delaying interaction between soils and spring snowmelt. The persistence of conditions favorable to biological activity and hydrologic transport suggest that water tracks may function as hot spots of greenhouse gas emissions in the cold season. Multiple linear regression results showed that most of the variation in active layer thermal conditions was explained by air temperature, feature, and snow depth. I used numerical models to further explore how those factors affect the thermal regime of the hillslope and water track active layer. I found that under the current climate, locations with deep snow can form taliks in warmer years, while in colder years, locations with shallow snow remain frozen for the majority of the

year. Further, groundwater flow redistributes heat, moderating active layer thermal regime in areas of aggregating flow, such as water tracks. The results of this study, together with the broad spatial extent of water tracks in permafrost watersheds, suggest that water tracks may play an underappreciated role in modulating the convolved hydrologic, geomorphic, and ecological responses of Arctic watersheds to climate change.

Keywords: Permafrost, Hydrology, Water tracks, Active layer, Climate change

Chapter 1: Introduction

The upland tundra accounts for approximately one third of the Arctic landscape (CAVM, 2003). It is a cold, windy desert (Liljedahl et al., 2017), but one that is underlain by thick, spatially continuous permafrost. By restricting the infiltration of water (Walvoord and Kurylyk, 2016), permafrost allowed peatlands to develop across much of the Arctic at the end of the last glaciation (MacDonald et al., 2006). During deglaciation, rapid warming triggered widespread mass wasting in upland landscapes, but at present the presence of peat and permafrost have raised the threshold for sediment transport, hillslope erosion, and stream network expansion (McNamara et al., 1999; McNamara and Kane, 2009; Mann et al., 2010). Instead, tundra hillslopes are commonly drained by zero-order flowpath features called water tracks (McNamara et al., 1997; Stieglitz et al., 2003). Peat and the seasonal snowpack buffer soils from both extremely cold and relatively warm seasonal air temperatures (Sturm et al., 1997; Baughman et al., 2015). The cold and wet soil regime slows decomposition, and in many places, organic matter has accumulated for millennia into a perennially frozen Arctic carbon pool containing ~50% of the global belowground organic carbon stocks (Tarnocai et al., 2009). Recent human-induced climate change is warming the Arctic at an amplified rate compared to lower latitudes (Manabe and Stouffer, 1980; Holland and Bitz, 2003; Serreze and Barry, 2011), threatening to destabilize local landscapes and ecosystem processes (Jorgenson et al., 2010). If permafrost thaws, it will make available for decomposition the Arctic carbon pool, which is twice that contained in the atmosphere (Schuur et al., 2008), and initiate a significant positive feedback with global climate change, depending on the magnitude, form, and rate of carbon release (Schuur et al., 2011).

Understanding the response of Arctic landscapes to climate change is thus a pressing but fundamentally difficult challenge, because the Arctic is a complex system, consisting of

interdependent components that are also interconnected with the broader Earth system (Figure 1, Hinzman et al., 2013). The Arctic system is characterized by low and extremely seasonal energy inputs from solar radiation (Hinzman et al., 1996). Energy and water fluxes are tightly coupled and non-linear due to latent heat exchange within the system (Atchley et al., 2017), affecting hydrological processes such as precipitation, evaporation, snowmelt, sublimation, and soil freeze-thaw (Hinzman et al., 1992). Liquid water, and thus most biological processes, occur aboveground and in the seasonally thawed active layer between the ground surface and permafrost during the brief summer warm season (Hinzman et al., 1991). Finally, water, energy, nutrients, and carbon spiral along potential gradients through heterogeneous watersheds (Fisher et al., 2004), where the properties of the soil, seasonal snowpack, and microclimate vary, often at different spatial and temporal scales (Taras et al., 2002).

The work presented in this dissertation approaches the challenge of understanding the response of Arctic landscapes to climate change by investigating the seasonal hydrological and thermal regimes of Arctic hillslopes and the water tracks draining them. Investigations at this temporal and spatial scale are rare and critical for understanding impacts across the landscape, since water tracks hydrologically connect hillslopes, a fundamental landscape unit (Jencso et al., 2009), to downslope aquatic ecosystems (Stieglitz et al., 2003). The dissertation is composed of three stand-alone chapters and their supporting information.

Chapter 2 investigates the hydrologic response of Arctic hillslopes and water tracks to summer rainfall patterns. Field observations collected at six hillslope watersheds drained by water tracks in the foothills region of the North Slope of Alaska showed that soil water storage and response to rainfall were spatially heterogeneous within the watersheds, and that water track runoff response was delayed relative to larger stream orders. Based on these findings, a piecewise linear

model was used to test the hypothesis that water track runoff response was primarily controlled by rainfall amount and antecedent water storage conditions.

Chapter 3 explores the relationship between the hydrologic and thermal regimes of Arctic hillslopes using a beta version of the USGS numerical modeling code SUTRA that couples the physical processes of groundwater flow and heat transport, including freeze-thaw. Snow cover, air, and ground temperature observations from Chapter 3 were used to construct 1-D and 3-D models representative of the study area. The 1-D model was used for a sensitivity analysis exploring the role of interannual variation in air temperature and snow cover in modifying the active layer thermal regime. The 3-D model, which assumes fully saturated conditions, was used to test the hypothesis that groundwater flow significantly alters the thermal regime in aggregation zones, such as water tracks.

Chapter 4 investigates the seasonal patterns and controls on the active layer thermal regime of Arctic hillslopes. Snow cover, air, and ground temperatures were monitored year-round adjacent to and within the six water tracks at the same field sites described in Chapter 2. The ground temperature records were used to compare the magnitude of seasonal temperature variations and the timing and duration of frozen, partially frozen, and thawed conditions inside and outside the water track. Multiple linear models were used to test the hypothesis that soil moisture exerts a stronger control on the active layer thermal regime on Arctic tundra hillslopes drained by water tracks than seasonal or interannual variations in snow cover or air temperature.

References

Atchley, A. L., Coon, E. T., Painter, S. L., Harp, D. R., & Wilson, C., (2016), Influences and interactions of inundation, peat, and snow on active layer thickness, *Geophysical Research Letters*, *43(10),* 5116-6123, doi.org/10.1002/2016GL068550.

Baughman, C. A., Mann, D. H., Verbyla, D. L., & Kunz, M. L., (2015), Soil surface organic layers in Arctic Alaska: Spatial distribution, rates of formation, and microclimatic effects, *Journal of Geophysical Research: Biogeosciences, 120*, 1150-1164, doi:10.1002/2015JG002983.

CAVM team. 2003. Circumpolar Arctic Vegetation Map. (1:7,500,000 scale). Conservation of Arctic flora and fauna (CAFF) Map No. 1. US Fish and Wildlife Service, Anchorage, Alaska. ISBN: 0-9767525-0-6, ISBN-13: 978-0-9767525-0-9.

Fisher, S. G., Sponseller, R. A., Heffernan, J. B., (2004), Horizons in stream biogeochemistry: Flowpaths to progress, *Ecology, 85(9),* 2369-2379.

Hinzman, L. D., Kane, D. L., Gieck, R. E., & Everett, K. R. (1991). Hydrologic and thermal properties of the active layer in the Alaskan Arctic. *Cold Regions Science and Technology, 19*, 95–110.

Hinzman, L. D., & Kane, D. L., (1992), Potential response of an Arctic watershed during a period of warming, *Journal of Geophysical Research, 97(D3)*, 2811-2820.

Hinzman, L. D., Kane, D. L., Benson, C. S., & Everett, K. R. (1996). Energy balance and hydrological processes in an arctic watershed. *Ecological Studies, 120*, 131–154.

Hinzman, L. D., Deal, C. J., McGuire, A. D., Mernild, S. H., Polyakov, I. V., & Walsh, J. E., (2013), Trajectory of the Arctic as an integrated system, *Ecological Applications, 23(3)*, 1837-1868.

Holland, M. M., & Bitz, C. M. (2003). Polar amplification of climate change in coupled models. *Climate Dynamics, 21*, 221–232.

Jencso, K. G., McGlynn, B. L., Gooseff, M. N., Wondzell, S. M., Bencala, K. E., & Marshall, L. A., (2009). Hydrologic connectivity between landscapes and streams: Transferring reach- and plot-scale understanding to the catchment-scale. *Water Resources Research, 45(W04428),* doi:10.1029/2008WR007225.

Jorgenson, M. T., Romanovsky, V., Harden, J., Shur, Y., O'Donnell, J., Schuur, E. A. G., Kanevskiy, M., & Marchenko, S., (2010), Resilience and vulnerability of permafrost to climate change. *Canadian Journal of Forest Resources 40*: 1219-1236.

Liljedahl, A. K., Hinzman, L. D., Kane, D. L., Oechel, W. C., Tweedie, C. E., & Zona, D., (2017), Tundra water budget and implications of precipitation underestimation. *Water Resources Research, S3*, 6472-6486, doi:10.1002/2016WR020001.

MacDonald, G.M., Beilman, D.W., Kremenetski, K.V., Sheng, Y., Smith, L.C., Velichko, A.A., (2006). Rapid early development of circumarctic peatlands and atmospheric CH4 and CO2 variations. *Science 314 (5797)*, 285-288.

Manabe, S., & Stouffer, R. J., (1980), Sensitivity of a global climate model to an increase of CO2 concentration in the atmosphere. *Journal of Geophysical Research: Oceans*, *85(C10),* 5529-5554, doi.org/10.1029/JC085iC10p05529.

Mann, D. H., Groves, P., Reanier, R. E., & Kunz, M. L., (2010). Floodplains, permafrost, cottonwood trees, and peat: What happened the last time climate warmed suddenly in arctic Alaska? *Quaternary Science Reviews, 29(27-28),* 3812-3830, doi: 10.1016/j.quascirev.2010.09.002.

McNamara, J. P., Kane, D. L., & Hinzman, L. D. (1997). Hydrograph separations in an arctic watershed using mixing model and graphical techniques. *Water Resources Research, 33(7)*, 1707–1719.

McNamara, J. P., Kane, D. L., & Hinzman, L. D. (1999). An analysis of an arctic channel network using a digital elevation model. *Geomorphology, 29*, 339–353.

McNamara, J. P., & Kane, D. L., (2009). The impact of a shrinking cryosphere on the form of arctic alluvial channels. *Hydrological Processes, 23*, 159-168, doi: 10.1002/hyp.7199.

Schuur, E. A. G., Bockheim, J., Canadell, J. G., Euskirchen, E., Field, C. B., Goryachkin, S. V., Hagemann, S., Kuhry, P., LaFleur, P. M., Lee, H., Mazhitova, G., Nelson, F. E., Rinke, A., Romanovsky, V. E., Shiklomanov, N. Tarnocai, C., Venevsky, S., Vogel, J. G. & Zimov, S. A. (2008). Vulnerability of permafrost carbon to climate change: Implication for the global carbon cycle. *BioScience, 58(8),* 701-714. doi: 10.1641/B580807.

Schuur, E. A. G., Abbott, B., & the Permafrost Carbon Network, (2011). High risk of permafrost thaw. *Nature, 480*, 32-33.

Serreze, M. C., Barrett, A. P., Stroeve, J. C., Kindig, D. N., & Holland, M. M., (2011). The emergence of surface-based Arctic amplification. *The Cryosphere, 3,* 11-19.

Stieglitz, M., Shaman, J., McNamara, J., Engel, V., Shanley, J., & Kling, G. W. (2003). An approach to understanding hydrologic connectivity on the hillslope and the implications for nutrient transport. *Global Biogeochemical Cycles, 17(4), 1105.* https://doi.org/10.1029/2003GB002041.

Sturm, M., Homgren, J., Konig, M., & Morris, K. (1997). The thermal conductivity of seasonal snow. *Journal of Glaciology, 43(143)*, 26-41.

Taras, B., Sturm, M., & Liston, G. E. (2002). Snow-ground interface temperatures in the Kuparuk River Basin, Arctic Alaska: Measurements and model. *Journal of Hydrometeorology*, *3*, 377-394.

Tarnocai, C., Canadell, J. G., Schuur, E. A. G., Kuhry, P., Mazhitova, G., & Zimov, S. (2009). Soil organic carbon pools in the northern circumpolar permafrost region. *Global Biogeochemical Cycles, 23*(GB2023), doi:10.1029/2008GB003327.

Walvoord, M. A., & Kurylyk, B. L. (2016). Hydrologic impacts of thawing permafrost-A review. *Vadose Zone Journal, 15(6),* doi:10.2136/vzj2016.01.0010.

Chapter 2: Rainfall-runoff responses on Arctic hillslopes underlain by continuous permafrost, North Slope, Alaska, USA

This chapter is published in Hydrological Processes and is reprinted here with permission of John Wiley and Sons under license number 4345640180000, issued on May 10, 2018.

2.1 Abstract

The Arctic hydrologic cycle is intensifying, as evidenced by increased rates of precipitation, evapotranspiration, and riverine discharge. However, the controls on water fluxes from terrestrial to aquatic systems in upland Arctic landscapes are poorly understood. Upland landscapes account for 1/3rd of the Arctic land surface and are often drained by zero-order geomorphic flowpath features called water tracks. Previous work in the region attributed rapid runoff response at larger stream orders to water tracks, but models suggest water tracks are hydrologically disconnected from the surrounding hillslope. To better understand the role of water tracks in upland landscapes, we investigated the surface and subsurface hydrologic responses of six water tracks and their hillslope watersheds to natural patterns of rainfall, soil thaw, and drainage. Between storms, both water track discharge and the water table in the hillslope watersheds exhibited diel fluctuations that, when lagged by five hours, were temporally correlated with peak evapotranspiration rate. Water track soils remained saturated for more of the summer season than soils in their surrounding hillslope watersheds. When rainfall occurred, the subsurface response was nearly instantaneous, but the water tracks took significantly longer than the hillslopes to respond to rainfall, and longer than the responses previously observed in nearby larger order Arctic streams. There was also evidence for antecedent soil water storage conditions controlling the magnitude of runoff response. Based on these observations, we used a broken stick model to test the hypothesis that runoff production in response to individual storms was primarily controlled by rainfall amount and antecedent water storage conditions near the water track outlet. We found that the relative

importance of the two factors varied by site and that water tracks with similar watershed geometries and at similar landscape positions had similar rainfall-runoff model relationships. Thus, the response of terrestrial water fluxes in the upland Arctic to climate change depends on the non-linear interactions between rainfall patterns and subsurface water storage capacity on hillslopes. Predicting these interactions across the landscape remains an important challenge.

2.2 Introduction

Across the Arctic, climate change is intensifying the hydrological cycle, as evidenced by increased rates of precipitation, evapotranspiration, and discharge from large rivers into the Arctic Ocean (Rawlins et al. 2010). Increased rates of precipitation are clearly due to atmospheric warming, because warmer air can hold more water vapor (Wentz et al., 2007), but it is less clear how Arctic landscapes are translating increased rates of precipitation into increased river discharge. Melting ground ice and associated ground subsidence have enhanced the hydrologic connectivity between land and rivers in the lowland Arctic (Liljedahl et al., 2016). However, enhanced runoff from the upland Arctic, where hillslopes have the potential to convey water to rivers more rapidly than low-gradient wetlands of the lowland Arctic, is another potential source for increased river discharge. Accurate assessment and prediction of the relative roles of the upland and lowland Arctic in changing patterns of river discharge depends on the mechanisms controlling the storage and runoff of precipitation from Arctic hillslopes.

The capacity for water storage and flow on Arctic hillslopes ranges widely over an annual cycle because of the extreme seasonality of the surface energy balance and seasonally thawed ground above continuous permafrost (Kane et al., 1989). Water on hillslopes is frozen and stored in the snowpack and soils except during a brief summer warm season, generally from May through September. During this period, the snowpack melts and the ground thaws progressively from the

surface downwards, allowing water storage and flow in the unfrozen soils of the "active layer," which is usually less than a meter thick depending on material properties and heat fluxes (e.g., Hinzman et al., 1991; Kane et al., 2001). Since the presence of permafrost inhibits infiltration to groundwater, the dominant pathways for water losses from the terrestrial upland are evapotranspiration and runoff (Hinzman et al., 1996). Arctic hillslopes are often drained by geomorphic features known as water tracks (McNamara et al. 1998; Paquette et al., 2017), which are curvilinear, unchannelized zones of preferential flow that develop a range of biophysical characteristics in the context of the local slope, climate, and surficial geology (Trochim et al., 2016a). Water tracks are zero-order extensions of the drainage network (McNamara et al., 1999) and they direct nutrients downslope to streams and lakes (Yano et al. 2010). A nested watershed investigation in Arctic Alaska attributed stormflow characteristics in low-order streams to water tracks (McNamara et al., 1998) and suggested that water tracks are the main source areas for runoff in response to summer rainfall (McNamara et al., 1997). This work implies that water fluxes from water tracks are the key linkage between terrestrial and aquatic systems in the upland Arctic, yet the controls on water track hydrologic response have not been directly investigated.

Hillslope hydrologic responses are often non-linear, and thus can be difficult to assess and predict. Investigations of hillslope hydrologic response in temperate regions have revealed threshold changes in the magnitude of hillslope runoff response to rainfall with increasing antecedent soil moisture (Western and Grayson, 1998; James and Roulet, 2007), subsurface saturation (Tromp-van Meerveld and McDonnell, 2006b), and/or rainfall (Detty and McGuire, 2010). These observations of runoff responses on hillslopes are part of a paradigm shift in the field of hydrology that recognizes threshold behavior as an emergent property of the hydrologic connection and disconnection of heterogeneous water storage components within watersheds of

all scales (Spence, 2010). Testing this paradigm requires field studies that reveal the mechanistic processes underlying observed emergent behaviors (Burt and McDonnell, 2015), and the utility of the paradigm lies in the ability to identify or predict the hierarchy of storage thresholds operating across different environments (Ali et al., 2013).

Multiple storage thresholds may be operating on hillslopes in permafrost regions like the Arctic. The active layer thaws seasonally, increasing the potential capacity for subsurface storage. On a barren Arctic hillslope in northern Canada, uneven frost table topography generated depression storage and isolated patches of soil saturation in an otherwise unsaturated active layer (Woo and Steer, 1983). In addition to the potential subsurface storage created by seasonal ground thaw, the effective storage capacity can also vary with spatial and temporal patterns of snowmelt, precipitation, and soil drainage characteristics. Runoff from both subarctic and arctic hillslopes in western Canada depended on antecedent water storage in highly transmissive surface organic soils (Carey and Woo, 2001; Quinton and Marsh, 1999). In a small watershed with water tracks in Arctic Alaska, runoff was produced in the stream in response to all storms larger than 15 mm even during dry periods when surface flow in the stream and water tracks had ceased (Kane et al. 1989). It is unclear whether a similar threshold runoff response should be expected from the hillslopes and water tracks themselves. A spatially-distributed rainfall-runoff model predicted that the hillslopes become hydrologically disconnected from the valley bottom as the active layer thaws, and the hillslopes and valley bottom only reconnect during storms with high antecedent soil moisture conditions (Stieglitz et al., 2003). Yet this seems at odds with the presence of water tracks on the same hillslopes, which are often described as saturated throughout the summer, and are thus predicted to be the source of initial runoff response in the stream network (McNamara et al., 1998).

In this study, we investigate the role of water tracks in Arctic hillslope runoff response to summer rainfall. We collected field observations of both surface and subsurface hydrological dynamics in hillslope watersheds with water tracks to address three questions: 1) How do arctic hillslope soils and water track runoff respond to summer hydrological dynamics?, 2) Do water tracks in different hillslope watersheds respond to summer rainfall in a similar way?, and 3) What controls water track runoff response to rainfall? Assessing the mechanisms underlying Arctic hillslope hydrologic functioning is essential for predicting the coupled trajectory of Arctic terrestrial and aquatic systems as the climate of the Arctic warms faster than the rest of the world (Holland and Bitz, 2003; IPCC, 2013) and the Arctic freshwater cycle intensifies (Rawlins et al., 2010).

2.3 Study area and field site descriptions

The Kuparuk River flows from the foothills region of the North Slope of Alaska north to the Arctic Ocean. In the Upper Kuparuk River watershed, water tracks cover an estimated 25% of the watershed area (Trochim et al., 2016b), draining hillslopes underlain by continuous permafrost and glacial drift deposits of the Sagavanirktok River Glaciation (Figure 1, Hamilton and Walker, 2003). The dominant vegetation type in this area is moist acidic tundra, which is characterized by tussock-forming graminoids such as *Eriophorum vaginatum*, small-stature shrubs such as dwarf birch and willow, and mosses (Walker et al., 1989). The hillslopes are generally covered in this porous and permeable vegetative mat, except in localized areas where glacial erratics, bedrock ridges, or frost boils occur at the surface. The typical soil profile consists of ~15 cm of peat overlying clay loam or sandy loam with a minor component of small pebbles (Hinzman et al., 1991). The peaty organic layer is approximately an order of magnitude more hydraulically conductive than the underlying loam (Hinzman et al., 1991). Active layer thickness is ~0.25 m on

non-track hillslope and upwards of a meter in some water tracks (Hinzman et al., 1991). Historically, summer rainfall has accounted for approximately two-thirds of annual precipitation (Kane et al., 2004). Total annual rainfall near the Upper Kuparuk River watershed outlet has ranged from 62 to 359 mm, with an average of 217 mm since a meteorological station was installed in 1994 by the Water and Environmental Resource Center (WERC) at the University of Alaska, Fairbanks (Kane et al., 2014). Since 1994, the average annual air temperature recorded at the station is -9 C, ranging from winter temperatures that are consistently colder than -40°C to summer temperatures as warm as 28°C (Kane and Hinzman, 2015).

Six hillslope watersheds containing water tracks (WTs) are the focus of this study (Figure 1). These watersheds were chosen because of their accessibility, proximity to the WERC meteorological station, and range of physical and biological characteristics (Table 1). According to the recent water track classification work of Trochim et al. (2016a), WT1 is an "organic-rich" water track, with a high abundance of graminoids, persistent active layer saturation, and thick organic soil layers. WT2 and WT3 are "steep" water tracks, because of their relatively high ground surface slopes, high abundance of dwarf shrubs, surface hummocks, and colluvial material including gravel at WT3. WT4 is a "wide" water track, because it is more than 8 m wide and has alluvial material in the subsurface. WT5 and WT6 are classified as "narrow" water tracks because they often have standing water in small pools, but lack hummocks or flarks- raised or depressed wetland features that are aligned perpendicular to flow. Half of the watersheds have a generally northeastern aspect (WT1, 2, 3), and half generally southwestern (WT4, 5, 6). WT1 drains to the Kuparuk River two kilometers northwest and downstream of the WERC meteorological station, and the other five watersheds (WT 2-6) are upstream of the meteorological system within four kilometers to the south or southeast.

2.4 Methods

2.4.1 Field data collection

Hourly rainfall data was recorded in 0.1 mm increments at the WERC Upper Kuparuk meteorological station, and runoff from the six water tracks was monitored from June through August in 2013 and 2014. Water flow through water tracks is unchannelized and often occurs in the subsurface. Seasonally freezing and thawing soils preclude constructing trenches to monitor runoff, as has been done in many studies of hillslope hydrology in temperate or tropical regions (e.g., Dunne and Black, 1970; McDonnell, 1990). Instead, we constructed plywood weirs across the six water tracks, wrapping the plywood in durable plastic sheeting to make the weirs water tight (Figure 2). The completed weirs extended through the active layer to the top of the frost table in late summer 2012, approximately 30-50 cm below the ground surface. The weirs channeled surface and subsurface runoff through 6-inch (15.24 cm) fiberglass Parshall flumes with stilling wells outfitted with Solinst Levelogger Edge pressure transducers, which recorded water temperature and temperature-corrected pressure at five-minute intervals. The pressure records were compensated for barometric pressure and elevation using a Solinst Barologger pressure transducer located at site WT6 and encased in vented white PVC pipe to reduce heating from insolation. Freeze-thaw processes beneath the flume and weir required us to level the flumes repeatedly, and we determined that creating rating curves for each site using manual measurements provided more accurate flow estimates than the rating curve associated with the flume. We calibrated the pressure records to manual stage measurements, then created a stage-discharge curve for each site with synoptic discharge measurements made using salt dilution gauging (Moore, 2005), in order to produce continuous discharge records. Flumes were mounted on the weirs following snowmelt and removed in late summer each year. Records at WTs 1-3 begin slightly

later than WTs 4-6 in 2013 because of logistical challenges in obtaining adequate early-season synoptic measurements at all six sites.

Nine fully-screened PVC wells 2.5-in (6.35 cm) in diameter were installed at each site to the depth of the frost table in August 2012 in order to monitor water table fluctuations throughout the summer seasons. The wells were arranged in three transects upslope from the weir and roughly perpendicular to the water track. Each transect includes two non-track wells located on the hillslope on either side of a central "water track" well located in the water track (Figure 2). In mid-June 2013 and 2014, ONSET Hobologger pressure transducers were suspended in the wells, recording pressure in five-minute intervals synchronous with the flume pressure transducers. Since the water in the wells froze over the winters, the pressure transducers had to be lowered deeper into the wells part way through the summer in many locations to collect more continuous pressure records. All records were corrected for this adjustment, compensated for barometric pressure, and reported relative to the ground surface to generate water table depth records. At roughly biweekly intervals, the depth of the frost table was determined by making depth-to-refusal frost probe measurements along two 60-m transects which crossed the water track and included the upper and lower well transects. Measurements were made every two meters on the non-track hillslope and every half-meter in the water track. The elevation of both the frost table and water table were determined at each measurement location by carefully surveying the ground surface relative to ground control points (large glacial erratics) using an automatic level and stadia rod. Finally, ground temperatures in the six water tracks and adjacent hillslopes were measured at 2- to 5-cm depth intervals from near the soil surface to a depth of 35 cm using thermocouple chains and Campbell Scientific dataloggers set to record every five minutes.

2.4.2 Data analysis

The watersheds of the six sites were delineated in ArcGIS 10 from 0.5-m or 1-m resolution digital elevation models (DEMs). The 0.5-m DEMs cover sites WT1, 5, and 6 and were created from terrestrial lidar data collected in August 2014 with BCAL Lidar Tools (https://bcal.boisestate.edu/tools/lidar) as described by Voytek et al. (2016). The 1-m DEM that includes the watersheds of WT2, 3, and 4 was created from aerial lidar data by the Alaska Division of Geological & Geophysical Surveys (Hubbard et al., 2011). Note that the delineated watersheds define the drainage divides for surface runoff but not necessarily subsurface runoff, because the topography of the frost table does not always follow the ground surface topography (Woo and Steer, 1983; Voytek et al. 2016). The ArcGIS Spatial Analyst toolbox was used to calculate the watershed areas and elevation distributions for each site from the DEMs.

Water track runoff responses to rainfall events were quantitatively assessed at four sites with the longest runoff and water table records and a range of drainage areas and elevation distributions: WT1, WT4, WT5, and WT6. We used the hydrograph separation methods of previous workers in permafrost hydrology (e.g., Carey and Woo, 2001; McNamara et al., 1998) to determine the magnitude of water track runoff in response to discrete periods of rainfall. First, the rainfall record for each summer was divided into discrete periods of rainfall, defined as periods of rainfall separated by an intervening period of least 24 hours with less than 0.3 mm of rainfall. Then, the hydrograph records for the four sites were examined for storm responses to the discrete periods of rainfall. When there was no distinguishable increase in discharge at the water track outlet, runoff production for that storm was designated as zero. When there was a distinguishable response, storm runoff was graphically separated from baseflow by projecting a horizontal line across the hydrograph from the beginning of the hydrograph rise to the time when discharge returned to the antecedent discharge (e.g., Carey and Woo, 2001). If the next period of rainfall

occurred before complete recession, the horizontal line was projected across the hydrograph to the time when discharge was 10% of the difference between the maximum storm discharge and the antecedent discharge (Tromp-van Meerveld and McDonnell, 2006a). Events not meeting either of these two conditions, and events that lasted longer than 10 days were excluded from the analyses. For each event, hyetograph and hydrograph characteristics (Dingman, 2002) were calculated for the water tracks in order to compare responses site-to-site and with those determined by McNamara et al. (1998) for the adjacent Imnavait Creek.

Based on initial water track hydrograph observations, we hypothesized that runoff production in response to individual storms was primarily controlled by rainfall amount and antecedent water storage conditions near the water track outlet, but that the relative importance of the two factors varied by site. To test this hypothesis, we constructed a broken stick linear model comparing runoff production with rainfall and antecedent water table depth under a set of simple assumptions. First, the model structure assumes that there is no runoff produced during events until after a break point value of the aggregated rainfall total and antecedent water table depth, that is, the water table depth at the onset of rainfall. Then after the break point, the model structure assumes that runoff production increases linearly with more rainfall or a higher antecedent water table. Thus,

$$q = \begin{cases} 0, if\ (r - F \times d) \leq p \\ a + m \times (r - F \times d), if\ (r - F \times d) > p \end{cases} \quad (1)$$

where q is runoff (mm), r is rainfall (mm), F is a scaling factor accounting for soil drainage properties, d is the depth to the water table (mm), p is the break point value of the x-axis (where $x = r - F \times d$) which is bounded by the values determined in Eq. 4, and a and m are the intercept and slope of the q - x relationship, respectively. The water table depth value (d) is from the well at each site with the most continuous record and seasonal water table fluctuations in excess of 10 cm.

These were the eastern hillslope well on the upper transect at WT1, the water track wells on the lower transect at WT4 and WT5, and the water track well on the middle transect at WT6. We chose to use a single well at each site rather than an aggregated metric of antecedent conditions across all wells at a site (e.g., Detty and McGuire, 2010). An aggregated metric was less accurate in this study because the water table sometimes declined below the level of the pressure transducer, especially in some hillslope wells. Thus, averages that include these dry wells underestimate variations in the depth to the water table.

We identified the best-fit model for each site by minimizing the sum of the squared error of the regression residuals (SSE). For each model, we tested 1000 values for the break point (p) ranging between the minimum and maximum x-values, 100 values between 0 and 2 for the slope of the line (m) after the break point, and 30 values ranging from 0 to 0.3 for the scaling factor (F) relating antecedent water table depth to rainfall. We express the uncertainty in the break point value by first calculating the standard error of the slope,

$$s_m = \frac{m}{\sqrt{n-2}} \times \sqrt{\frac{1}{\rho^2} - 1} \tag{2}$$

where s_m is the standard error of m, the slope of the regression line above the break point, n is the number of storms, and ρ is the Pearson correlation coefficient. Minimum and maximum intercepts of the regression can be determined from the standard error of the slope, such that

$$b_{min} = \bar{q} - \bar{x} \times (m - s_m), b_{max} = \bar{q} + \bar{x} \times (m - s_m) \tag{3}$$

where b_{min} and b_{max} are the minimum and maximum intercepts, respectively, and $\bar{x}$ and $\bar{q}$ are the mean x and q values of the samples used to generate the regression. Finally,

$$p_{min} = \frac{-b_{min}}{m + s_m}, p_{max} = \frac{-b_{max}}{m + s_m} \tag{4}$$

where p_{min} and p_{max} are minimum and maximum values of the break point based on the standard error of the slope of the regression line.

Finally, we investigated the potential role of evapotranspiration losses on hillslope runoff patternsby analyzing the timing of diel cycles at the focal water tracks. Following the cross-correlation methods of Barnard et al. (2010) and Post and Jones (2001), we calculated the Pearson's correlation coefficient between our discharge measurements (averaged to half-hour intervals), and evapotranspiration rates estimated from instantaneous water flux measurements made at the Arctic Observatory Network tussock tundra eddy covariance tower in the Imnavait Creek watershed 2.5 km southeast of WT6 (Euskirchen et al., 2012). We identified the lag with the largest Pearson's coefficient for lags from 30 minutes to 12 hours. We removed evapotranspiration rate estimates that were derived from "poor quality" water fluxes using the quality check system of Mauder and Foken (2004), which accounted for less than 10% of the time period analyzed.

2.5 Results and discussion

2.5.1. Summer rainfall-runoff dynamics

More rain fell between mid-June and the end of August in 2014 (195.4 mm) than during the summer of 2013 (147.7 mm). The average cumulative rainfall over the same period is 175.8 mm, based on the 14 years with continuous rainfall data at the meteorological station, making summer 2014 relatively wet and summer 2013 relatively dry. However, the cumulative rainfall over this period is also highly variable, from a minimum of 83.2 mm in 2011 to a maximum of 275.4 mm in 1997, and 2013 and 2014 fall within one standard deviation (53.6 mm). Both summers were characterized by low intensity rainfall, with rainfall briefly reaching a maximum hourly intensity of 6.5 mm/hr on June 29, 2014. Low intensity rainfall is typical of the area, again based

on the available summer records. For example, rainfall intensities exceeding 2 mm/hr account for 7.1% of rainfall in the historical records, compared with 7.4% of rainfall in 2013 and 3.6% of the rainfall in 2014 (Figure S1). Neither summer 2013 nor 2014 included a period of time without rainfall longer than one week.

Runoff from the six water tracks was ephemeral or intermittent, ranging from 0 to 10 L/s (Figure 3, S2). Diel cycles in both water track discharge and water table fluctuations were observed at all sites and well locations, particularly in the dry periods between storms. Figure 4 shows a particularly clear example of this behavior from August 4th to August 15th, 2014 at WT6. A previous mechanistic investigation of diel cycles in hillslope discharge during the snow and ice-free season on a temperate hillslope found that the diel fluctuations resulted from plants drawing down soil moisture for transpiration (Barnard et al., 2010). In that study, hillslope runoff and transpiration were most tightly coupled as the hillslope was drying, and during that time, peak transpiration was correlated with minimum hillslope discharge, with a lag of two hours. We expected a similar correlation and lag between peak evapotranspiration rates, estimated from water fluxes measured at a nearby eddy covariance station, and minimum water track discharge at our sites. We found that peak evapotranspiration rate has the highest correlation with minimum water track discharge 5 hours later (Figure S3, $r = -0.54$, $p < 0.01$). We infer that plant water use has a significant impact on diel cycles in water track discharge on these Arctic hillslopes. Unlike the temperate system previously mentioned, it is also possible that melting ground ice could contribute to the diel cycles in water track discharge and water table fluctuations. Assuming an average mineral soil heat flux of 5 W/m^2 based on summer measurements by Hinzman et al. (1991), and assuming that all incoming heat is used for melting ice, potential daily contributions are ~0.43 L/s. However, all incoming heat is very unlikely to be used for melting ice given that ground ice

contents vary spatially and part of the incoming heat flux is partitioned to increased sensible heat; in fact, we measured soil temperature variations up to ~2.5ºC at a depth of 35 cm during this period using thermocouple chains. Contributions from melting ground ice to diel cycles in Arctic hillslope hydrologic dynamics could be further investigated by using tracers to fingerprint the potential water sources, or by isolating ground ice contributions from unvegetated Arctic hillslopes or water tracks in Antarctica.

2.5.2 Timing and magnitude of subsurface response

Both the timing and magnitude of water table response to rainfall varied with landscape position and from site to site. The magnitude of water table fluctuations at individual wells ranged from less than 6 cm to more than 30 cm over the course of each summer season (Figures 3 and 5 and S4-6). The median duration of full saturation in the water-track soils was 24% and 58% of the 2013 and 2014 seasons, respectively, while it was 0% for both seasons in the non-track hillslope soils ($p < 0.05$ using the Friedman test). Water track soils at WT1, WT5, and WT6 were previously found to regulate nutrient dynamics by strongly retaining inorganic phosphorus but not inorganic nitrogen when saturated (Harms and Ludwig, 2016). The frequency of soil saturation we observed in the water tracks relative to the adjacent hillslope suggests that the potential for nutrient regulation is common in water tracks both spatially and throughout the growing season.

To explore the spatial variations in the magnitude and rate of subsurface response, we focus on a mid-summer storm that began on July 31, 2014, for which there is continuous water level data for most wells (Figure 6). On all well transects except the upper transect at WT6, the magnitude of water table rise on the non-track hillslopes was greater than the rise in the water tracks. At WT1, the water track wells experienced almost no water table rise, while the hillslope wells rose as much

as 15 cm over the course of the 3-cm storm. At most hillslope well locations, the water table responded immediately, rose more rapidly than discharge at the watershed outlet, and then receded at a similar rate, producing a counter-clockwise hysteretic relationship, while the water table rose and fell in tandem with discharge at some water track well locations or even produced a clockwise hysteretic pattern (Figure 7). Even at water track sites with clockwise hysteresis (e.g., WT6 in Figure 7), there is a smaller water table rise for the same change in discharge. Framed within the fill-and-spill paradigm (Spence and Woo, 2003; Tromp-van Meerveld et al., 2006b), these characteristics suggest that the water track locations are generally closer to their storage capacity and more liable to spill water downslope, either as surface runoff or through soil. In contrast, the hillslope locations store water in the soil column, at least temporarily, increasing the local hydraulic gradient towards the water track. This inference is supported by observations that the soil organic layer, which is an order of magnitude more hydraulically conductive than the mineral soil (Hinzman et al., 1991), is thicker in the water tracks than the non-track hillslope at our sites and in many water tracks in this region (Baughman, 2013).

Finally, in contrast with the relatively slow water track runoff response times relative to small Arctic streams (McNamara et al., 1998), the water table responded immediately to the storm on July 31st, 2014 at almost all water track and hillslope well positions (Figure 6). The exceptions were the water track wells (solid lines) at WT1 and WT3 and two hillslope wells (dashed blue and black lines) at WT3 (Figure 6). The stable water tables at WT1 are unsurprising, because the water table was almost always above the ground surface and fluctuated the least of all wells throughout the season (Figure S4). In contrast, the water table does fluctuate in the water track wells at WT3, but the rainfall response is delayed by several hours at the water track wells. This suggests that wells with the delayed response were hydrologically disconnected prior to the storm, and

reconnected as the storm progressed. The discontinuous nature of the water table time series as thaw progresses precludes seasonal comparisons of the spatial variation in the magnitude and rates of subsurface response for most storms.

2.5.3 Water track runoff response timing characteristics

Quantitative descriptions of the rainfall and hydrograph characteristics averaged for all storms and sites used in the broken stick runoff modeling are shown in Table 2, and characteristics for each site and each storm are included as Supplemental Tables 1-4. The initial abstraction (P_{abst}) is the amount of precipitation that falls prior to initial hydrograph rise. The average initial abstractions were low, ranging from 2.6-5.5 mm, but not as low as the average reported at nearby Imnavait Creek (1.52 mm, McNamara et al., 1998). The water track initial abstractions also had a broader range (0.1-8.1 mm at WT1 to 0.4-17.4 mm at WT4) than those at Imnavait Creek (0-6.5 mm). However, like Imnavait Creek and subarctic hillslopes (McNamara et al., 1998; Carey and Woo, 2001), the initial abstractions were not correlated with five-day antecedent precipitation (P_{5ant}) or the antecedent discharge (q_{ant}), both metrics of antecedent watershed wetness. The initial response time (T_{r1}) is the time from first rainfall to initial hydrograph rise and reflects the time required to fill water storage deficits and connect to the watershed outlet. WT1, which has the largest drainage area, had the lowest average initial abstraction (2.6 mm) and fastest average initial response time (9.1 hours), while WT6, which has the smallest drainage area, had the slowest average initial response time (19.1 hours). WT4 had the largest initial abstraction (5.5 mm). Although McNamara et al. (1998) hypothesized that runoff from water tracks responds immediately to precipitation, causing the fast initial response times observed at Imnavait Creek (average: 2.15 hours), a response time of zero was only observed once, on 6/25/2014 at WT1. The majority of response times were much longer than the average response time observed at Imnavait

Creek and the average response time at each of the four sites relative to Imnavait Creek was 3-7 times longer (Table 2). While our analysis included some complex storms and those in the Imnavait Creek rainfall-runoff analysis did not, our results suggest that the rapid runoff responses to small amounts of rainfall observed at Imnavait Creek were not due to a response on the hillslope water tracks. Instead, we hypothesize that the rapid responses may be attributed to the valley bottom. In contrast with the longer initial abstraction and initial response times, the average lag-to-peak, T_{lp}, and the average centroid lag, T_{lc}, at WT4, WT5, and WT6 were similar to Imnavait Creek (McNamara et al., 1998), and shorter at WT1. The lag-to-peak and centroid lag both characterize the aggregate watershed response time (Dingman, 2002). The lag-to-peak is a measure of the difference between rainfall centroid and hydrograph rise, while the centroid lag is a measure of the difference between hyetograph centroid and hydrograph centroid, and thus the aggregate response time includes information about both the hydrograph rise and recession. The similarity in aggregated response time between Imnavait Creek and the water tracks in this study suggests that, although higher-order streamflow responses are initiated in the valley bottom, upslope water tracks are the dominant source areas for streamflow once water track runoff is initiated and the hillslopes become hydrologically connected to the valley bottom. This finding underscores the importance of understanding the mechanisms controlling water track runoff generation processes.

2.5.4 Evidence for storage-mediation of water track rainfall-runoff responses

Despite the presence of permafrost and mineral soils with low hydraulic conductivity, which limit subsurface water storage (Hinzman et al., 1991), the patterns of water track discharge and water table fluctuations observed at the study sites provide evidence that storage mediates water track runoff responses to rainfall. This mediation is evident in the hydrologic responses to two similarly-sized, sequential rainstorms in July 2013 (Figure 8). On July 15th-17th, 19.9 mm of

rainfall was recorded at the Upper Kuparuk meteorological station after 6.25 days without rainfall, and there was a distinguishable runoff response at the two water tracks with the largest drainage areas (WT1 and WT4), but not at the four water tracks with smaller drainage areas (WT 2, 3, 5, and 6, as exemplified by WT5 discharge in Figure 8). The variation in flow seen at WT5 during the beginning of this period better reflects the diel patterns discussed in section 4.1, and even this variation is absent immediately following the storm on the 17th. However, the water table at all sites rose abruptly, filling previously available subsurface storage capacity. Two days later, before the observed water tables at all locations had receded to antecedent levels, an additional 15.9 mm of rainfall was recorded, the water tables rose further, and discharge from all six water tracks increased dramatically. Notably, the hydrograph at WT4 exhibited a distinct double peak in response to the second storm, which was not observed at other sites or in the hyetograph, suggesting that storage exceedance occurred in two parts of the hillslope watershed, with a delayed hydrologic connection from one part to the other. Similar double-peak hydrograph responses to other large events occurred at this site in summer 2013, but not in summer 2014. We hypothesize that this interannual difference is due to subtle changes in thaw at this site. The WT4 watershed is narrow and slopes gently near the ridgeline, then flattens out into a wide, mid-slope wetland (represented by a sharp peak in the elevation-area curve in the Figure 1 inset). Below the wetland, the slope increases again near the base of the hillslope where the weir is located (Figure 1). Slight differences in the location and timing of thaw at the transitions between the wetland and lower hillslope could affect the routing of water from the upper hillslope, potentially altering fill-and-spill patterns (Spence and Woo, 2006) and runoff response at the weir. Fine-scale observations of thaw in this transition zone could be used to test this hypothesis, but our thaw transects are

downslope of the wetland and cannot directly address the effect of interannual differences in thaw location and timing on the hydrograph response characteristics.

2.5.5 Controls on water track runoff response to rainfall

The best-fit broken stick models (see section 3.2 for details) indicate that runoff production at all four sites increases as storm size increases, but information about local antecedent water table depth has a variable contribution to model fit by site (Table 3, Figure 9). The best-fit model has a scaling factor (*F*) of zero at WT1, meaning that information about antecedent water table depth near the watershed outlet does not improve model prediction of runoff production. This result is consistent with observed seasonal hydrologic dynamics at WT1, where the water table depth in the water track near the weir varies little in response to rainfall or throughout the season (e.g., Figure 6, Figure S1). In contrast, the best-fit model at WT4 suggests that runoff production depends strongly on antecedent water table depth, as indicated by an *F* of 0.25. Both WT1 and WT4 are similar in the steep gains in runoff production following the break point, as indicated by model slopes of 1.31 and 1.41. This behavior could be due to an abrupt increase in the hydrologically connected watershed area contributing to runoff, as already suggested by the hillslope geometry and double-peaked 2013 hydrographs at WT4. WT1, on the other hand, responds most rapidly to rainfall and produces some runoff even during small storms (Table 3, Figure 8), which are likely contributions from the saturated water track near the weir. The large rate of increase in runoff production at both sites after the break point may be attributed to the large fraction of the respective watershed areas which is concentrated in a narrow range of elevations (Figure 1 inset). In fact, half the watershed area is in a 10- or 12-m elevation band that accounts for only 28 or 11% of the total watershed area at WT1 and WT4, respectively. Once storage is exceeded in the relatively flat parts of the two watersheds, those large fractions of the watershed, which were previously

hydrologically disconnected from the watershed outlet, become connected, generating a steep slope > 1 in the R-P relationship that may have been lower if more large events had been observed. At the other two sites, WT5 and WT6, the best-fit models suggest that runoff production depends on antecedent water table depth to a similar, relatively moderate degree (F = 0.09 and 0.07) with similar, lower model slopes (m = 0.48 and 0.38) after relatively small break points (p = -1.13 and 5.61 mm). WT5 and WT6 are similar to one another compared to the other sites, with both water tracks draining small hillslope watersheds on the west-facing moraine in close proximity to one another. In contrast with WT1 and WT4, elevation is more consistently distributed throughout each watershed at WT5 and WT6 (Figure 1 inset), which may explain the differences in the slopes of the linear models.

The broken stick model is a simple tool to test for information on the emergent behaviors that arise from the hydrologic complexity in each hillslope system due to site-specific characteristics. In reality, runoff from a hillslope watershed is the aggregated outcome of a complex set of heterogeneous and hysteretic hydrologic connections and disconnections along flowpaths that exist on the scale of individual soil pores, the soil profile, and geomorphic features such as water tracks. We interpret our simple runoff production model results as indicating that a range of complex, storage-mediated threshold rainfall responses and hillslope hydrologic connectivity processes control water track runoff. WT1 is wetter and hydrologically connected along the water track, while WT4 develops local storage deficits that affect the timing of runoff response as reflected in their initial and watershed response times (Table 2, Section 4.3). At both of these sites, storage thresholds are exceeded during large storms not only within each water track, but throughout the watershed, which contributes to strong runoff response. In contrast, we infer that the water tracks at WT5 and WT6 remain hydrologically disconnected and receive lower

contributions from the surrounding hillslope over the range of storms observed. Both WT5 and WT6 fall under the same classification as “narrow” water tracks, while WT4 is a “wide” water track and WT1 is an “organic-rich” water track, suggesting that the classification scheme recently developed by Trochim et al. (2016b) for remotely sensing water tracks has some utility in predicting site-to-site similarity in hydrologic response to rainfall, but it is important to consider the larger watershed controls as well. Predicting hydrological processes and characteristics from remotely sensed information remains an important challenge in upland Arctic landscapes.

The interplay between rainfall patterns, soil drainage, and watershed structure is also likely to affect nutrient cycling and flux in Arctic watersheds, as the magnitude of the hydrologic response at all sites suggests that water tracks are significant conduits for water and solute export from Arctic hillslopes. Climate change has the potential to influence several of the observed controls on the hydrologic response of Arctic hillslope systems. Global climate model simulations predict increases in pan-Arctic precipitation and evapotranspiration (Rawlins et al., 2010), as well as extreme precipitation events (Tebaldi et al., 2006), which will increase runoff from water tracks if increased precipitation occurs in the summer and outpaces losses from evapotranspiration. Gradual active layer thaw processes can affect runoff routing and the hydrologically connected area contributing to runoff (Woo and Steer, 1983; Quinton et al., 2009), particularly in hillslope watersheds with sensitive geometries, such as WT4. Abrupt thermal erosion processes have also been documented to destabilize and incise water tracks (Bowden et al. 2008, Trochim et al., 2016a), which would impact both the soil drainage properties in the water track and the hydrologic connectivity of water track with the rest of the hillslope watershed, and may affect nutrient export patterns (e.g., Abbott et al., 2015).

2.6 Conclusions

Here we analyzed surface and subsurface hydrological dynamics at six Arctic hillslope watersheds drained by water tracks. Over two summer seasons, water track soils remained saturated for a longer duration of the season than soils on the adjacent hillslope. Diel cycles were observed in both water table records and water track discharge at all sites and observation locations, particularly in the periods between rainfall, likely due to plant water uptake. Hydrograph analysis indicates that the initial runoff response from water tracks is delayed relative to a headwater stream in the adjacent watershed, but that the overall response timing is similar. This suggests a revised understanding of runoff generation from upland Arctic watersheds: early contributions to stream stormflow are likely sourced from valley bottoms, while water tracks shape the stream peak flow and recession characteristics. Further, not all water tracks respond to rainfall in the same way. Thresholds for runoff generation depended on rainfall amount at all sites, but to varying degrees on antecedent water storage conditions near the watershed outlets. We attribute this variability to differences in the patterns of hydrologic connectivity between watersheds, which are controlled by soil drainage and the topography of the surface and subsurface. Based on these findings, we expect that climate change will influence the hydrologic response more in some hillslope watersheds with water tracks than others. In those watersheds with little storage mediation of inputs, larger or more intense storms may lead to higher runoff, and perhaps additional erosion. Watersheds in which subtle subsurface thaw affects hydrological responses may be particularly sensitive to warming because of shifts in subsurface watershed boundaries. The observations presented here should improve our ability to predict the spatial distribution and temporal dynamics of water storage capacity and hydrologic connectivity along hillslope flowpaths in the upland Arctic. In order to generalize the understanding of the controls on runoff generation beyond the watersheds in this study, future work should focus on (1) modeling the

interaction between the process controls identified from field observations and (2) applying process understanding to remotely sensed and spatially distributed information about the upland Arctic landscape.

2.7 Acknowledgements

Funding from the National Science Foundation's Division of Polar Programs and Division of Environmental Biology award numbers 1259930 and 1026843, the United States Geological Survey Northwest Climate Science Center, and the University of Idaho College of Natural Resources McCall Outdoor Science School supported this work. Four anonymous reviewers and editor Dr. John L. Nieber provided constructive criticism which greatly improved this work. The staff of Toolik Field Station, CH2MHill Polar Services, UNAVCO, and the other members and volunteers of the Water Tracks Team provided field support and data collection assistance. Special thanks to Colin Edgar for his assistance in acquiring data from the eddy flux station. Data from this study are available online in the International Arctic Research Center Data Archive (P.I. Sarah Godsey) and in the UNAVCO TLS Archive (Project U-035).

2.8 Figures and Tables

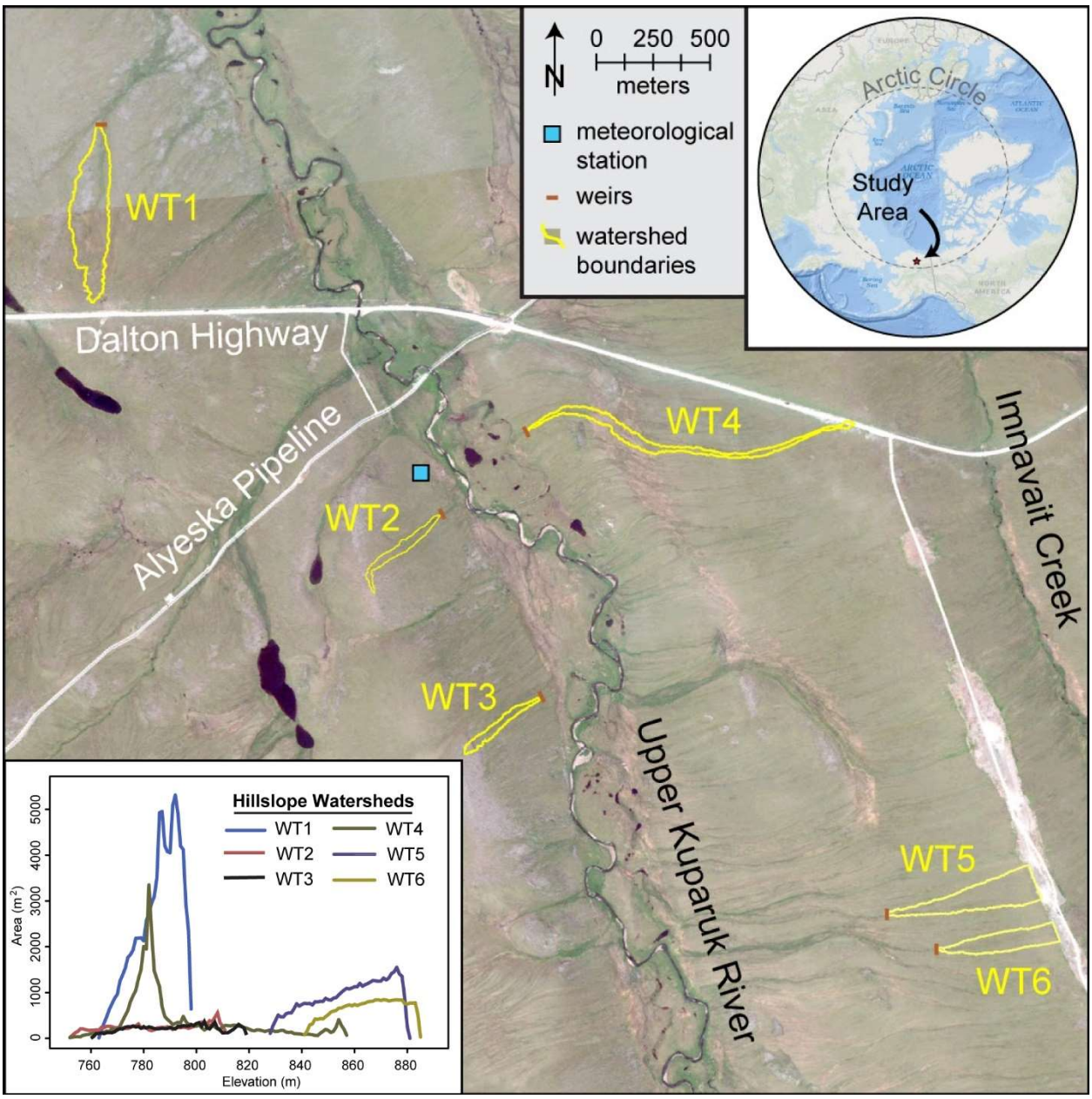

Figure 1. The study area and six water track (WT) watersheds draining the hillslopes of the Upper Kuparuk River in Arctic Alaska, USA (inset). Numerous water tracks are visible as bands of greener vegetation that terminate at the valley bottom, while roads and pipeline stand out in white and water bodies in dark blue. The true color background image combines imagery from the Quickbird-2 satellite on July 18, 2009 (upper image) and the Worldview-2 satellite on July

10, 2011 (lower image). The border between the two images passes through WT1. Commercial imagery (Copyright 2012, DigitalGlobe, Inc.) obtained courtesy of the Polar Geospatial Center at the University of Minnesota.

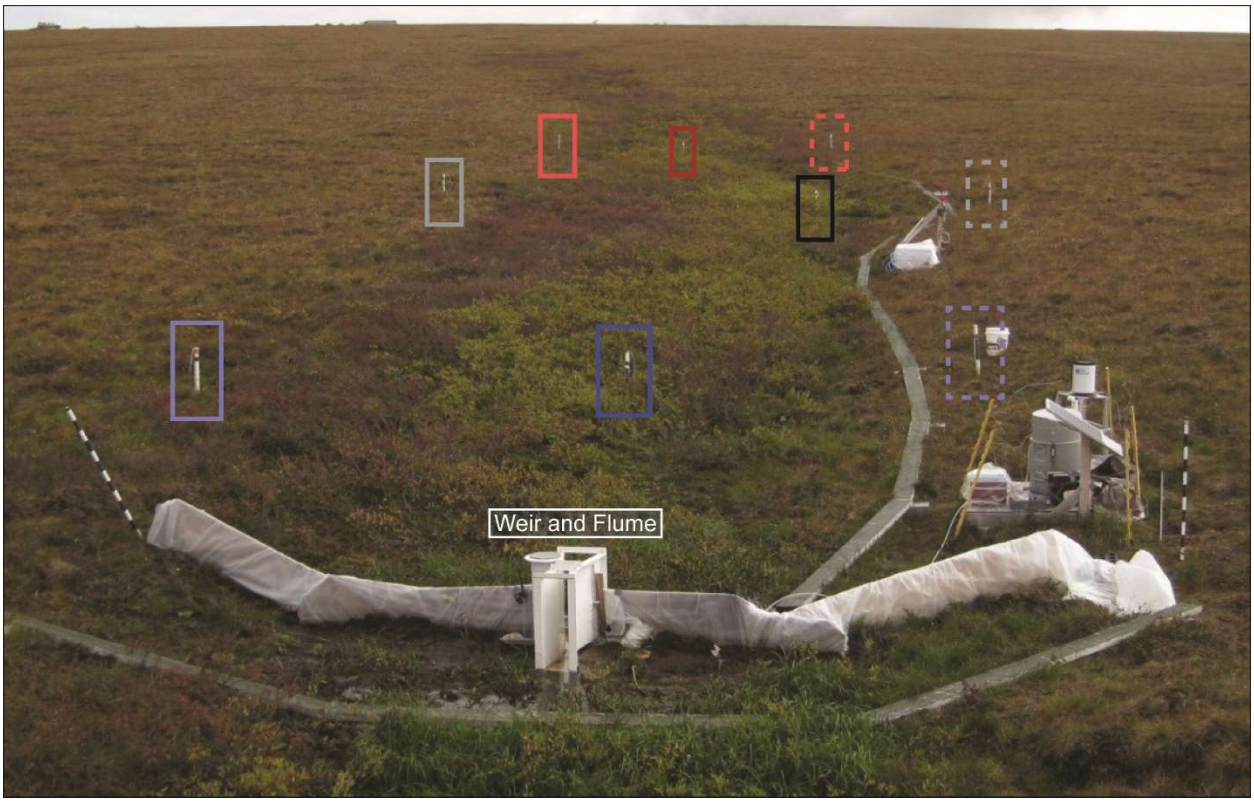

Figure 2. An example from WT6 of the monitoring scheme at each site: the weir and flume used to record flow out of the hillslope watershed are in the foreground, and the nine PVC wells used to monitor water table fluctuations are highlighted with boxes in the middle ground within 100 meters of the watershed outlet. The color and line type of the boxes correspond with the water table time series shown in Figures 3-8. The green foliage of the shrubs in the water track feature distinguishes it from the brown tussock tundra of the surrounding hillslope at the time of year the photo was taken (August 20th, 2014). Photograph taken by Emily Voytek with a camera at the top of a 13' (3.96 m) stadia rod looking upslope.

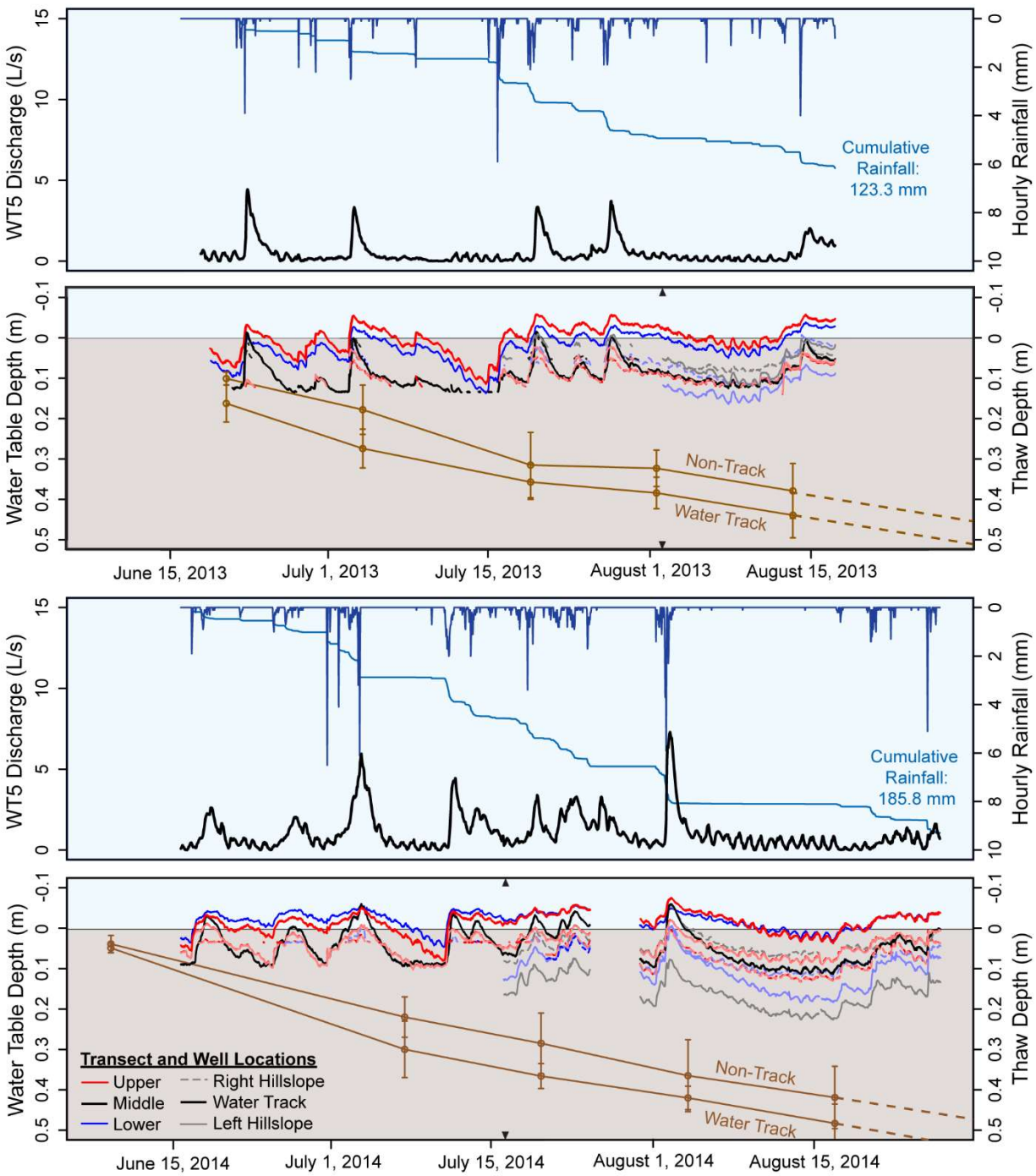

Figure 3. Surface and subsurface hydrological dynamics at WT5 observed in summers 2013 and 2014. The top panels for each year show the water track hydrograph (black), hourly rainfall (dark blue), and cumulative rainfall (bright blue). The bottom panels for each year show (1) the average depth to the frost table inside and outside the water track measured from depth-to-refusal

frost probing (dark gray lines) and (2) the depth to the water table recorded in the shallow groundwater monitoring wells (red, blue, and gray-scale lines). Colors and line types for the water table depth correspond to the boxes shown around each well in Figure 2. Fully saturated line colors indicate water track wells and unsaturated line colors indicate non-track wells. Triangles indicate when the pressure transducers were lowered deeper into the wells in each field season.

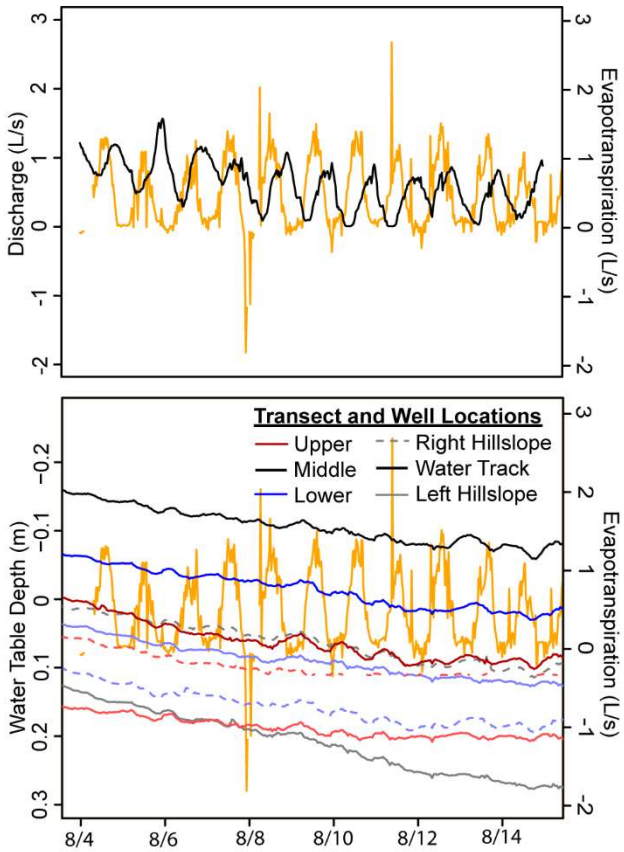

Figure 4. Diel cycles in water track discharge (top panel) and water table depth (bottom panel) during a baseflow period in August 2014 at WT6 compared evapotranspiration rates (orange) derived from water flux measurements made at the Arctic Observatory Network tussock tundra eddy flux tower located in the Imnavait Creek watershed, 2.5 km southeast of WT6. Colors and line types for the water table depths as in Figure 3.

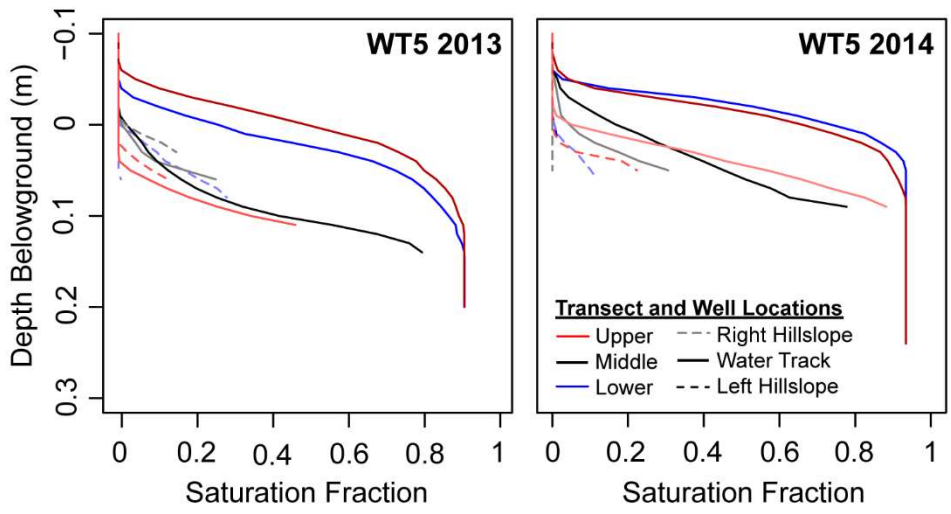

Figure 5. Saturation fraction, or the duration of saturation expressed as a fraction of the study season as a function of depth at each well location for the two seasons at WT5. The maximum depth displayed for each well is the depth of initial pressure transducer deployment, so that the saturation fraction shown represents the entire period of record. Colors and line types for the water table depth correspond to the boxes shown around each well in Figure 2.

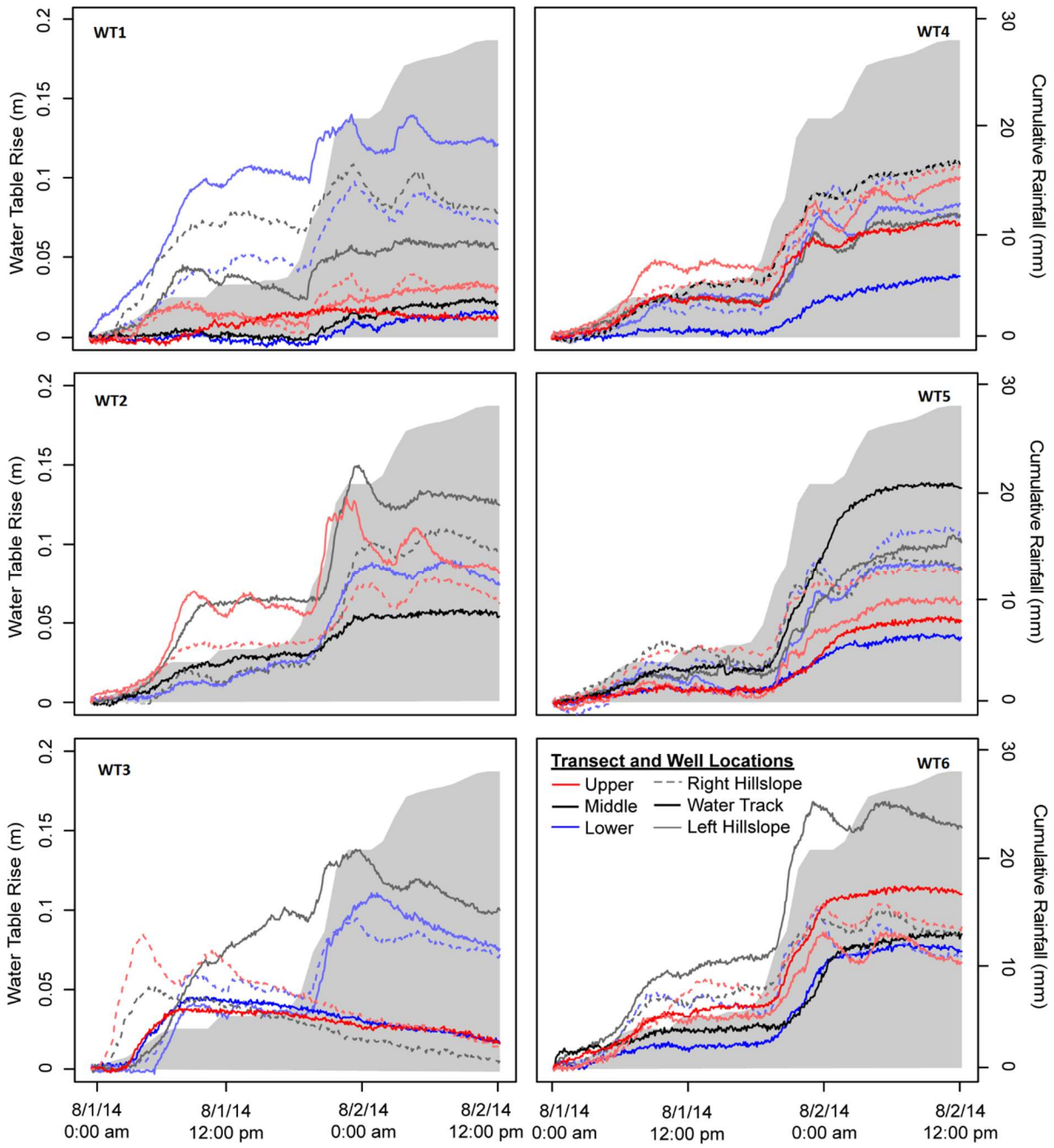

Figure 6. Water table response at each well that responded to a 30.4 mm rainfall event on July 31st 2014. Cumulative rainfall at the Upper Kuparuk meteorological station is shown with the gray region. Colors and line types for the water table rise as in Figure 2.

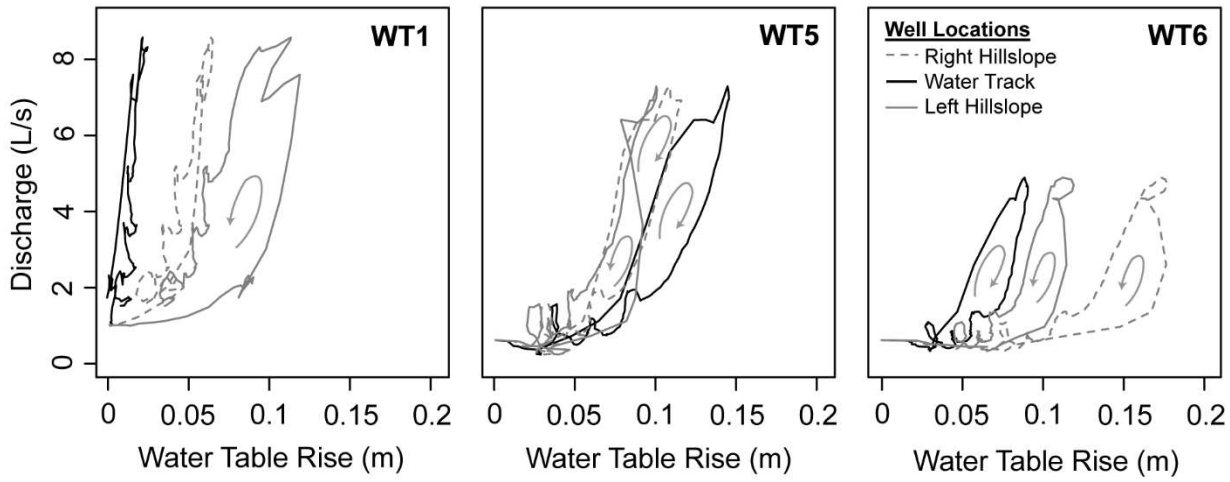

Figure 7. The magnitude of water table rise in the three wells along the middle well transects at WT1, WT5, and WT6 plotted against discharge from each watershed during the rainfall event on July 31st, 2014. As in Figure 6, the amount of water table rise is relative to the initial water table height in each well at the onset of precipitation. Line types for the water table rise correspond to the boxes around each well in Figure 2.

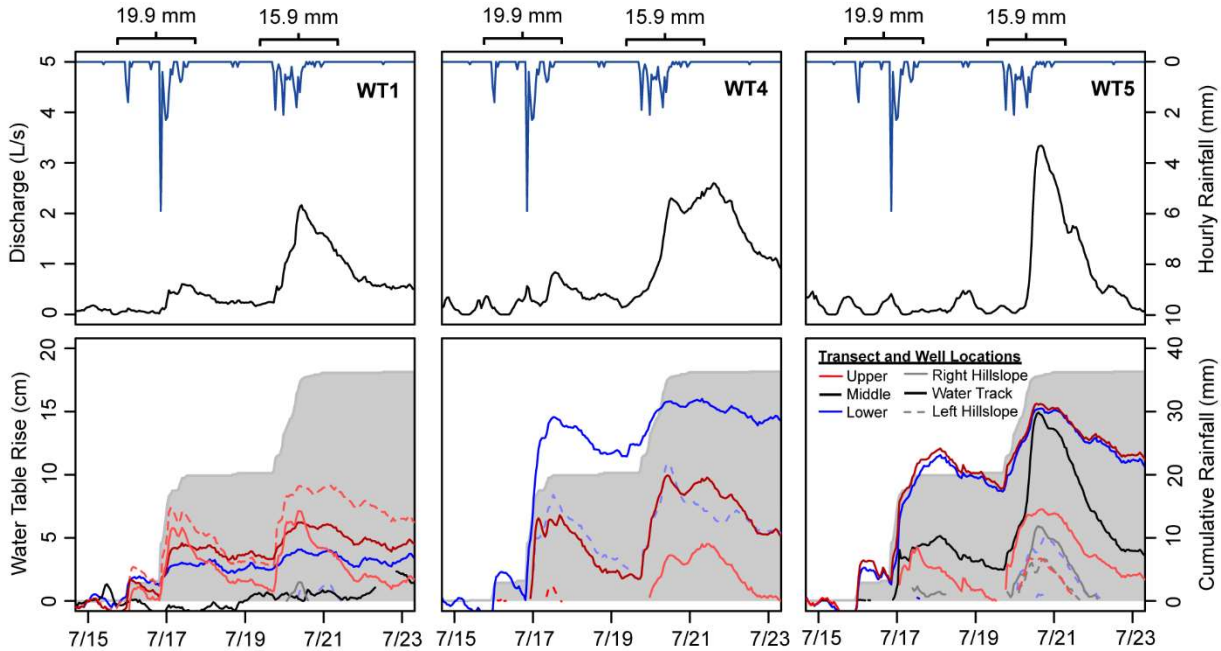

Figure 8. Storage-filling responses to two sequential rainfall events of similar size in July 2013 for WT1, 4, and 5, which highlight three distinct response characteristics observed at all WTs. The total rainfall for each event is shown at the top of the two panels shown for each site. Cumulative rainfall is shown in gray in the lower panel as in Figure 6. Colors and line types for the water table rise as in Figure 3.

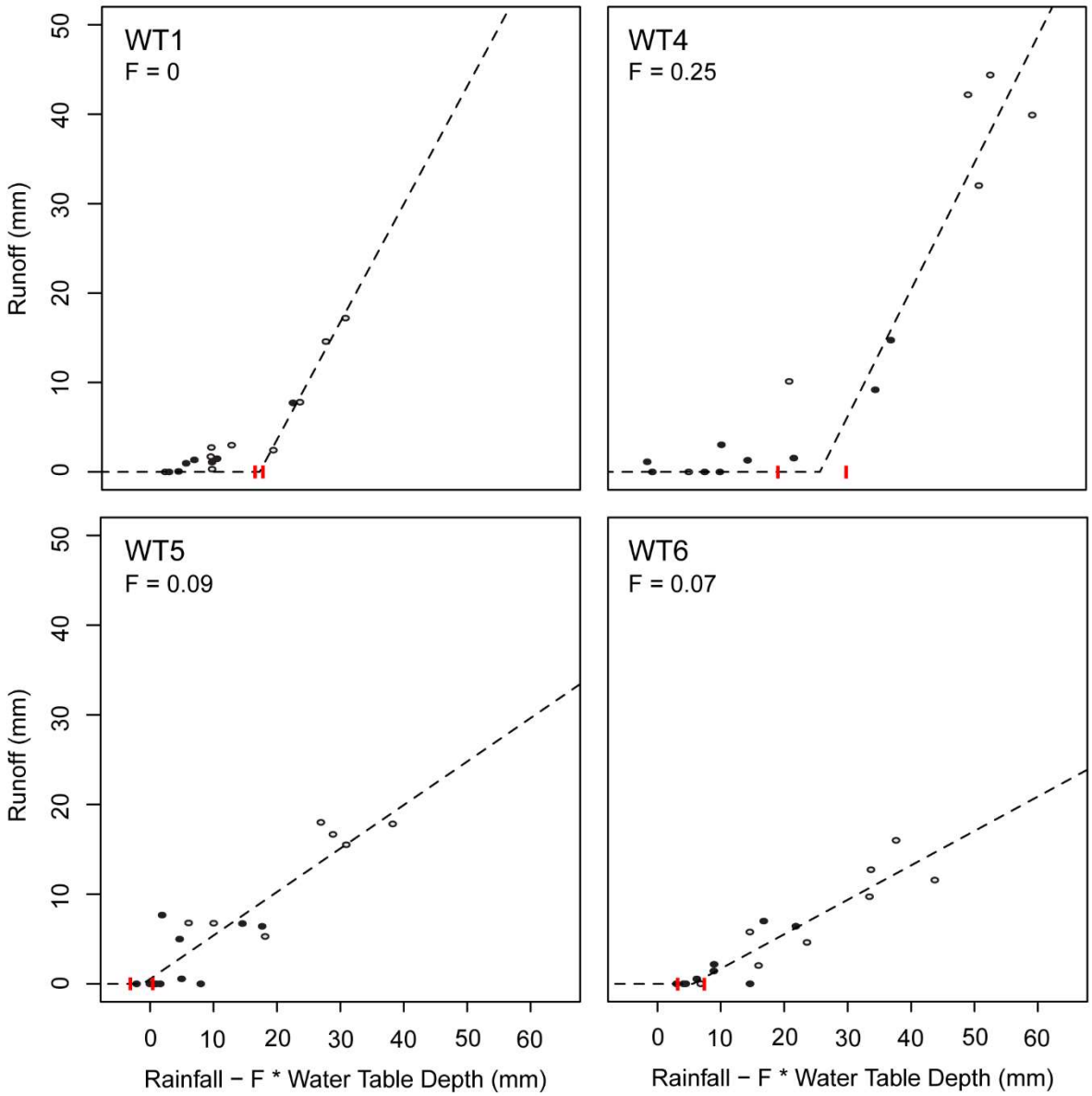

Figure 9. Water track runoff production in response to discrete rainstorms, as a function of total rainfall less the water table depth multiplied by a scaling factor (F), which is indicated in the top left-hand corner of each plot below the site name. Events from 2013 are shown with closed circles and events from 2014 are shown with open circles. The best-fit model is shown with a dashed line. The minimum and maximum threshold values based on the uncertainty in the slope of the line above the threshold are shown with red bars.

Table 1. Hillslope watershed characteristics

Site	Drainage Area (km^2)	Mean Aspect (°)	Cardinal Aspect	Relief (m)	Mean Slope (°)	Water Track Width (m)	Classification
WT1	0.089	1.0	north	35	3.6	12.5	organic-rich
WT2	0.014	72	east	59	8.0	9.5	steep
WT3	0.013	61.0	northeast	59	8.8	7.5	steep
WT4	0.039	225.0	southwest	105	3.6	10.5	wide
WT5	0.049	258.0	west	53	5.1	7	narrow
WT6	0.029	263.0	west	44	4.8	5	narrow

Table 1. Hillslope watershed characteristics. The drainage area, mean aspect, relief, and slope characteristics were determined from DEMs, as described in Section 3.2 of the text. The water track width was in the field by measuring the width of the water track feature at the lower well transect of each site. The water track classification comes from Trochim et al. (2016b), as described in Section 2 of the text.

Table 2. Summary of event-based rainfall-runoff analyses

Statistic	T_p (hrs)	T_{ep} (hrs)	P_{pk} (mm)	P_t (mm)	P_{abst} (mm)	P_{5ant} (mm)	I (mm/hr)	I_{max} (mm/hr)	T_{r1} (hrs)	T_{r2} (hrs)	T_r (hrs)	T_{lp} (hrs)	T_{lc} (hrs)	T_b (days)	q_{ant} (L/s)	q_{pk} (L/s)	R (mm)
Site WT1, n=19																	
Minimum	3.0	-0.3	2.7	1.3	0.1	0.0	0.0	0.6	0.0	-97.3	0.2	-12.4	5.4	0.0	0.1	0.9	0.0
Maximum	128.0	127.2	27.6	30.7	8.1	20.3	1.2	6.5	23.7	1.1	55.6	30.0	49.7	8.5	1.6	9.5	17.2
Mean	44.7	39.4	12.0	12.6	2.6	6.4	0.3	2.7	9.1	-19.6	19.8	8.6	21.9	3.0	0.8	3.5	3.3
Standard Error	8.0	9.7	2.0	2.0	0.6	1.7	0.1	0.4	2.1	7.1	4.7	2.6	3.4	0.7	0.1	0.7	1.2
Site WT4, n=16																	
Minimum	3.0	1.8	5.5	1.3	0.4	0.0	0.0	0.6	1.1	-82.8	7.8	-10.8	13.4	1.7	0.1	0.8	0.0
Maximum	209.0	166.0	39.7	39.8	17.4	20.3	0.5	6.5	43.0	6.2	155.5	90.7	62.7	10.9	1.6	10.4	44.4
Mean	60.8	64.8	17.8	15.7	5.5	5.3	0.3	2.7	12.3	-17.8	47.0	30.7	37.6	4.9	0.6	3.8	12.7
Standard Error	13.7	14.1	3.1	3.3	1.3	1.6	0.0	0.5	3.7	8.1	12.2	7.7	4.2	0.8	0.1	1.0	4.2
Site WT5, n=18																	
Minimum	3.0	11.0	6.8	1.3	0.2	0.0	0.1	0.6	1.2	-94.9	9.3	-3.6	18.5	1.9	0.0	0.5	0.0
Maximum	128.0	109.9	37.3	37.3	9.6	20.3	0.5	6.5	33.3	11.1	105.5	70.9	42.1	7.3	0.5	7.4	18.0
Mean	55.7	62.5	16.6	14.3	4.2	5.7	0.3	2.6	12.9	-28.5	34.0	20.1	28.5	4.1	0.2	3.8	6.3
Standard Error	9.3	8.9	2.7	2.6	0.9	1.6	0.0	0.4	2.8	10.8	8.1	5.7	2.0	0.4	0.0	0.5	1.6
Site WT6, n=18																	
Minimum	3.0	-49.9	5.5	1.3	0.4	0.0	0.1	0.6	3.8	-94.9	4.8	-3.6	13.9	0.6	0.0	0.6	0.0
Maximum	128.0	110.3	37.3	37.3	9.7	20.3	0.5	6.5	62.9	57.9	101.5	71.0	61.8	5.8	0.4	5.0	16.0
Mean	55.7	51.5	15.7	14.3	4.7	5.7	0.3	2.6	19.1	-22.4	29.2	22.9	28.6	3.3	0.2	2.1	4.8
Standard Error	9.3	11.8	2.6	2.6	0.7	1.6	0.0	0.4	4.9	12.1	7.4	6.3	3.3	0.4	0.0	0.3	1.2

Table 2. Summary of event-based rainfall-runoff analyses for all storms and sites used in the broken stick runoff modeling (see Figure 9). Site-specific event values are available in Tables S1-S4 of the supplemental information. T_p, duration of rainfall; T_{ep}, time from initial hydrograph rise to the end of rainfall; P_{pk}, rainfall prior to hydrograph peak; P_t, total rainfall; P_{abst}, rainfall prior to initial hydrograph rise; P_{5ant}, rainfall during the five days prior to the event; I, average rainfall intensity; I_{max}, maximum rainfall intensity determined on an hourly basis; T_{r1}, time from first rainfall to initial hydrograph rise; T_{r2}, time from end of rainfall to hydrograph peak; T_r, duration of hydrograph rise; T_{lp}, time from hyetograph centroid to hydrograph peak; T_{lc}, time from hyetograph centroid to

hydrograph centroid; T_b, time from initial hydrograph rise to the return to antecedent discharge; q_{ant}, antecedent discharge; q_{pk}, peak discharge; R, runoff; n, the number of rainfall events that make up the summary statistics.

Table 3. Best-fit model runoff production model results for the four sites

Site	SSE	F	m	se_m	p_{min}	p_{max}
WT1	27.91575	0	1.31	0.10	16.52	17.64
WT4	320.2928	0.25	1.41	0.33	19.11	29.80
WT5	134.9868	0.09	0.48	0.06	-3.14	0.39
WT6	62.66418	0.07	0.38	0.05	3.25	7.37

Table 3. Best-fit runoff production results for the four sites used in the broken stick runoff modeling (see Figure 9). SSE is the sum of the squared error of the model residuals (mm^2), F is the factor relating water table depth to rainfall, m is the slope of the line after the break point, se_m is the standard error of the slope, and p_{min} and p_{max} are the minimum and maximum break points predicted by se_m.

2.9 References

Abbott, BW, Jones, JB, Godsey, SE, Larouche, JR, Bowden, WB. 2015. Patterns and persistence of hydrologic carbon and nutrient export from collapsing upland permafrost. *Biogeosciences* **12**: 3725:3740.

Ali G, Oswald CJ, Spence C, Cammeraat ELH, McGuire KJ, Meixner T, Reaney SM. 2013. Towards a unified threshold-based hydrological theory: necessary components and recurring challenges. *Hydrological Processes* **27**: 313-318.

Barnard HR, Graham CB, Van Verseveld WJ, Brooks JR, Bond BJ, McDonnell JJ. 2010. Mechanistic assessment of hillslope transpiration controls of diel subsurface flow: a steady-state irrigation approach. *Ecohydrology* **3**: 133-142.

Baughman CA. 2013. Soil surface organic layers in the arctic foothills: Distribution, development, and microclimatic feedbacks. MS Thesis, University of Alaska, Fairbanks.

Bowden WB, Gooseff MN, Balser A, Green A, Peterson BJ. 2008. Sediment and nutrient delivery from thermokarst features in the foothills of the North Slope, Alaska: Potential impacts on

headwater stream ecosystems. *Journal of Geophysical Research* **113**(G02026). doi:10.1029/2007JG000470.

Burt TP, McDonnell JJ. 2015. Whither field hydrology? The need for discovery science and outrageous hydrological hypotheses. *Water Resources Research* **51**: 5919-5928. doi:10.1002/2014WR016839.

Carey SK, Woo MK. 2001. Slope runoff processes and flow generation in a subarctic, subalpine catchment *Journal of Hydrology* **253**: 110-129.

Detty JT, McGuire KM. 2010. Threshold changes in storm runoff generation at a till-mantled headwater catchment. *Water Resources Research* **46**: W07525. DOI:10.1029/2009WR008102.

Dingman, SL. 2002. Physical Hydrology (2nd ed.). Upper Saddle River, NJ: Prentice Hall.

Dunne T, Black RD. 1970. An experimental investigation of runoff production in permeable soils. *Water Resources Research* **6**(2): 478-490.

Euskirchen ES, Bret-Harte MS, Scott GJ, Edgar C, Shaver GR. 2012. Seasonal patterns of carbon dioxide and water fluxes three representative tundra ecosystems in northern Alaska. *Ecosphere* **3**(1): 4.

Hamilton TD, Walker, DA. 2003. *Glacial geology of Toolik Lake and the Upper Kuparuk River region.* Alaska Geobotany Center, Institute of Arctic Biology, University of Alaska–Fairbanks: Fairbanks, AK. 24 pages.

Harms TK, Ludwig SM. 2016. Retention and removal of nitrogen and phosphorus in saturated soils of arctic hillslopes. *Biogeochemistry* **127**(2): 291-304. doi: 10.1007/s10533-016-0181-0.

Hinzman LD, Kane DL, Gieck RE, Everett, KR. 1991, Hydrologic and thermal properties of the active layer in the Alaskan Arctic, *Cold Regions Science and Technology* **19**: 95-110.

Hinzman, LD, Kane, DL, Benson, CS, Everett, KR. 1996. Energy balance and hydrological processes in an arctic watershed, *Ecological Studies* **120**: 131-154.

Holland MM, Bitz CM. 2003. Polar amplification of climate change in coupled models. *Climate Dynamics* **21**: 221-232.

Hubbard TD, Koehler RD, Combellick RA. 2011. High-resolution lidar data for Alaska infrastructure corridors, in DGGS Staff, LiDAR Datasets of Alaska: Alaska Division of Geological & Geophysical Surveys Raw Data File 2011-3, 291 pp.

IPCC. 2013. Climate Change 2013: The physical science basis. Contribution of Working Group I to the *Fifth Assessment Report of the Intergovernmental Panel on Climate Change*. Stocker TF, Qin D, Plattner G-K, Tignor M, Allen SK, Boschung J, Nauels A, Xia Y, Bex V, Midgley PM (eds). Cambridge University Press, Cambridge, United Kingdom and New York, NY, USA, 1535 pp. doi:10.1017/CBO9781107415324.

James AL, Roulet NT. 2007. Investigating hydrologic connectivity and its association with threshold change in runoff response in a temperate forested watershed. *Hydrological Processes* **21**: 3391-3408.

Kane DL, Hinzman LD, Benson CS, Everett KR. 1989. Hydrology of Imnavait Creek, an arctic watershed. *Holarctic Ecology* **12**(3): 262-269.

Kane DL, Hinkel KM, Goering DJ, Hinzman LD, Outcalt SI. 2001. Non-conductive heat transfer associated with frozen soils. *Global and Planetary Change* **29**: 275-292.

Kane DL, Gieck RE, Kitover DC, Hinzman LD, McNamara JP, Yang D. 2004. *Hydrologic cycle on the North Slope of Alaska*. International Association of Hydrological Sciences Publication 290, 224-236.

Kane DL, Youcha EK, Stuefer SL, Myerchin-Tape G, Lamb E, Homan JW, Gieck RE, Schnabel WE, Toniolo H. 2014. *Hydrology and meteorology of central Alaskan Arctic: data collection and analysis*, *final report*, Report INE/WERC 14.05, 168 pp. University of Alaska Fairbanks, Water and Environmental Research Center: Fairbanks, Alaska.

Kane DL, Hinzman LD. 2015. Climate data from the North Slope Hydrology Research project. University of Alaska Fairbanks, Water and Environmental Research Center. URL: http://ine.uaf.edu/werc/projects/NorthSlope/. Accessed September 8, 2016.

Liljedahl AK, Boike J, Daanen RP, Fedorov AN, Frost GV, Grosse G, Hinzman LD, Iijma Y, Jorgenson JC, Matveyeva N, Necsoiu M, Raynolds MK, Romanovsky VE, Schulla J, Tape KD, Walker DA, Wilson CJ, Yabuki H, Zona D. 2016. Pan-Arctic ice-wedge degradation in warming permafrost and its influence on tundra hydrology. *Nature Geoscience*. DOI: 10.1038/NGEO2674.

Mauder M, Foken T. 2004. Documentation and instruction manual of the eddy covariance software package TK2. Garmisch-Partenkirchen, Germany: Abt. Mikrometeorologie.

McDonnell J. 1990. A rationale for old water discharge through macropores in a steep, humid catchment. *Water Resources Research* **26**(11): 2821-2832.

McNamara JP, Kane DL, Hinzman LD. 1997. Hydrograph separations in an arctic watershed using mixing model and graphical techniques. *Water Resources Research* **33**(7): 1707-1719.

McNamara J, Kane D, Hinzman L. 1998. An analysis of streamflow hydrology in the Kuparuk River Basin, Arctic Alaska: a nested watershed approach. *Journal of Hydrology* **206**: 39-57.

McNamara JP, Kane DL, Hinzman LD. 1999. An analysis of an arctic channel network using a digital elevation model. *Geomorphology* **29**: 339-353.

Moore RD. 2005. Slug injection using salt in solution. *Streamline Watershed Management Bulletin* **8**(2): 1-6.

Paquette M, Fortier D, Vincent WF. 2017. Water tracks in the High Arctic: a hydrological network dominated by rapid subsurface flow through patterned ground. *Arctic Science* **3**: 334-353.

Post, DA, Jones JA. 2001. Hydrologic regimes of forested, mountainous, headwater basins in New Hampshire, North Carolina, Oregon, and Puerto Rico. *Advances in Water Resources* **24**: 1195-1210.

Quinton WL, Marsh P. 1999. A conceptual framework for runoff generation in a permafrost environment. *Hydrological Processes* **13**(16): 2563-2581.

Quinton WL, Bemrose RK, Zhang Y, Carey SK. 2009. The influence of spatial variability in snowmelt and active layer thaw on hillslope drainage for an alpine tundra hillslope. *Hydrological Processes.* DOI: 10.1002/hyp.7327.

Rawlins MA, Steele M, Holland MM, Adam JC, Cherry JE, Francis JA, Groisman PA, Hinzman, LD, Huntington TG, Kane DL, Kimball JS, Kwok R, Lammers RB, Lee CM, Lettenmaier DP, McDonald KC, Podest E, Pundsack JW, Rudels B, Serreze MC, Shiklomanov A, Skagseth O, Troy TJ, Vorosmarty CJ, Wensnahan M, Wood EF, Woodgate R, Yang D, Zhang K, Zhang T. 2010. Analysis of the arctic system for freshwater cycle intensification: Observations and expectations. *Journal of Climate* **23**: 5715-5737.

Shaver GR, Johnson LC, Cades DH, Murray G, Laundre JA, Rastetter EB, Nadelhoffer KJ, Giblin AE. 1998. Biomass and CO2 flux in wet sedge tundras: Responses to nutrients, temperature, and light. *Ecological Monographs* **68**(1): 75-97.

Spence C, Woo, M. 2003. Hydrology of subarctic Canadian Shield: soil-filled valleys. *Journal of Hydrology* **279**: 151-166.

Spence C, Woo, M. 2006. Hydrology of subarctic Canadian Shield: heterogeneous headwater basins. *Journal of Hydrology* **317**: 138-154.

Spence C. 2010. A paradigm shift in hydrology: storage thresholds across scales influence catchment runoff generation. *Geography Compass* **4**(7): 819-833.

Stieglitz M, Shaman J, McNamara J, Engel V, Shanley J, Kling GW. 2003. An approach to understanding hydrologic connectivity on the hillslope and the implications for nutrient transport. *Global Biogeochemical Cycles* **17**(4): 1105. DOI:10.1029/2003GB002041.

Tebaldi C, Hayhoe K, Arblaster JM, Meehl GA. 2006. Going to the extremes: An intercomparison of model-simulated historical and future changes in extreme events. *Climatic Change* **79**: 185-211. DOI: 10.1007/s10584-006-9051-4.

Trochim ED, Jorgenson MT, Prakash A, Kane DL. 2016a. Geomorphic and biophysical factors affecting water tracks in northern Alaska. *Earth and Space Science* **3**: DOI: 10.1002/2015EA000111.

Trochim ED, Prakash A, Kane DL, Romanovsky VE. 2016b. Remote sensing of water tracks. *Earth and Space Science* **3**: DOI: 10.1002/2015EA000111.

Tromp-van Meerveld, HJ, McDonnell JJ. 2006a. Threshold relations in subsurface stormflow: 1. A 147-storm analysis of the Panola hillslope. *Water Resources Research* **42:** W02410. DOI: 10.1029/2004WR003778.

Tromp-van Meerveld HJ, McDonnell JJ. 2006b. Threshold relations in subsurface stormflow: 2. The fill and spill hypothesis. *Water Resources Research* **42:** W02411. DOI: 10.1029/2004WR003800.

Voytek EB, Rushlow CR, Godsey SE, Singha K. 2016. Identifying hydrologic flowpaths on arctic hillslopes using electrical resistivity and self potential. *Geophysics* **81**(1): WA225–WA232.

Walker D, Binnian E, Evans B, Lederer N, Nordstrand E, Webber P. 1989. Terrain, vegetation and landscape evolution of the R4D research site, Brooks Range foothills, Alaska, *Holarctic Ecology* **12**: 238-261.

Wentz FJ, Ricciardulli L, Hilburn K, Mears C. 2007. How much more rain will global warming bring? *Science* **317**(317): 233-235. DOI: 10.1126/science.1140746.

Western AW, Grayson RB. 1998. The Tarrawarra data set: soil moisture patterns, soil characteristics and hydrological flux measurements. *Water Resources Research* **34**(10): 2765–2768.

Woo M, Steer P. 1983. Slope hydrology as influenced by thawing of the active layer, Resolute, N.W.T. *Canadian Journal of Earth Sciences* **20**: 978-986.

Yano Y, Shaver GR, Giblin AE, Rastetter EB, Nadelhoffer KJ. Nitrogen dynamics in a small arctic watershed: retention and downhill movement of ^{15}N. *Ecological Monographs*. **80**(2): 331-351.

2.10 Supplemental Tables and Figures

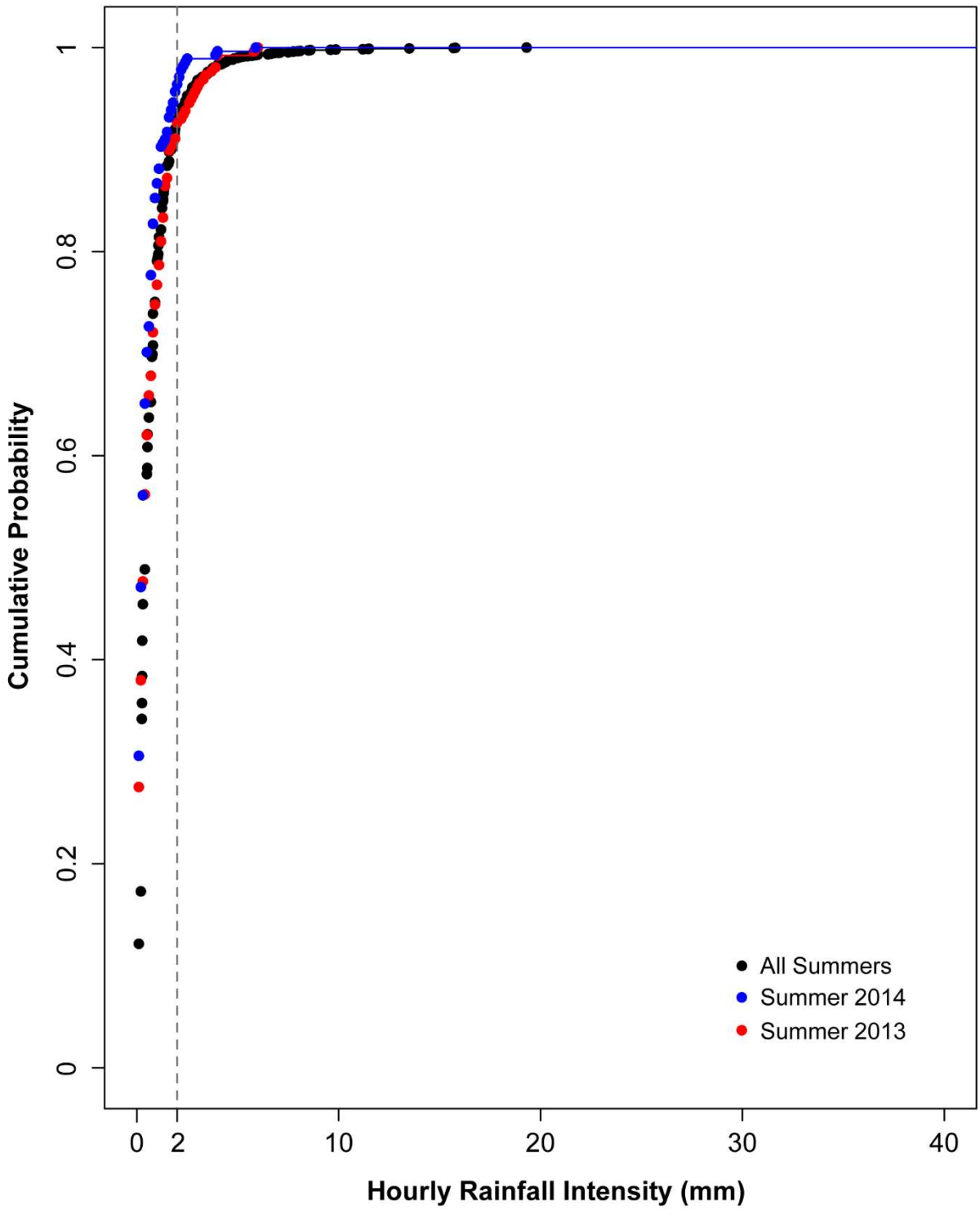

Figure S1. Cumulative distribution function of hourly rainfall intensity for the two study summers (2013 in red and 2014 in blue) compared to the long-term record (in black) at the Water and Environmental Research Center's meteorological station near the Upper Kuparuk watershed outlet.

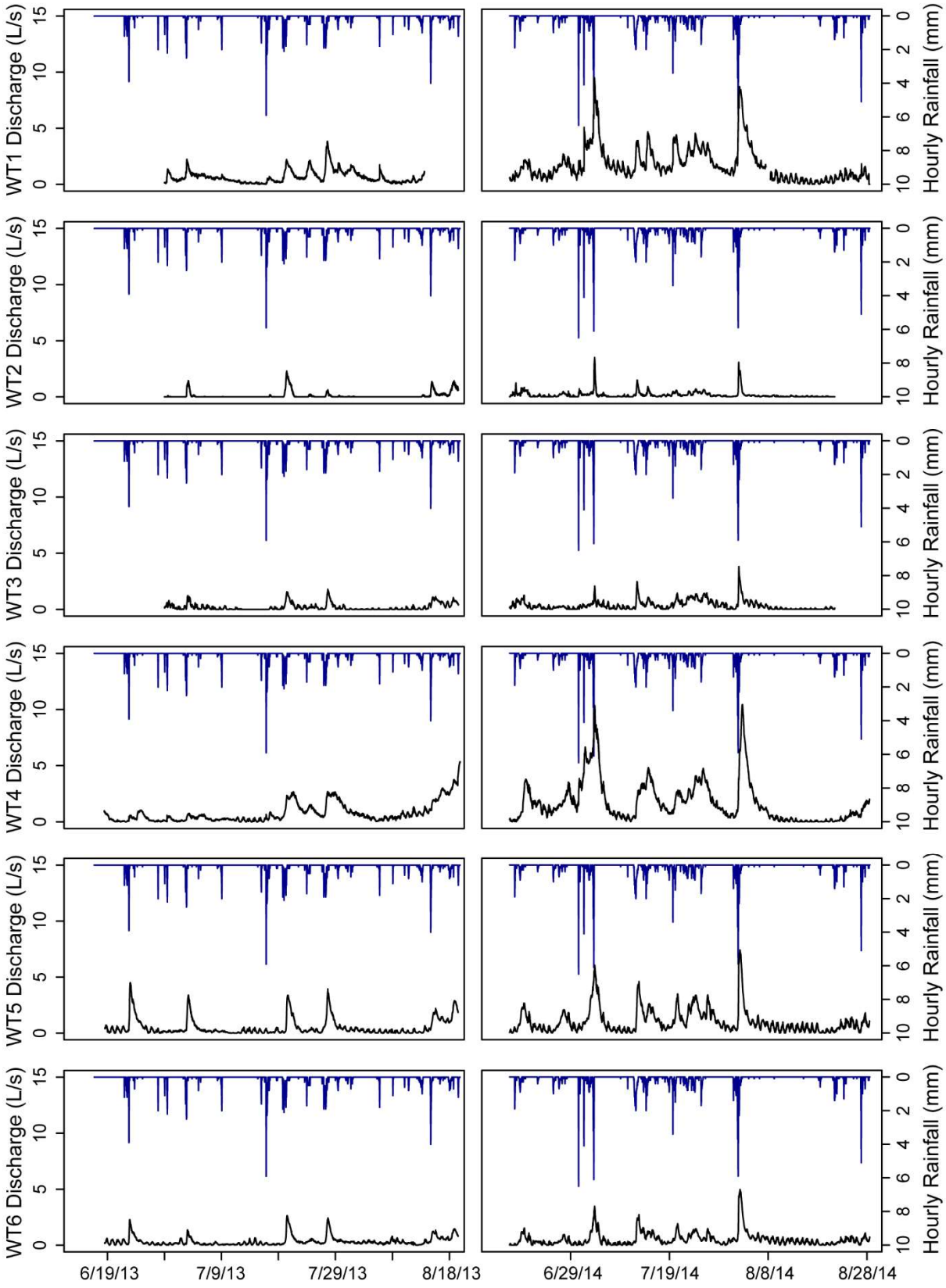
WT1 Discharge (L/s)
WT2 Discharge (L/s)
WT3 Discharge (L/s)
WT4 Discharge (L/s)
WT5 Discharge (L/s)
WT6 Discharge (L/s)
Hourly Rainfall (mm)
0
5
10
15
0
2
4
6
8
10
6/19/13
7/9/13
7/29/13
8/18/13
6/29/14
7/19/14
8/8/14
8/28/14

Figure S2. Hydrographs (black line) for the six study sites and the hyetograph (blue line) from the Upper Kuparuk meteorological station for the two study summers

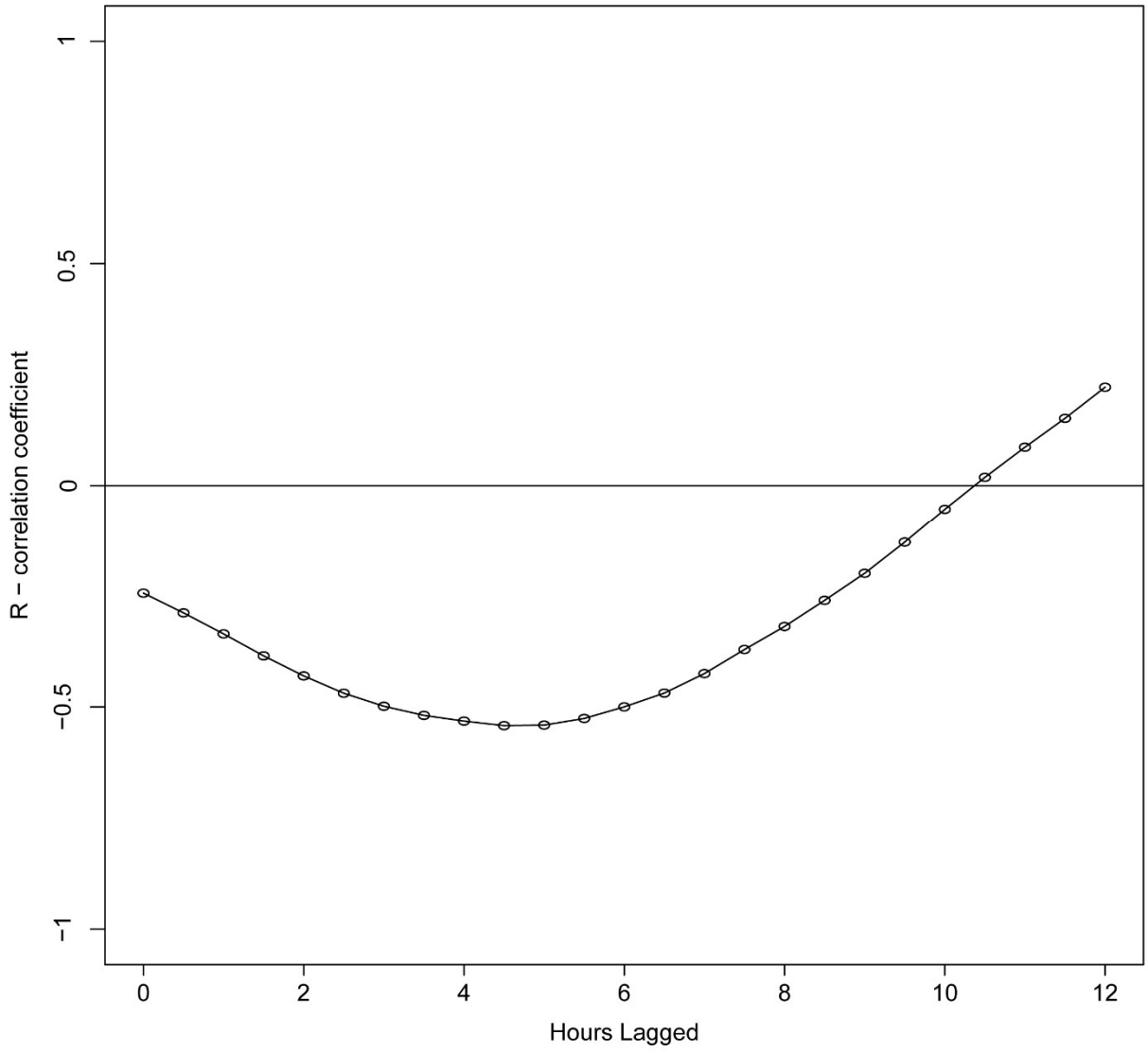

Figure S3. Cross-correlation between daily maximum evapotranspiration rate and minimum discharge at WT6 for lags between 30 min and 12 hours during the period of record shown in Figure 4 of the main text. This analysis follows the approach outlined in Barnard et al. (2010) and Post and Jones (2001).

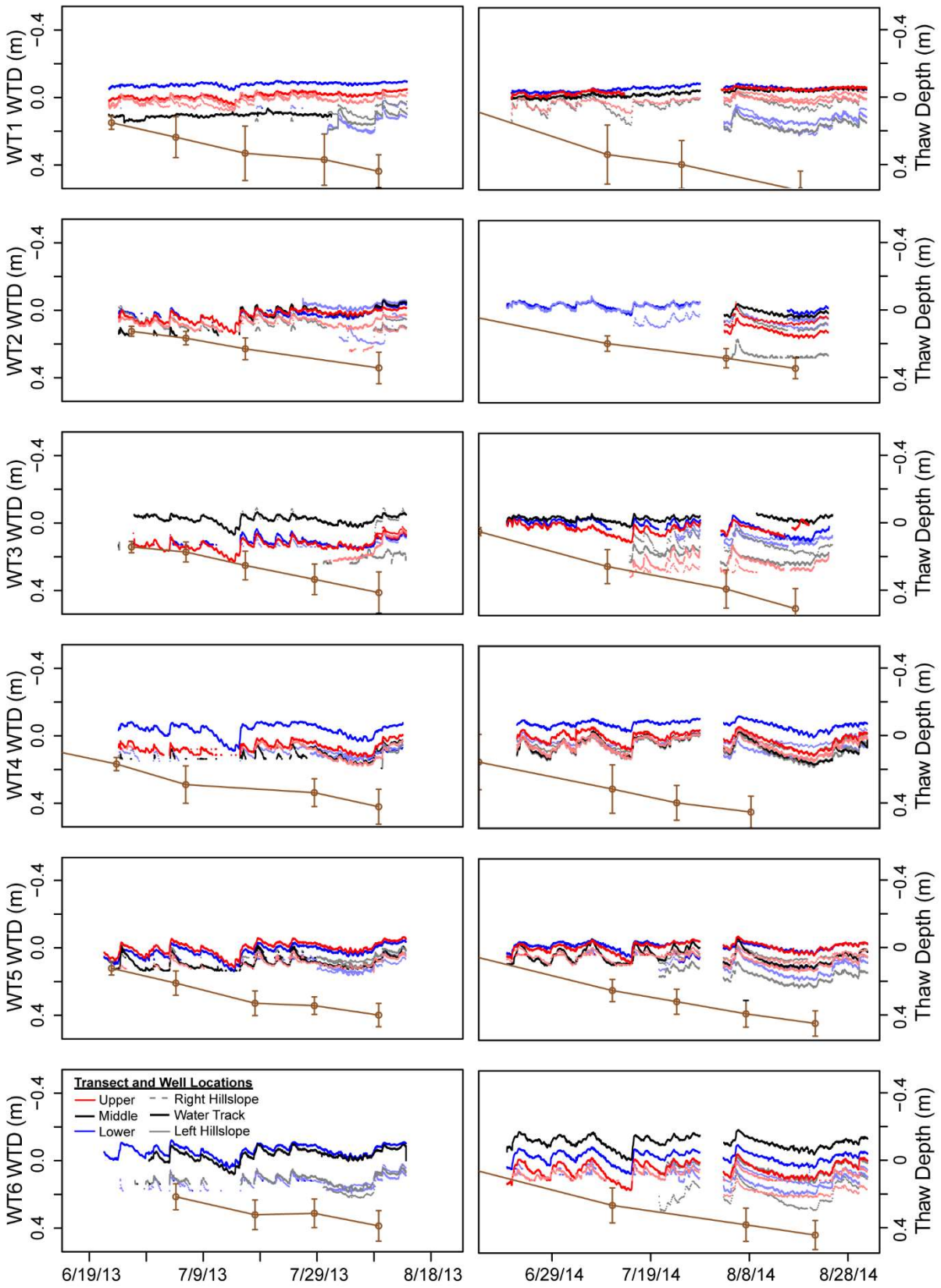
WT1 WTD (m)
WT2 WTD (m)
WT3 WTD (m)
WT4 WTD (m)
WT5 WTD (m)
WT6 WTD (m)
Thaw Depth (m)
0.4
0.0
−0.4
0
Transect and Well Locations
Upper
Middle
Lower
Right Hillslope
Water Track
Left Hillslope
6/19/13
7/9/13
7/29/13
8/18/13
6/29/14
7/19/14
8/8/14
8/28/14

Figure S4. The average depth to the frost table measured from depth-to-refusal frost probing (brown lines) and the depth to the water table (WTD) recorded in the shallow groundwater monitoring wells (red, blue, and black lines). Colors and line types for the water table depth as in Figure 3 in the main text.

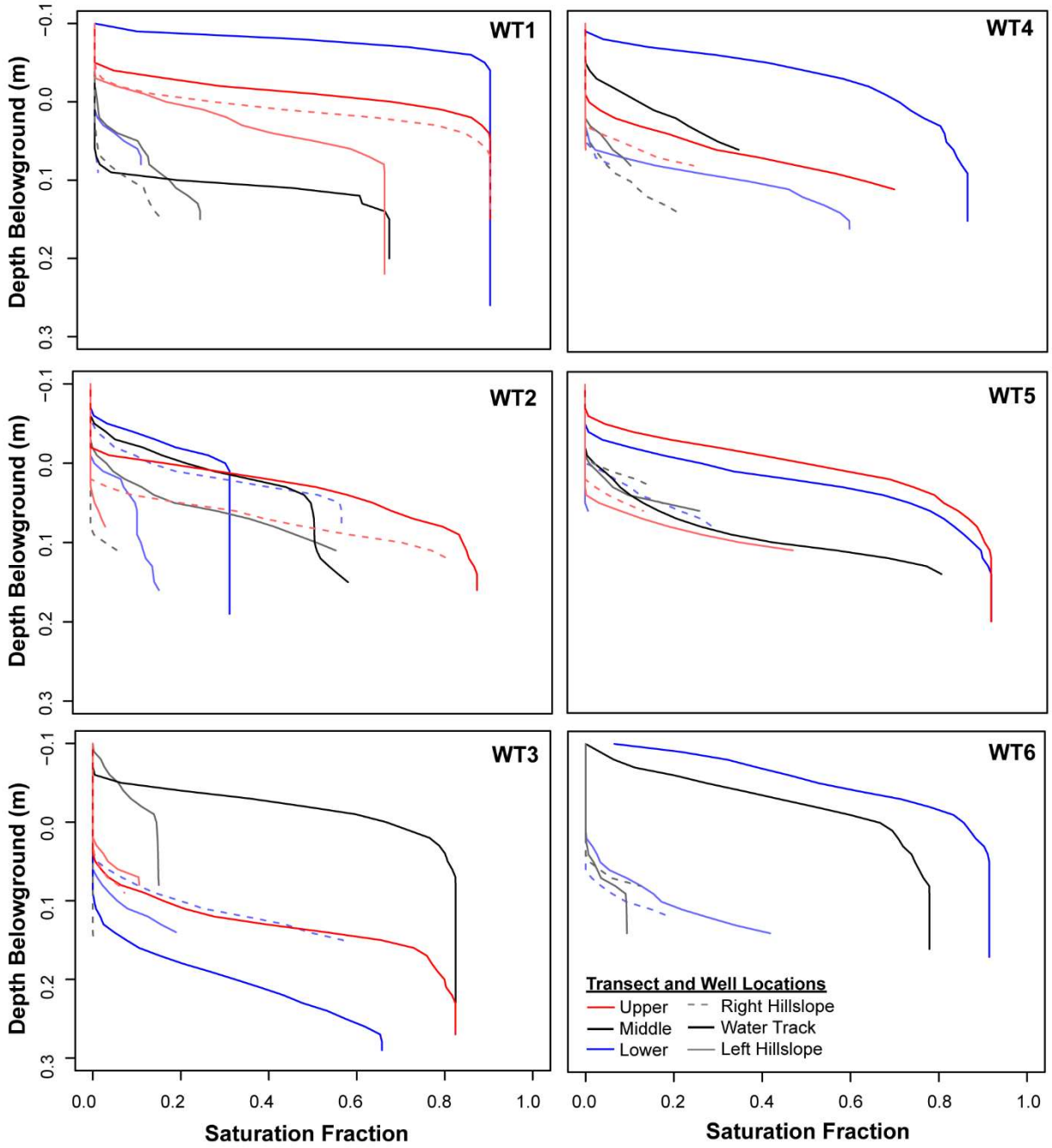

Figure S5. Saturation fraction, or the duration of saturation expressed as a fraction of the study period in 2013, as a function of depth at each well. The maximum depth displayed for each well is the depth of initial pressure transducer deployment, so that the saturation fraction shown represents the entire period of record. Colors and line types for the water table depth as in Figure 3 in the main text.

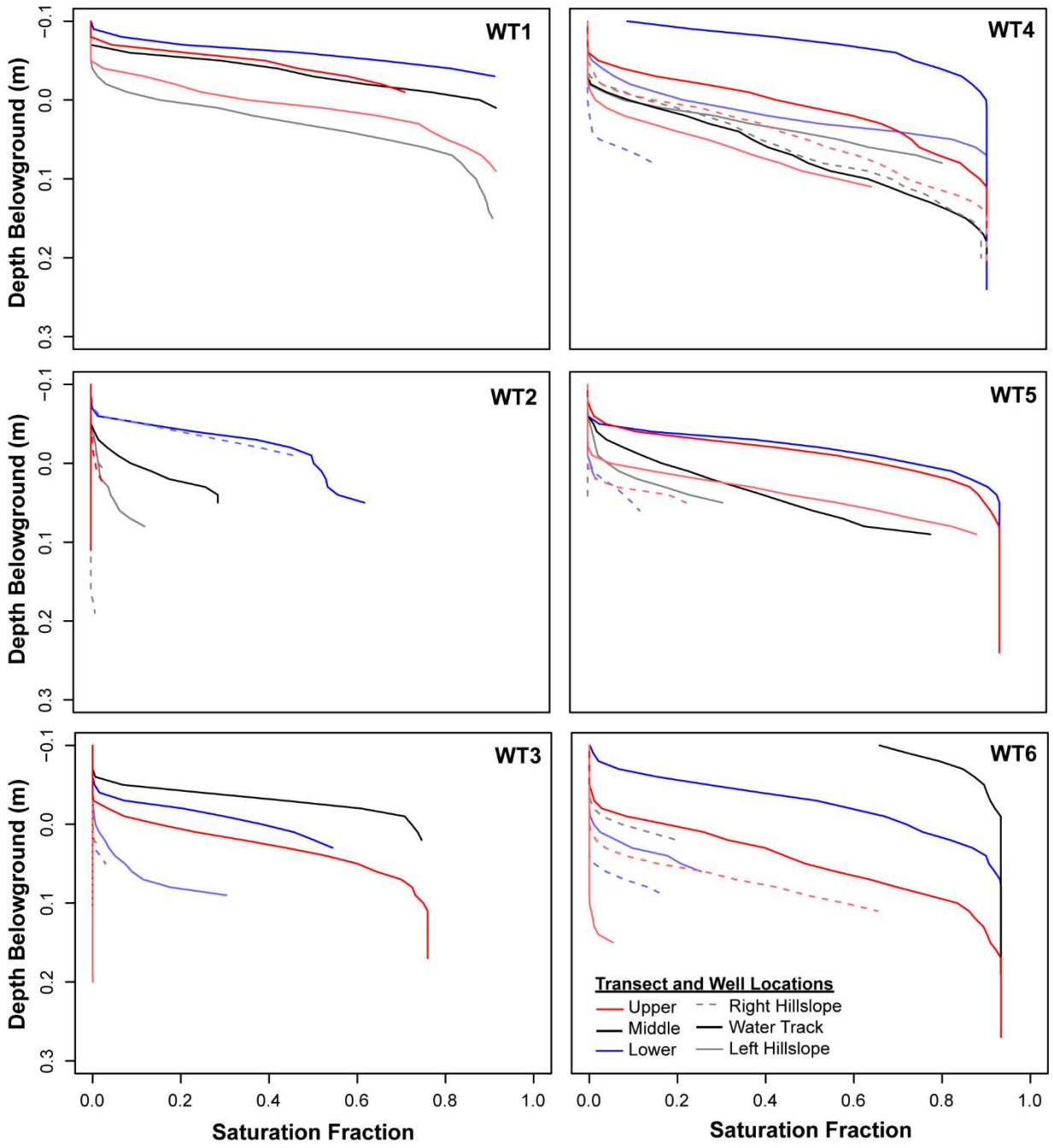

Figure S6. Saturation fraction, or the duration of saturation expressed as a fraction of the study period in 2014, as a function of depth at each well. The maximum depth displayed for each well is the depth of initial pressure transducer deployment, so that the saturation fraction shown represents the entire period of record. Colors and line types for the water table depth as in Figure 3 in the main text.

Table S1. Event-based rainfall-runoff analyses at WT1

Storm date	T_p (hrs)	T_{ep} (hrs)	P_{pk} (mm)	P_t (mm)	P_{abst} (mm)	P_{5ant} (mm)	I (mm/hr)	I_{max} (mm/hr)	T_{r1} (hrs)	T_{r2} (hrs)	T_r (hrs)	T_{1p} (hrs)	T_{1c} (hrs)	T_b (days)	q_{ant} (L/s)	q_{pk} (L/s)	R (mm)
6/17/2014	52.0	28.3	9.1	9.4	4.4	0.0	0.2	1.9	23.7	-3.4	24.9	30.0	33.6	2.3	0.9	2.2	1.7
6/25/2014	68.0	68.0	8.4	9.5	0.6	1.4	0.1	1.0	0.0	-18.9	49.1	25.8	23.7	3.7	1.0	2.7	2.7
6/30/2014	8.0	6.9	9.6	9.6	8.1	8.1	1.2	6.5	1.1	0.2	7.2	6.4	5.5	0.5	0.9	2.1	0.3
7/1/2014	49.0	48.8	27.6	27.6	4.1	14.3	0.6	6.1	0.2	1.1	49.9	18.5	30.9	6.2	1.2	9.5	14.6
7/11/2014	36.0	30.7	17.2	19.3	3.8	0.8	0.5	2.0	5.3	-20.2	10.5	6.4	18.2	2.1	1.2	3.9	2.4
7/13/2014	45.0	21.8	10.7	12.0	3.7	20.0	0.3	2.0	23.2	-12.6	9.3	8.8	20.5	2.0	1.4	4.7	3.0
7/21/2014	121.0	104.7	16.4	23.5	0.8	17.2	0.2	1.7	16.3	-49.1	55.6	10.8	27.4	6.0	1.6	4.5	7.8
7/31/2014	128.0	127.2	27.4	30.7	0.1	0.0	0.2	5.9	0.7	-97.3	29.9	8.2	43.2	7.3	0.8	8.7	17.2
8/18/2014	14.0	-	-	2.2	-	0.1	0.2	0.6	-	-	-	-	-	-	-	-	0.0
6/21/2013	44.0	35.6	9.0	10.2	2.0	0.0	0.2	3.9	8.4	-24.3	11.3	3.0	8.9	1.5	0.5	2.3	1.5
6/29/2013	13.0	6.3	5.5	5.5	1.8	2.2	0.4	2.2	6.8	1.0	7.2	5.8	17.6	1.9	0.1	1.4	1.0
7/2/2013	37.0	27.0	9.0	9.6	1.9	7.5	0.3	2.5	10.0	-21.5	5.5	2.4	18.2	2.1	0.6	2.2	1.1
7/8/2013	19.0	1.6	4.3	4.3	4.3	1.4	0.2	0.8	17.4	0.1	1.7	3.2	5.4	0.3	0.5	0.9	0.1
7/15/2013	37.0	-	-	19.8	-	0.1	0.5	5.9	-	-	-	-	-	-	-	-	0.0
7/19/2013	67.0	-	-	16.0	-	20.3	0.2	2.1	-	-	-	-	-	-	-	-	0.0
7/23/2013	23.0	18.4	6.8	6.8	0.4	16.4	0.3	1.7	4.6	0.8	19.2	10.4	15.3	2.2	0.6	2.1	1.3
7/26/2013	73.0	66.3	15.9	19.3	0.8	6.9	0.3	1.9	6.7	-50.7	15.6	-12.4	49.7	8.5	0.3	3.8	7.7
8/6/2013	12.0	-0.3	2.7	2.7	2.7	1.6	0.2	1.8	12.3	0.5	0.2	2.1	9.7	0.8	0.5	1.7	0.3
8/8/2013	3.0	-	-	1.3	-	2.7	0.0	1.1	-	-	-	-	-	0.0	-	-	0.0
Mean	44.7	39.4	12.0	12.6	2.6	6.4	0.3	2.7	9.1	-19.6	19.8	8.6	21.9	3.0	0.8	3.5	3.3
Standard Error	8.0	9.7	2.0	2.0	0.6	1.7	0.1	0.4	2.1	7.1	4.7	2.6	3.4	0.7	0.1	0.7	1.2

T_p, duration of rainfall; T_{ep}, duration of effective rainfall, which is defined as the time from initial hydrograph rise to the end of contributing rainfall; P_{pk}, rainfall prior to hydrograph peak; P_t, total rainfall; P_{abst}, rainfall prior to initial hydrograph rise; P_{5ant}, rainfall during the five days prior to the event; I, average rainfall intensity; I_{max}, maximum rainfall intensity; T_{r1}, time from first rainfall to initial hydrograph rise; T_{r2}, time from end of rainfall to hydrograph peak; T_r, duration of hydrograph rise; T_{1p}, time from hyetograph centroid to hydrograph peak; T_{1c}, time from hyetograph centroid to hydrograph centroid; T_b, time from initial hydrograph rise to the return to antecedent discharge; q_{ant}, antecedent discharge; q_{pk}, peak discharge; R, runoff; n, the number of rainfall events that make up the summary statistics. Site-specific event values are available in Table S1-S4 of the supplemental information.

Table S2. Event-based rainfall-runoff analyses at WT4

Storm date	T_p (hrs)	T_{ep} (hrs)	P_{pk} (mm)	P_t (mm)	P_{abst} (mm)	P_{5ant} (mm)	I (mm/hr)	I_{max} (mm/hr)	T_{r1} (hrs)	T_{r2} (hrs)	T_r (hrs)	T_{1p} (hrs)	T_{1c} (hrs)	T_b (days)	q_{ant} (L/s)	q_{pk} (L/s)	R (mm)
6/25/2014	68.0	66.8	9.5	9.5	1.4	1.4	0.1	1.0	1.3	6.2	73.0	50.9	40.2	4.8	0.8	3.5	10.1
6/30/2014	76.0	74.9	20.3	37.4	8.1	8.1	0.5	6.5	1.1	3.2	78.1	35.3	23.5	5.6	1.6	10.3	44.4
7/11/2014	118.0	109.7	30.4	32.9	8.3	0.8	0.3	2.0	8.2	-47.4	62.3	41.9	53.2	7.6	0.4	4.8	32.0
7/17/2014	209.0	166.0	39.7	39.8	4.4	15.0	0.0	3.4	43.0	-10.5	155.5	90.7	62.7	10.9	0.7	4.7	39.9
7/31/2014	128.0	118.3	30.4	30.7	5.1	0.0	0.2	5.9	9.7	-82.8	35.5	22.7	46.5	6.8	0.5	10.4	42.2
8/18/2014	14.0	-	-	2.2	-	0.1	0.2	0.6	-	-	-	-	-	-	-	-	0.0
6/21/2013	76.0	56.8	10.3	10.4	8.9	0.0	0.1	3.9	19.2	-6.0	50.8	53.2	45.9	3.5	0.4	1.4	3.7
6/29/2013	13.0	1.8	5.5	5.5	3.2	2.2	0.4	2.2	11.2	6.1	7.9	10.9	19.1	1.7	0.1	0.8	1.3
7/2/2013	37.0	26.0	9.5	9.6	3.5	7.5	0.3	2.5	11.0	-13.8	12.2	10.1	49.4	4.5	0.3	0.9	3.0
7/8/2013	19.0	-	-	4.3	-	1.4	0.2	0.8	-	-	-	-	-	-	-	-	0.0
7/15/2013	37.0	6.6	19.8	19.8	17.4	0.1	0.5	5.9	30.4	1.2	7.8	17.0	31.1	2.0	0.5	1.3	1.1
7/19/2013	67.0	65.8	15.9	16.0	2.3	20.3	0.2	2.1	1.2	-21.3	44.6	35.6	32.5	3.6	0.9	3.1	9.2
7/23/2013	23.0	19.2	6.8	6.8	0.4	16.4	0.3	1.7	3.8	0.8	20.0	10.4	13.4	1.9	0.8	1.5	1.5
7/26/2013	73.0	65.9	15.9	22.4	2.7	6.9	0.3	1.9	7.1	-49.1	16.8	-10.8	33.2	6.2	0.5	2.7	14.7
8/6/2013	12.0	-	-	2.7	-	1.6	0.2	1.8	-	-	-	-	-	-	-	-	0.0
8/8/2013	3.0	-	-	1.3	-	2.7	0.4	1.1	-	-	-	-	-	-	-	-	0.0
Mean	60.8	64.8	17.8	15.7	5.5	5.3	0.3	2.7	12.3	-17.8	47.0	30.7	37.6	4.9	0.6	3.8	12.7
Standard Error	13.7	14.1	3.1	3.3	1.3	1.6	0.0	0.5	3.7	8.1	12.2	7.7	4.2	0.8	0.1	1.0	4.2

T_p, duration of rainfall; T_{ep}, duration of effective rainfall, which is defined as the time from initial hydrograph rise to the end of contributing rainfall; P_{pk}, rainfall prior to hydrograph peak; P_t, total rainfall; P_{abst}, rainfall prior to initial hydrograph rise; P_{5ant}, rainfall during the five days prior to the event; I, average rainfall intensity; I_{max}, maximum rainfall intensity; T_{r1}, time from first rainfall to initial hydrograph rise; T_{r2}, time from end of rainfall to hydrograph peak; T_r, duration of hydrograph rise; T_{1p}, time from hyetograph centroid to hydrograph peak; T_{1c}, time from hyetograph centroid to hydrograph centroid; T_b, time from initial hydrograph rise to the return to antecedent discharge; q_{ant}, antecedent discharge; q_{pk}, peak discharge; R, runoff; n, the number of rainfall events that make up the summary statistics. Site-specific event values are available in Table S1-S4 of the supplemental information.

Table S3. Event-based rainfall-runoff analyses at WT5

Storm date	T_p (hrs)	T_{ep} (hrs)	P_{pk} (mm)	P_t (mm)	P_{abst} (mm)	P_{5ant} (mm)	I (mm/hr)	I_{max} (mm/hr)	T_{r1} (hrs)	T_{r2} (hrs)	T_r (hrs)	T_{lp} (hrs)	T_{lc} (hrs)	T_b (days)	q_{ant} (L/s)	q_{pk} (L/s)	R (mm)
6/17/2014	52.0	42.2	9.0	9.4	3.6	0.0	0.2	1.9	9.8	-8.3	33.8	25.1	28.5	3.1	0.1	2.7	6.8
6/25/2014	68.0	66.8	8.5	9.5	1.4	1.4	0.1	1.0	1.2	-15.5	51.3	29.2	34.1	4.7	0.1	2.1	6.8
6/30/2014	76.0	60.6	37.3	37.3	9.6	8.1	0.5	6.5	15.4	3.2	63.8	35.3	35.0	5.0	0.3	6.0	17.8
7/11/2014	118.0	109.7	19.0	32.9	8.3	0.8	0.3	2.0	8.2	-92.8	16.9	-3.6	31.0	5.1	0.1	4.6	16.7
7/13/2014	66.0	32.7	16.3	16.3	1.2	15.0	0.2	3.4	33.3	7.7	40.4	25.4	25.5	3.1	0.4	3.5	5.3
7/21/2014	121.0	94.4	23.5	23.5	2.9	17.2	0.2	1.7	26.6	11.1	105.5	70.9	42.1	7.3	0.5	3.4	18.0
7/31/2014	128.0	109.9	28.2	30.7	7.1	0.0	0.2	5.9	18.1	-94.9	15.0	10.6	32.3	4.8	0.3	7.4	15.5
8/18/2014	14.0	-	-	2.2	-	0.1	0.2	0.6	-	-	-	-	-	-	-	-	0.0
6/21/2013	76.0	60.3	9.2	10.4	5.0	0.0	0.1	3.9	15.8	-50.9	9.3	8.3	27.2	3.4	0.2	4.5	7.7
6/29/2013	13.0	-	-	5.5	-	2.2	0.4	2.2	-	-	-	-	-	-	-	-	0.0
7/2/2013	37.0	32.2	9.5	9.6	0.2	7.5	0.3	2.5	4.7	-15.1	17.2	8.8	20.7	3.3	0.2	3.4	5.0
7/8/2013	19.0	-	-	4.3	-	1.4	0.2	0.8	-	-	-	-	-	-	-	-	0.0
7/15/2013	37.0	-	-	19.8	-	0.1	0.5	5.9	-	-	-	-	-	-	-	-	0.0
7/19/2013	67.0	58.9	15.4	16.0	7.3	20.3	0.2	2.1	8.1	-43.6	15.3	13.2	25.8	3.2	0.0	3.4	6.7
7/23/2013	23.0	11.0	6.8	6.8	3.0	16.4	0.3	1.7	12.0	6.2	17.2	15.7	21.7	1.9	0.1	0.5	0.6
7/26/2013	73.0	71.5	15.9	19.3	0.5	6.9	0.3	1.9	1.5	-49.0	22.5	2.3	18.5	4.2	0.3	3.9	6.4
8/6/2013	12.0	-	-	2.7	-	1.6	0.2	1.8	-	-	-	-	-	-	-	-	0.0
8/8/2013	3.0	-	-	1.3	-	2.7	0.4	1.1	-	-	-	-	-	-	-	-	0.0
Mean	55.7	62.5	16.6	14.3	4.2	5.7	0.3	2.6	12.9	-28.5	34.0	20.1	28.5	4.1	0.2	3.8	6.3
Standard Error	9.3	8.9	2.7	2.6	0.9	1.6	0.0	0.4	2.8	10.8	8.1	5.7	2.0	0.4	0.0	0.5	1.6

T_p, duration of rainfall; T_{ep}, duration of effective rainfall, which is defined as the time from initial hydrograph rise to the end of contributing rainfall; P_{pk}, rainfall prior to hydrograph peak; P_t, total rainfall; P_{abst}, rainfall prior to initial hydrograph rise; P_{5ant}, rainfall during the five days prior to the event; I, average rainfall intensity; I_{max}, maximum rainfall intensity; T_{r1}, time from first rainfall to initial hydrograph rise; T_{r2}, time from end of rainfall to hydrograph peak; T_r, duration of hydrograph rise; T_{lp}, time from hyetograph centroid to hydrograph peak; T_{lc}, time from hyetograph centroid to hydrograph centroid; T_b, time from initial hydrograph rise to the return to antecedent discharge; q_{ant}, antecedent discharge; q_{pk}, peak discharge; R, runoff; n, the number of rainfall events that make up the summary statistics. Site-specific event values are available in Table S1-S4 of the supplemental information.

Table S4. Event-based rainfall-runoff analyses at WT6

Storm date	T_p (hrs)	T_{ep} (hrs)	P_{pk} (mm)	P_t (mm)	P_{abst} (mm)	P_{5ant} (mm)	I (mm/hr)	I_{max} (mm/hr)	T_{r1} (hrs)	T_{r2} (hrs)	T_r (hrs)	T_{1p} (hrs)	T_{1c} (hrs)	T_b (days)	q_{ant} (L/s)	q_{pk} (L/s)	R (mm)
6/17/2014	52.0	45.0	9.0	9.4	3.4	0.0	0.2	1.9	7.0	-5.4	39.6	28.0	28.3	3.2	0.0	1.5	5.8
6/25/2014	68.0	58.6	8.5	9.5	3.9	1.4	0.1	1.0	9.4	-15.3	43.3	29.3	20.7	2.5	0.2	0.9	2.0
7/1/2014	76.0	52.7	37.3	37.3	9.7	8.1	0.5	6.5	23.3	2.6	55.2	34.7	32.3	3.7	0.0	3.5	11.6
7/11/2014	118.0	110.3	19.2	32.9	6.7	0.8	0.3	2.0	7.7	-92.8	17.5	-3.6	29.2	5.1	0.3	2.7	12.7
7/17/2014	66.0	21.8	16.3	16.3	4.4	15.0	0.2	3.4	44.2	7.8	29.6	25.5	29.0	2.9	0.2	1.9	4.6
7/21/2014	121.0	90.3	23.5	23.5	4.3	17.2	0.2	1.7	30.7	11.2	101.5	71.0	34.8	5.8	0.2	1.5	9.7
7/31/2014	128.0	109.8	28.3	30.7	7.1	0.0	0.2	5.9	18.2	-94.9	14.9	10.6	32.7	4.6	0.4	5.0	16.0
8/18/2014	14.0	-	-	2.2	-	0.1	0.2	0.6	-	-	-	-	-	-	-	-	0.0
6/21/2013	76.0	60.7	9.2	10.4	5.0	0.0	0.1	3.9	15.3	-53.5	7.2	5.7	26.2	3.7	0.1	2.3	5.9
6/29/2013	13.0	-49.9	5.5	5.5	5.5	2.2	0.4	2.2	62.9	57.9	8.0	62.7	61.8	0.6	0.1	0.6	0.5
7/2/2013	37.0	23.4	9.3	9.6	6.4	7.5	0.3	2.5	13.6	-18.6	4.8	5.3	13.9	1.4	0.2	1.4	2.2
7/8/2013	19.0	-	-	4.3	-	1.4	0.2	0.8	-	-	-	-	-	-	-	-	0.0
7/15/2013	37.0	-	-	19.8	-	0.1	0.5	5.9	-	-	-	-	-	-	-	-	0.0
7/19/2013	67.0	61.8	15.2	16.0	4.0	20.3	0.2	2.1	5.3	-47.4	14.3	9.4	24.5	3.4	0.2	2.6	7.0
7/23/2013	23.0	19.2	6.8	6.8	0.4	16.4	0.3	1.7	3.8	6.2	25.3	15.7	19.4	2.6	0.2	0.6	1.4
7/26/2013	73.0	66.2	15.9	19.3	0.8	6.9	0.3	1.9	6.7	-48.4	17.8	2.8	18.8	3.7	0.2	2.4	6.4
8/6/2013	12.0	-	-	2.7	-	1.6	0.2	1.8	-	-	-	-	-	-	-	-	0.0
8/8/2013	3.0	-	-	1.3	-	2.7	0.4	1.1	-	-	-	-	-	-	-	-	0.0
Mean	55.7	51.5	15.7	14.3	4.7	5.7	0.3	2.6	19.1	-22.4	29.2	22.9	28.6	3.3	0.2	2.1	4.8
Standard Error	9.3	11.8	2.6	2.6	0.7	1.6	0.0	0.4	4.9	12.1	7.4	6.3	3.3	0.4	0.0	0.3	1.2

T_p, duration of rainfall; T_{ep}, duration of effective rainfall, which is defined as the time from initial hydrograph rise to the end of contributing rainfall; P_{pk}, rainfall prior to hydrograph peak; P_t, total rainfall; P_{abst}, rainfall prior to initial hydrograph rise; P_{5ant}, rainfall during the five days prior to the event; I, average rainfall intensity; I_{max}, maximum rainfall intensity; T_{r1}, time from first rainfall to initial hydrograph rise; T_{r2}, time from end of rainfall to hydrograph peak; T_r, duration of hydrograph rise; T_{1p}, time from hyetograph centroid to hydrograph peak; T_{1c}, time from hyetograph centroid to hydrograph centroid; T_b, time from initial hydrograph rise to the return to antecedent discharge; q_{ant}, antecedent discharge; q_{pk}, peak discharge; R, runoff; n, the number of rainfall events that make up the summary statistics. Site-specific event values are available in Table S1-S4 of the supplemental information.

Chapter 3: The influence of snow cover, air temperature, and groundwater flow on the active layer thermal regime of Arctic hillslopes drained by water tracks

3.1 Abstract

Permafrost occurs beneath many Arctic watersheds and limits biological activity to a thin, seasonally-thawed active layer beneath the ground surface. Freeze-thaw patterns in this active layer can affect hillslope drainage architecture and hydrologic connectivity to the stream network. This study uses a coupled groundwater flow and heat transport model with freeze-thaw capabilities to examine potential controls on the timing and duration of freeze-thaw conditions and the magnitude of temperature fluctuations within the active layer of Arctic hillslopes and common hillslope drainage features called water tracks. Varying the mean annual air temperatures and the depth and duration of snow cover over the historic range for the study watershed had a stronger effect on the timing and duration of frozen and partially frozen conditions compared to the timing and duration of thaw, and on the mean and minimum annual temperatures compared to the maximum annual temperature. Notably, while the length of the shallow active layer thaw season varied by one month across the full range of scenarios, the shallow active layer never froze in the warmest and deepest snow scenario and fully froze for over seven months in the coldest and shallowest snow scenario. Groundwater flow had a subtle moderating effect on the active layer thermal regime, decreasing summer temperatures and slightly increasing winter temperatures, shifting the first day of thaw and last day of partial freeze later, extending the duration of partial thaw and reducing the duration of thaw and full freezing up to two weeks. The models presented here elucidate key mechanisms driving small-scale variation in the active layer thermal regime of tundra hillslopes under the current climate.

3.2 Introduction

The polar climate of Arctic watersheds causes their structure and function to differ considerably from watersheds in more temperate regions. Water and energy fluxes are extremely seasonal and affected by the presence of continuous permafrost just below the ground surface (Hinzman et al., 1991). Liquid water and the biological activity that depends upon it occur at the surface during the brief summer warm season and in the shallow soils of the seasonally-thawed "active layer" between the surface and permafrost. Thus, the thermal regime and moisture status of the active layer exert a primary control of the distribution, transformations, and flows of water, energy, carbon, and nutrients in Arctic watersheds (e.g., Walvoord and Kurylyk, 2016). Despite their critical importance for ecosystem processes, it remains difficult to predict active layer conditions throughout Arctic watersheds (Jorgenson et al., 2010). Conditions at the ground surface are influenced by seasonal snow cover, vegetation, and topography (e.g., Zhang, 20005). Within the active layer, latent heat exchange associated with freezing and melting of soil water couples hydrological and thermal conditions (e.g., Atchley et al., 2016). Further, as water moves through the active layer along potential gradients, it distributes solutes along with it, which are subject to the successive conditions encountered along the flowpath (Stieglitz et al., 2003).

In Arctic tundra watersheds, the flowpath network extends up the hillslope along zero-order drainage features called water tracks (Hastings et al., 1989; Walker et al., 1989; McNamara et al., 1999). Where present, water tracks affect the delivery of runoff and nutrients from terrestrial hillslopes to downstream aquatic ecosystems (McNamara et al., 1998; Harms and Ludwig, 2016; Rushlow and Godsey, 2017). The active layer conditions of tundra water tracks contrast strongly with those of the hillslope watersheds they drain, and consistently across sites, despite differences in vegetation and watershed structure (Rushlow et al., 2017). Water tracks spend significantly more of the thaw season saturated than the non-track hillslope (Rushlow and Godsey, 2017), thaw

more deeply, experience muted diel and seasonal temperature fluctuations, and are frozen weeks or months and for less time (Rushlow et al., *in prep*). Several factors could explain this consistent spatial patterning in active layer conditions, but the relative roles and interactions of those factors are unclear. For example, since water tracks tend to accumulate more snow and their soils are more saturated than the surrounding hillslope, either greater insulation from cold winter temperature or the release of latent heat by water freezing could cause the active layer of water tracks to experience protracted partially frozen temperatures (Sturm et al., 1997; Matsuoka and Hirakawa, 2000; French, 2013; Rushlow et al., *in prep*).

Numerical models are powerful tools for simulating the effects of complex physical processes under a range of historical or potential conditions. Over the past three decades, numerical models of permafrost watersheds have advanced from simulating vertical heat conduction to fully coupling groundwater flow and heat transport in variably saturated, multi-dimensional environments with freeze-thaw processes (Kane et al., 1991; McKenzie et al., 2013; Karra et al., 2014). Recent studies have demonstrated that groundwater flow can accelerate permafrost degradation over century timescales (McKenzie and Voss, 2013) and cause pulses of soil warming in conjunction with the warming of adjacent shallow water bodies (Sjoberg et al., 2016). The question is no longer whether, but where and when heat advection affects freeze-thaw dynamics and dependent processes in permafrost landscapes (Fritz et al., 2015), and how significant advective heat transport is relative to other intrinsic and extrinsic factors affecting the watershed energy balance. The paucity of such studies and the specificity of the results underscore the need to better understand coupled heat and water flow processes across the diverse range of permafrost landscapes and to ground modeling endeavors with small-scale field observations from well-instrumented watersheds (Walvoord and Kurylyk, 2016).

Here, we use a physically-based numerical model to the simulate the relative effects of snow cover, air temperature, and groundwater redistribution of heat on the active layer thermal regime of Arctic hillslopes. We drive and compare our results with field observations collected in water tracks and the hillslope watersheds they drain. We focused on seasonal dynamics to elucidate the sensitivity of Arctic hillslope active layer to realistic variations in environmental conditions that occur on spatial and temporal scales that are relevant for ecological processes. Based on previous work and field observations, we expected that warmer air temperatures, deeper snow, and increased groundwater flow would warm active layer temperatures and extend the duration of thawed conditions. We used a conduction-only soil column model to (1) examine how observed differences in snowpack thickness and duration between a water track and the adjacent non-track hillslope affect their active layer thermal regimes and (2) explore how interannual variations snowpack and air temperatures affect active layer thermal regime of the hillslope. Further, we used a fully coupled groundwater flow and heat transport model that represented a half-hillslope watershed to (1) determine the relative impact of groundwater flow on the active layer thermal regime throughout a hillslope and (2) define both the long-term and seasonal subsurface volume contributing groundwater flow to the water track.

3.3 Methods

3.3.1 Field Observations

We measured active layer temperatures in a hillslope watershed ("WT6," Harms and Ludwig, 2016; Voytek et al., 2016; Rushlow and Godsey, 2017) in Upper Kuparuk watershed of northern Alaska (Figure 1) from May 24, 2012 through April 22, 2015. At this site and many others across the Arctic, the subsurface consists of a porous and permeable peat mat overlying silty mineral soil and glacial till (e.g., Hinzman et al., 1991; Quinton et al., 2004). Ground temperatures

were measured at depths of 2, 4, 6, 8, 10, 15, 20, 25, 30, and 35 cm using two vertical chains of thermocouples, one inside the water track draining the hillslope watershed and the other 3.5 meters away on the non-track hillslope adjacent to the water track. Temperatures were logged at five-minute intervals from snowmelt through the end of the summer and at 30-minute intervals during the winter using a solar-powered Campbell Scientific CR1000 datalogger complexed to a AM16/32B multiplexer. At the water track thermocouple chain, the water track drains an estimated 0.035 square kilometers of the hillslope, based on analysis of a digital elevation model generated from terrestrial lidar data (Voytek et al., 2016; Rushlow and Godsey, 2017), while the drainage area at the non-track thermocouple profile is less than 10 square meters. Air temperature was measured at half-hourly intervals at an eddy covariance tower on the ridgeline of the adjacent Imnavait Creek watershed operated by the Arctic Observatory Network ("AON," Euskirchen et al., 2012), and deep ground temperatures were measured in a borehole on the ridgeline (Romanovsky, 2017).

Over most of the snow cover season, from initial accumulation to ablation, snow depth was inferred from miniature temperature loggers deployed at several heights above the ground along a vertical stake (Lewkowicz, 2008). When an individual temperature sensor was buried in the snowpack, it recorded muted temperatures relative to temperature sensors exposed to air. Since the loggers were set to record every four hours, abrupt damping in the amplitude of diel temperature fluctuations at lower loggers that coincided with little change at higher loggers were used to infer the onset of the snow cover up to the height of the lower loggers (Rushlow et al., *in prep*). Manual snow depth measurements were also made for two weeks of the spring ablation period near the snow stakes. Together, the manual measurements and temperature sensor information provided daily time series of snow depth on the hillslope and in the water track.

3.3.2 Numerical Modeling

3.3.2.1 Model Overview

We simulated the effects of snow cover, climate warming, and lateral flow on the active layer thermal regime of an Arctic hillslope using a version of SUTRA (Voss and Provost, 2010) that was modified to incorporate freeze-thaw dynamics in groundwater flow and heat transport through porous media (McKenzie et al., 2007). The modified code accounts for the contribution of the latent heat of fusion to the subsurface energy budget as well as the changes in permeability, heat capacity, and thermal conductivity associated with pore water freeze and melt. Since we assumed fully saturated conditions, the porous media consists of two components: solid matrix and pore water. We set the proportion of pore water that is liquid or frozen to vary with temperature from 5% to 100% between -2 and 0°C according to a piecewise linear function. Effective permeability also decreases linearly between 0 and -2°C by six orders of magnitude. The code treats heat capacity and thermal conductivity in each element as a volumetric average of the components (ice, liquid water, or solid matrix). Parameter values are provided in Table 1.

3.3.2.2 Conduction-Only Soil Column Model

The soil column model simulates conductive heat transfer and represents a generalized soil profile at the field site, with peat-rich organic soil overlying a sandy loam (Figure 2B). We used an inverse analytical approach and literature values to characterize the thickness and material properties of each soil layer, since properties were not measured directly in the field. To determine layer thickness, we iteratively solved Fourier's Law for the solid grain thermal conductivity between adjacent pairs of thermocouples in the profile installed on the hillslope. This approach assumes that heat flux is steady through the entire profile for the analysis period, and calculating unique solutions required assuming an effective thermal conductivity at one of the thermocouple

locations. We addressed the first assumption by solving over time windows in which the entire profile was either fully frozen or fully thawed, and the second by assigning an effective thermal conductivity to the lowest pair, which was likely to be mineral soil. We chose the value for the assumed effective thermal conductivity based on the work on Hinzman et al. (1991), who directly measured soil thermal properties in the Imnavait Creek watershed, which is adjacent to the study site and has experienced a nearly identical climatic and glacial history (Hamilton, 1986). The solid grain thermal conductivity for the remaining layers were calculated using the mean temperature at each thermocouple for the analysis period and iteratively varying the porosity. In these solutions, there was a clear break in conductivity values above and below 20 centimeters, and this depth was chosen as the transition between organic and mineral soil properties in our models. There was also a transition between the uppermost layer and the layer beneath it, which we interpreted as an unsaturated zone in the organic soil. These organic and mineral layers were then assigned literature values for the permeability, porosity, heat capacity, and solid grain thermal conductivity (Table 1; Hinzman et al., 1991, Kane et al., 1991, and Quinton et al., 2008).

We used the field observations of air temperature and snow depth described in Section 3.3.1 to assess how well our parameterization of the conduction-only model represented the active layer thermal regimes of the hillslope and water track (Figure 3). A thermal boundary layer was applied to the top of the model, simulating the two-way conduction of heat between the atmosphere and the ground through the snowpack or air (McKenzie and Voss, 2013). The thermal boundary layer had a constant heat transfer coefficient of 1.25 $W/m^2/K$ during the snow-free period (McKenzie and Voss, 2013), and was a function of the effective thermal conductivity of the snowpack divided by the snow depth when snow was present, up to a maximum value of 1.25 $W/m^2/K$. Values for the effective thermal conductivity were based on the multi-year averages

reconstructed using inverse modeling of field data at Franklin Bluffs, AK, a moist tundra site with continuous snow cover measurements (Jafarov et al., 2014). A specified temperature of -3.86°C was applied to the bottom of the model domain based on multi-year observations at 60 m depth within a borehole located on the ridgeline of the field site (Romanovsky, 2017). The model was initialized by running a steady-state simulation with a specified temperature of -1.59°C, the mean 2-cm ground temperature measured in the field in 2013, applied to the top of the model. After initialization, the thermal boundary layer conditions for the water track and hillslope snow depth scenarios were each applied for ten annual cycles to ensure that the model had reached a dynamic steady-state. Since our primary goal was to simulate the temporal dynamics of the active layer thermal regime at the two locations, we qualitatively compared the seasonal progression of the modeled and observed active layer temperatures for the following characteristics: freezing from the surface downwards, prolonged zero curtain temperatures, deep winter cold, rapid warming during snowmelt, and thawing from the surface downwards (e.g., Sturm et al., 2005). Capturing the magnitude of seasonal active layer temperature fluctuations was of secondary importance and assessed by regressing modeled and observed active layer temperatures for a full annual cycle.

The conduction-only model was used for a sensitivity analysis exploring the effects of warming mean annual air temperature and variable snowpack depth and duration on the active layer thermal regime, independent of groundwater flow. A thermal boundary layer was applied to the top of the model using synthetic air temperature and snow depth time series. A sinusoidal daily air temperature time series was generated by fitting the mean monthly air temperatures reported for a long-term monitoring station in the Upper Kuparuk watershed (Kane et al., 2014). The snow depth for the thermal boundary layer was set to increase linearly, beginning on the first fall day with an air temperature less than 0°C and peaking on the last spring day with an air temperature

less than 0°C. Then, to represent meltwater interaction with the ground surface during spring ablation, the air temperature was damped to zero and the heat transfer coefficient was set to 2 $W/m^2/K$ for 3-15 days, scaled linearly to the peak snow depth. Model scenarios reduced the snow cover duration from 240 to 224 days by incrementally warming the mean annual air temperature by 2°C, from -7.7°C to - 5.7°C (Figure 3). At the same time, scenarios varied the peak snow depth from 0.2 to 1.5 m, or approximately 0.5 to 3 times the mean end-of-winter snow depth (0.43±0.1 m) measured at a long-term (26-year record) monitoring location in the Imnavait Creek watershed (Kane et al., 2014). Since the heat transfer coefficient covaries with snow depth and effective thermal conductivity, we did not vary the values for the effective thermal conductivity of the snowpack between scenarios, and instead simply scaled them to the snow cover duration. In this way, the effective thermal conductivity increased linearly from 0.05 to 0.2 W/m/K when the snowpack had reached 75% of its maximum depth, and then remained constant until the period of ablation. For each simulation, we calculated three metrics of the annual active layer thermal regime: (1) the *magnitude* of active layer temperatures, including the minimum, mean, and maximum temperatures, (2) the *timing* of active layer conditions, including the first and last day of thaw and the last day of partially thawed conditions, and (3) the *duration* of frozen, partially frozen, and thawed conditions.

3.3.2.3 Fully Coupled Groundwater Flow and Heat Transport Half-Hillslope Model

The 3-D model fully coupled groundwater flow and heat transport and represented a half-hillslope. This model was used to assess the effect of advection on the active layer thermal regime. The half-hillslope had dimensions analogous to the field site, measuring 500 meters long, 40 meters wide, and 60 meters thick (Figure 1 and 2A). The model domain had a vertical relief of 50 meters, and thus a constant downhill slope of 0.1. The model domain also sloped downward from

the outside lateral edge of the model, representing a groundwater divide, to the inside lateral edge of the model, representing the water track. Elements were 5 meters long and 2 meters wide. The pressure at the top boundary was specified as zero, representing the water table. Hydrostatic pressure was specified at the downslope outlet face and the base, sides, and upslope face were no-flow boundaries. All sides of the model were no-heat flux boundaries. Models were initialized by running 1000-year transient simulation with yearly time steps with a specified temperature of -1.59°C applied to the top of the model. Mean daily 2-cm temperatures measured at the hillslope field location were then applied to the top boundary of the model and repeated for 26 years in order to reach dynamic steady state. Due to data storage and computational constraints associated with the dimensionality of the half-hillslope model, output data was only produced at daily intervals for a subset of observation points, and at monthly time intervals for all elements and nodes. We used the daily outputs to calculate the same three metrics of the thermal regime that were used in the sensitivity analysis at locations on the inside and outside edge of the half-hillslope (Figure 2), which represent the water track and non-track hillslope measurement locations and have large and no contributing areas, respectively. The monthly outputs were used for an initial visually assessment of the model behavior based temperature and pressure distribution within the model (e.g., Figure S1).

We used an additional capture zone analysis (*sensu* Frind et al., 2006) with the half-hillslope model to delineate the contributing areas that are drained by the water track over long timescales and the short thaw season. With heat as a tracer, a specified temperature of 10°C was applied to the "water track" nodes on the inside edge of the half-hillslope model (Figure 2). The sign of gravity was reversed to cause water to flow upslope, opposite the natural direction. Incoming water had a specified temperature of 0°C. Material properties were the same as in the

other experiments, except for (1) the thermal conductivity, which was set to zero such that all heat redistribution within the model was due to water flow, (2) the permeability between 0.18 and 60 m depth was set to 1 x 10^{-19} m^2 to simulate the continuous presence of permafrost, and (3) the dispersivity, which was set to 2 in the longitudinal direction and 0.01 in the transverse direction, to maintain numerical stability. Under these conditions, the capture zone is the simulated volume with a temperature above 0°C. We defined the extent and shape of the long-term and thaw-season capture zones using a steady-state simulation and a 90-day transient simulation, respectively.

3.4 Results and Discussion

3.4.1 Water Track and Hillslope Conductive Heat Transfer Processes

The conduction-only model produced reasonable representations of the annual active layer thermal regime in the water track and on the adjacent hillslope (Figure 4). The fall freeze-up period is well-represented, illustrating the dual role of latent heat exchange and subtle differences in snowpack accumulation in controlling the duration of zero-curtain conditions. Since the simulations represent locations only a few meters apart, and the only difference between the hillslope and water track simulations is the rate of heat transfer through the snowpack, these results highlight the need for measuring and predicting seasonal snowpack characteristics at small spatial and temporal scales to accurately infer active layer dynamics across the snow cover season. Overall, both simulations produced slightly colder active layer temperatures than those observed in the field, with linear regressions between the temperatures at the measured and modeled depths yielding a root mean square error ranging from 2.27-3.86°C and 1.52-1.82°C and adjusted R^2 values ranging from 0.84-0.95 and 0.94-0.95 for the hillslope and water track scenarios, respectively (Figure S2). The mismatch is greater in the summer, particularly at shallow depths on the hillslope. Since the simulations assume saturated conditions and the hillslopes are drier than

the water track in the summer (Rushlow and Godsey, 2017), the effective thermal conductivity in the modeled active layer is typically higher than would be expected at the field site, which would enhance heat conduction. Surface heat transfer processes that are not represented in the model, such as radiative heat transfer and variable shading by vegetation (e.g., Briggs et al., 2014), are therefore more likely than soil properties to explain the discrepancy between the modeled and field observations. Future work on thaw season dynamics should focus on describing the role of these processes in modifying the active layer thermal regime across the landscape.

3.4.2 Sensitivity to Snow Cover and Climate Warming

The sensitivity analysis explores the relative role of climate warming and changing snow cover as measured by shifts in the timing, duration, and magnitude of changes in the active layer thermal regime. The conditions in the sensitivity analysis represent a realistic range for the interannual variation in air temperatures and snow cover, coupled with the microclimatic variations which can occur due to wind redistribution of snow across variable microtopography, as observed within the water tracks at the field site. The results of the four end-member scenarios of the sensitivity analysis show that this experiment encompassed the range of winter active layer conditions, but, similar to the experiments with observed conditions, underestimates the variation in summer (thaw season) temperatures (Figure 5).

As expected, deeper, longer snow cover and warmer air temperatures increases the duration of thaw and partially frozen conditions and decreases the duration of frozen conditions. However, the explored range in snow cover has a stronger effect than the range of mean annual air temperatures. Variations in both drivers have a much stronger effect on the timing and duration of partially frozen and frozen conditions and the mean and minimum annual temperatures than on the timing and duration of thaw and the maximum annual temperatures (Figure 6). As air temperatures

warm and snow cover increases, the number of thawed days at 2 cm depth increases from 83 to 117 per year, the number of partially frozen days increases from 63 to 251 per year, and the number of fully frozen days decreases from 218 to none per year (Figure 6). While increasing the mean annual air temperature by 2°C increases the number of days with air temperatures above freezing in the model scenarios by 16, from 125 days to 141 days (Figure 4), it increases the number of thaw days at 2-cm depth by a range of 20-27 (depending on snow depth), decreases the number of frozen days by 20-141, and increases the number of partially frozen days by 0-119 (Figure 6). In comparison, increasing the maximum snow depth from 0.2 to 1.5 m and the snow cover duration by 15 days, from 224 to 240 days, decreases the number of thaw days by 6-9 (depending on air temperature), increases the number of partially frozen days by 67-186, and decreases the number of frozen days by 74-195 (Figure 6). Our results suggest that the active layer is relatively sensitive to changes in precipitation and temperature during the cold season and relative insensitivity during the thaw season. In years and locations with the deepest snow and warmest winters under the current climate, the active layer may never fully freeze, allowing for year-round movement of water and solutes. Since microbial respiration increases exponentially with soil temperature both above and below freezing (Mikan et al., 2002) and partially frozen conditions have been previously linked to enhanced cold season greenhouse gas emissions (Zona et al., 2016), the substantial shifts in the cold season active layer conditions suggest corresponding variability in greenhouse gas production both interannually and spatially throughout upland tundra watersheds. Further, global models not only project that the Arctic climate will change the most in the winter (Bitanja and Krikken, 2016), but we expect that the active layer thermal regime will be most responsive then as well.

3.4.3 The Role of Groundwater Flow in Altering the Active Layer Thermal Regime

Groundwater flow modestly moderates the active layer thermal regime in the region representing the water track (dark colored lines, Figure 7), relative to the non-track hillslope (light colored lines, Figure 7). At water track observation nodes (Figure 2), groundwater flow cools the maximum temperature in the summer by 0.74-2.67°C and warms the minimum winter temperature by 0.17-0.78°C but has little effect on the mean annual temperature relative to the hillslope observation nodes (Figure 8). The first day of thaw and the last day of partial thaw shifts later by 1-12 and 4-17 days, respectively, at water track locations, while the last day of thaw shifts only a few days later or earlier, or not at all, depending on the depth and distance upslope (Figure 8). Groundwater flow also reduces the duration of thawed and frozen conditions by 1-14 and 1-12 days, respectively, and extends the duration of partially frozen conditions by 5-15 days (Figure 8). The duration of thawed and frozen conditions show significant trends with depth, with the duration of thaw shifting the most in the deep active layer and the duration of frozen conditions shifting the most in the shallow active layer (Figure 8).

The difference in the extent of the long-term and thaw season groundwater capture zones explains the modest effect of groundwater flow on the active layer thermal regime (Figure 9). The thaw season capture zone is a shallow wedge circumscribing the organic soil layers, as dictated by the model parameterization, and extending only a few meters laterally and upslope (Figure 9). The long-term capture zone circumscribes a scoop-shaped region with flowpaths extending tens of meters below ground into deep, low-permeability material and laterally and upslope towards the groundwater divides on the sides and upslope face of the half-hillslope domain. Under the long-term, steady-state conditions, the flow rate through the half-hillslope outlet face (0.13 L/s, equivalent to 0.26 L/s for a full hillslope model) was similar to the mean discharge measured from mid-June through mid-August at the study site in 2013 and 2014 (0.35 L/s and 0.53 L/s,

respectively, Rushlow and Godsey, 2017). Simulated reverse flow through the region upslope of the water track is directed out of half-hillslope, representing return flow and thus the surface water capture zone of the water track. These results suggest that water and solute export during the thaw season from the water track mixes return flow contributions from the region upslope with lateral groundwater contributions from a small contributing area in the shallow soils of the proximal hillslope watershed. Based on the shape of the capture zone simulated here, we expect that meter-scale undulations, such as those associated with tussock-forming sedges typically found on tundra hillslopes (Dingman, 1973), in either the surface or subsurface topography would produce substantial exchange between surface water and shallow groundwater.

3.4.4 Recommendations for Future Investigations

This study used a simple numerical modeling approach for initial evaluation of the controls on the active thermal regime on a permafrost hillslope, and several of the assumptions present fruitful avenues for future work using numerical models:

- All simulations in this study assumed fully saturated conditions in isotropic, non-deformable porous media. Previous work documented variable saturation in both space and time at the study hillslope (Rushlow and Godsey, 2017), and in similar cold-region environments, enhanced flow occurs between tussocks (Dingman, 1973) and through soil pipes (Carey and Woo, 2000). The melting of interstitial ice that accompanies active layer thawing can cause ground deformation on seasonal timescales (Rushlow and Godsey, 2017) and, where ice wedges are present, abrupt ground failures called thermokarst (Bowden et al., 2008).
- The subsurface architecture was assumed to be invariant among the one-dimensional model scenarios and throughout the domain of the three-dimensional model. However, the organic

layer thickness is known to vary significantly across tundra landscapes (Baughman et al., 2015) and was recently found to have a greater effect on active layer thickness than snow thickness (Atchley et al., 2016).

- The hillslope geometry was idealized as a smooth, sloping box. In reality, meter-scale variations in surface topography likely drive the differences in snow accumulation between the water track and hillslope (Sturm et al., 2005) and generate zones of groundwater upwelling and downwelling along the water track flowpath (Voytek et al., 2016).

3.5 Conclusions

This study investigated how snow cover, air temperature, and groundwater flow affects active layer temperatures and freeze-thaw state of two common features in upland permafrost landscapes: a hillslope and the water track that hydrologically connects it to downslope aquatic ecosystems. Soil column simulations using observed differences in snow cover largely explain the contrasting winter thermal regimes of the two locations, but not thaw season dynamics. A generalized sensitivity analysis using the same soil column model shows that realistic spatial and interannual variations in seasonal snow cover and mean annual air temperatures strongly affect the thermal regime of the active layer, modifying the duration and timing of freeze-thaw conditions and the magnitude of seasonal temperature fluctuations. Fully coupling groundwater and heat flow in a three-dimensional half-hillslope domain reveals a modest but moderating year-round effect of groundwater flow on the active layer thermal regime, which has not been noted in previous studies. This study improved understanding of the complex processes underlying spatiotemporal heterogeneity in the active layer, a critical zone of interaction for hydrological and ecological processes. The results also indicate the need for future work investigating the physical basis for Arctic hillslope active layer dynamics should focus on accurate representation of the spatial

variation in summer heat transfer, snow cover (especially spring ablation), and soil moisture across realistic topography.

3.6 Acknowledgements

This work was supported by a Pathfinder Fellowship from the Consortium of Universities for the Advancement of Hydrologic Science, Incorporated and funding from the National Science Foundation's Division of Polar Programs and Division of Environmental Biology award numbers 1259930 and 1026843, the United States Geological Survey Northwest Climate Science Center, the University of Idaho College of Natural Resources McCall Outdoor Science School, and the Idaho State University Geosciences Department. Data from this study are available online in the International Arctic Research Center Data Archive (P.I. Sarah Godsey) and in the UNAVCO TLS Archive (Project U-035). The work presented here would not have been possible without the guidance of Dr. Audrey Sawyer of The Ohio State University and Dr. Cliff Voss of the United States Geological Survey.

3.7 Figures and Tables

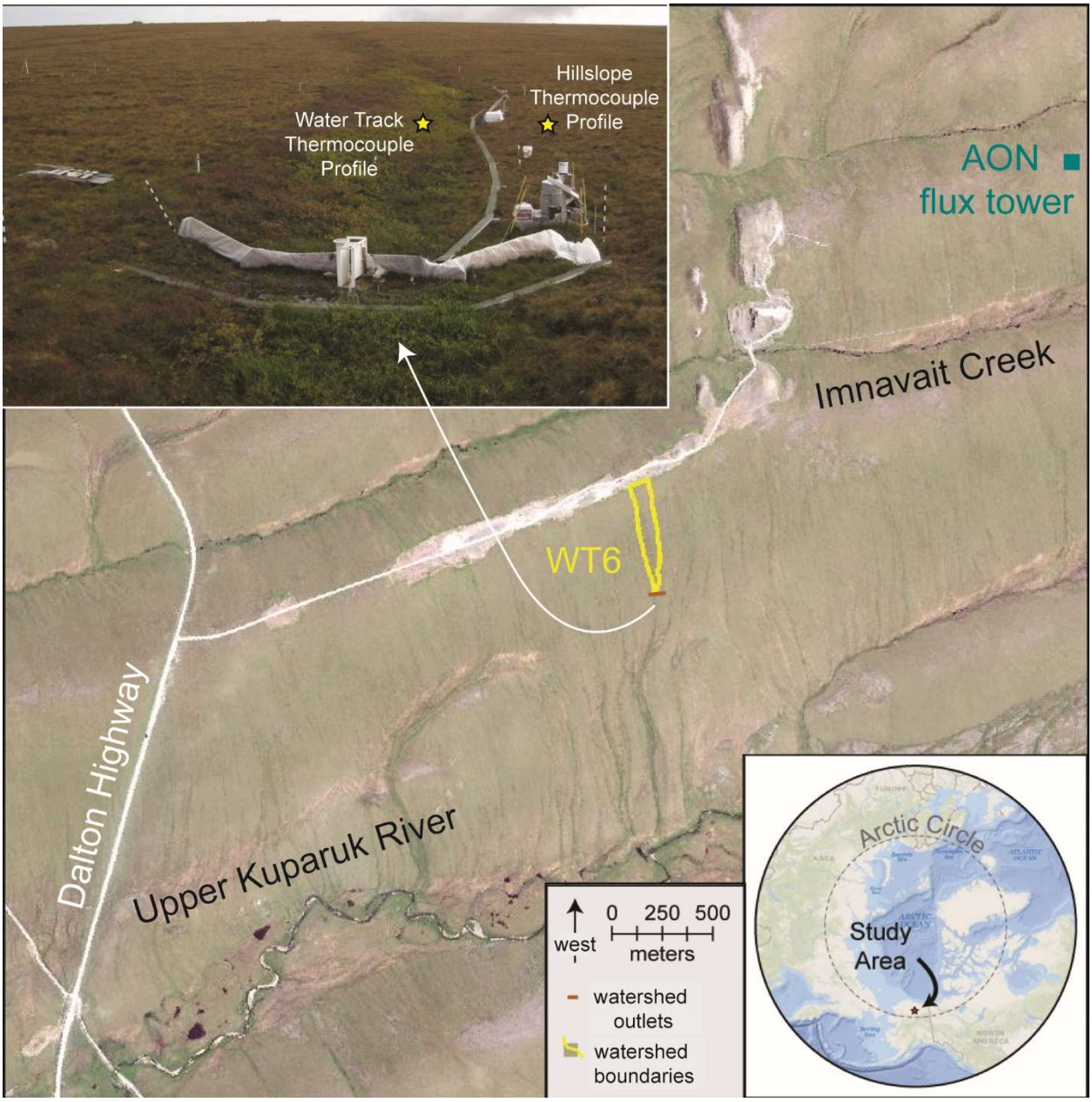

Figure 1. The study area in the central foothills of the North Slope of Alaska. The watershed boundaries of the field site ("WT6") are shown in yellow and a teal square indicates the location of the Arctic Observatory Network ("AON") flux tower where air temperatures were recorded. The lower inset is a polar projection showing the regional location of the study area. The upper inset is a photograph of the field site with the locations of the water track and hillslope thermocouple profiles marked with a yellow star. The photograph was taken in August 2014 by

Dr. Emily Voytek. In it, the water track feature is distinguishable from its hillslope watershed by the brighter green shrubby vegetation relative to the brown-red of the senescing grasses on the surrounding hillslope. Commercial imagery (Copyright 2012, DigitalGlobe, Inc.) obtained courtesy of the Polar Geospatial Center at the University of Minnesota.

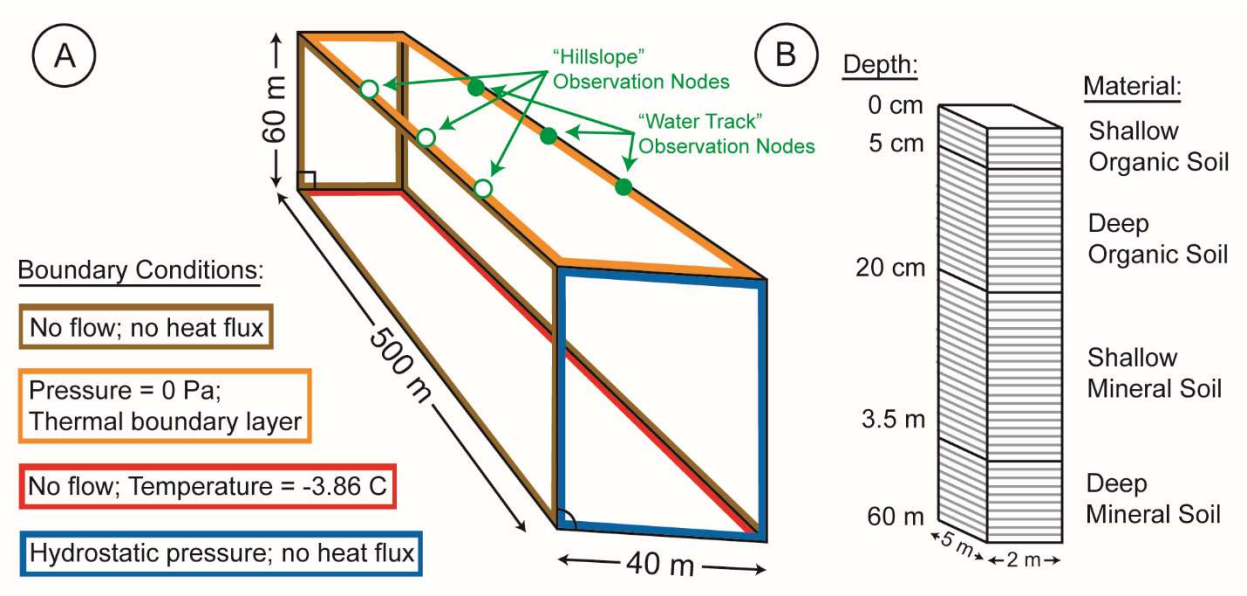

Figure 2. Schematic representations of the (A) half-hillslope model, boundary conditions, and nodes where water track conditions were applied and (B) vertical structure and discretization within both the column and half-hillslope models. Element dimensions shown at the base of the vertical column apply to the half-hillslope model only. Note that these schematic representations are conceptual and not drawn to scale.

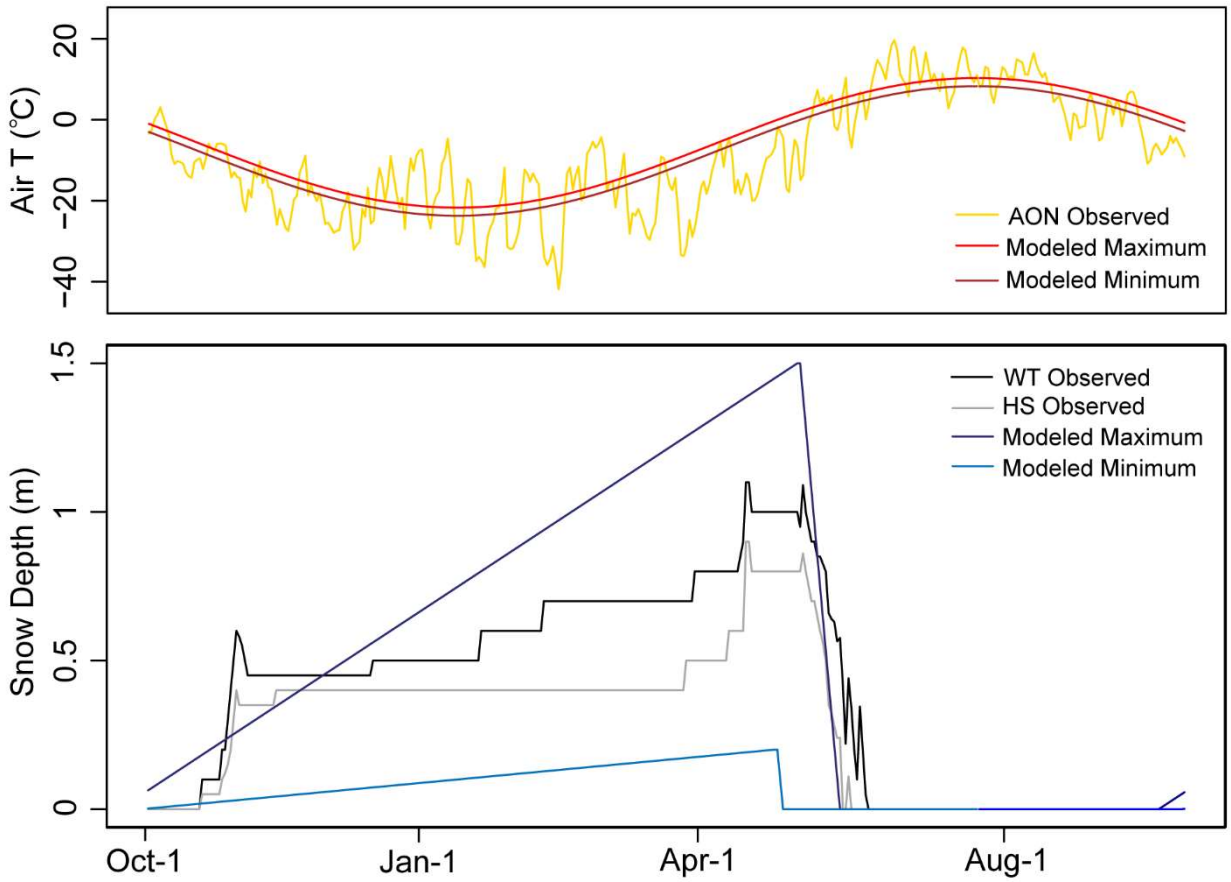

Figure 3. Thermal boundary layer conditions for the conduction-only modeling experiments. The top panel shows the observed mean daily air temperatures from October 1, 2012 through September 30, 2013 ("AON Observed," gold line) and the end-member sinusoidal daily temperature time series used in the sensitivity analysis ("Maximum modeled" and "Minimum Modeled," red lines). The bottom panel shows the inferred daily snow depths in the water track ("WT Observed," black line) and on the adjacent hillslope ("HS Observed," gray line) and the end-member snow depth time series used in the sensitivity analysis ("Maximum Modeled" and "Minimum Modeled," blue lines).

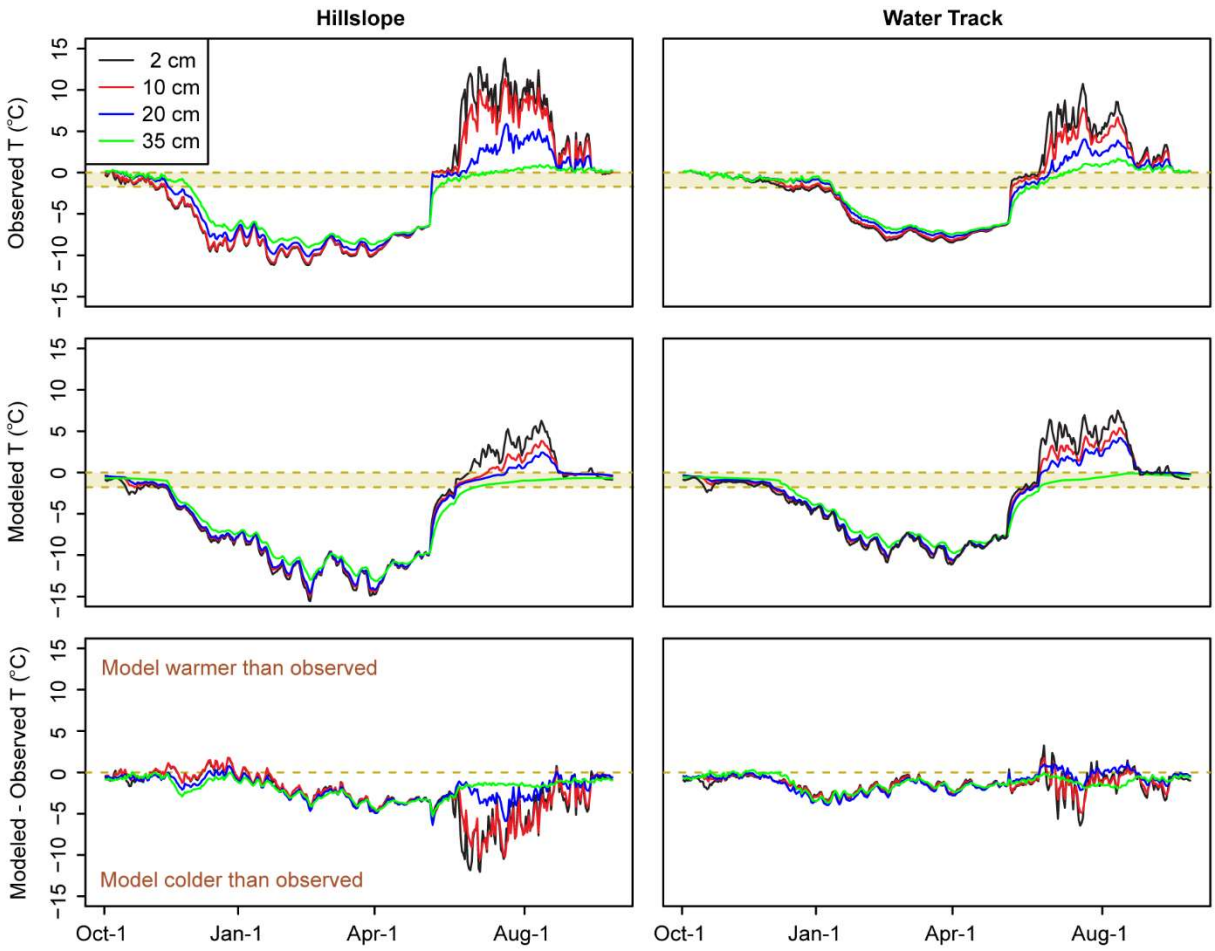

Figure 4. Observed (top) and modeled (middle) ground temperatures at the hillslope (left) and water track (right) field locations, and the difference between the modeled and observed ground temperatures (bottom) through time for four depths below ground: 2 (red), 10 (green), 20 (blue), and 35 (black) cm. The dashed yellow line highlights temperatures or temperature differences of 0 and 2°C, and the light yellow band indicates the zero curtain window and zone of partial freezing.

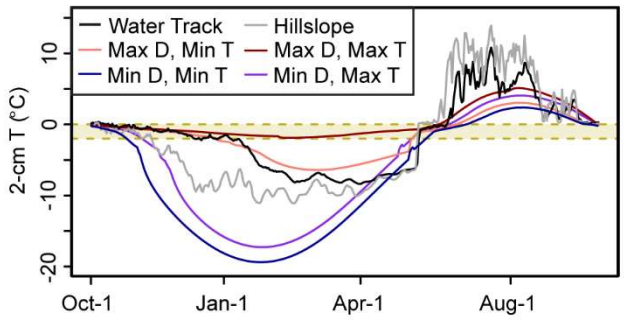

Figure 5. Observed 2-cm ground temperatures in the water track (black line) and on the hillslope (gray line) compared to the four end-member scenarios of the snow cover and climate warming sensitivity analysis. In pink, 1.5 m maximum snow depth ("Max D") and 0°C warming ("Min T"). In red, 1.5 m maximum snow depth ("Max D") and 2°C warming ("Max T"). In blue, 0.2 m maximum snow depth ("Min D") and 0°C warming ("Min T"). In lavender, 0.2 m maximum snow depth ("Min D") and 2°C warming ("Max T").

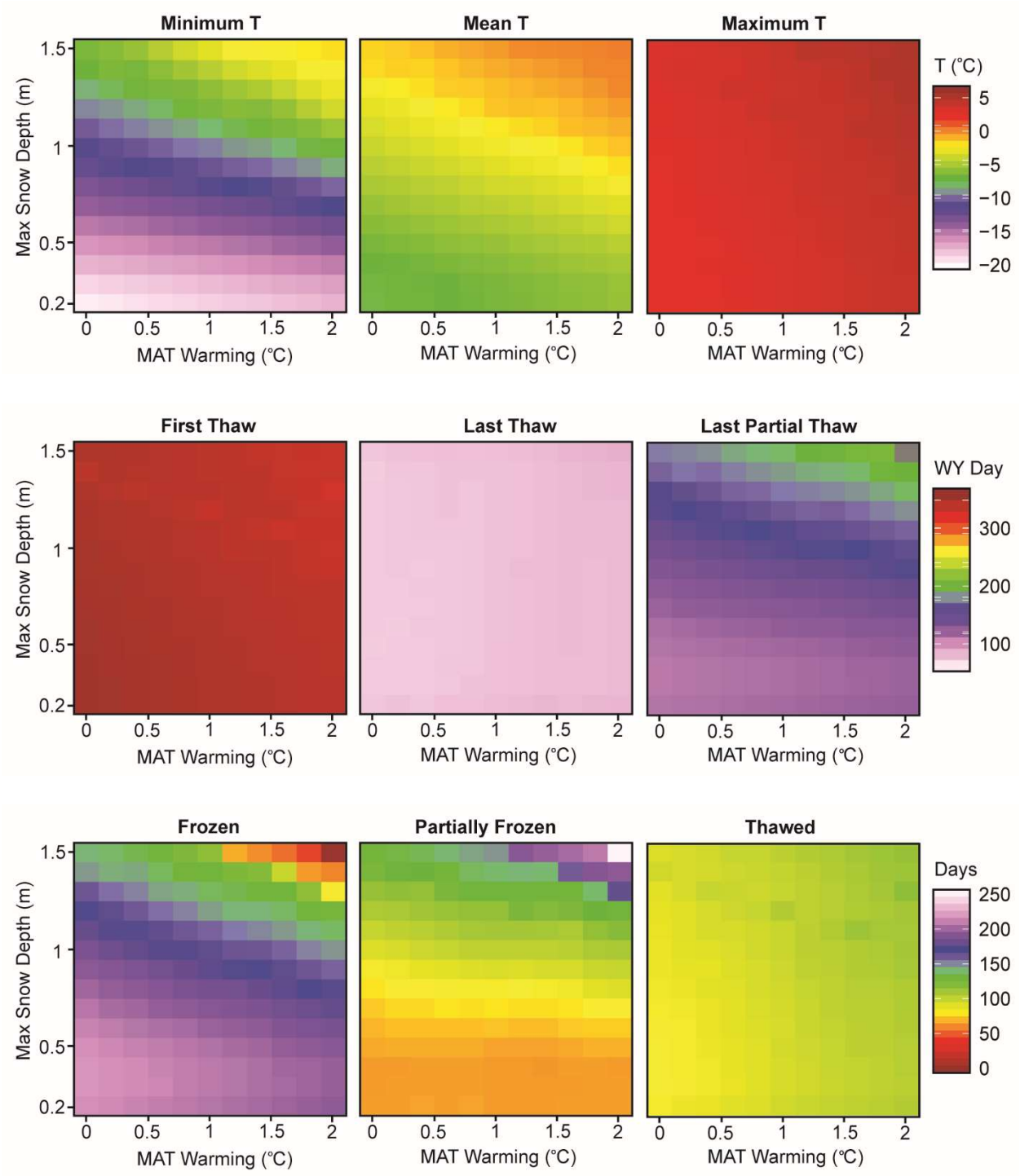

Figure 6. Heat maps of the variation in the minimum, mean, and maximum annual temperatures (top row), the timing of first and last day of thaw and last day of partial thaw (middle row), and the annual duration in days (bottom row) of fully frozen (T < -2°C), partially frozen (-2 < T <

0°C), and thawed (T > 0°C) conditions at a depth of 2 cm in the column model as the mean annual temperature (MAT) is warmed by 0 to 2°C, and the maximum snow depth is increased from 0.2 to 1.5 m. "WY Day" stands for the day of the water year, with day 1 on October 1st.

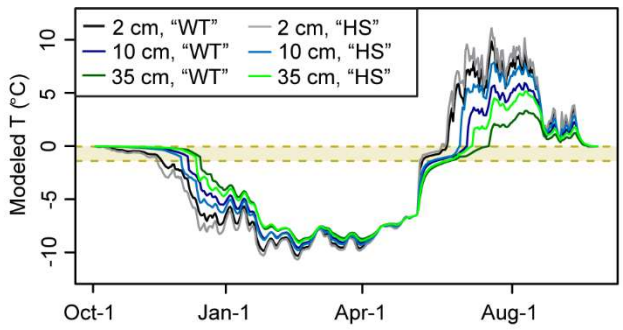

Figure 7. Comparison of daily modeled active layer temperatures at observation nodes with high groundwater flow on the inside "water track" ("WT," dark-colored lines) edge of the half-hillslope model and nodes with no groundwater flow on the outside "hillslope" ("HS", light-colored lines) edge Temperatures at depths of 2 (black/gray), 10 (dark blue/bright blue), and 20 (dark green/bright green) cm are shown. Model observation nodes are 150 m upslope of the model outlet face (Figure 2; circles in Figure 8).

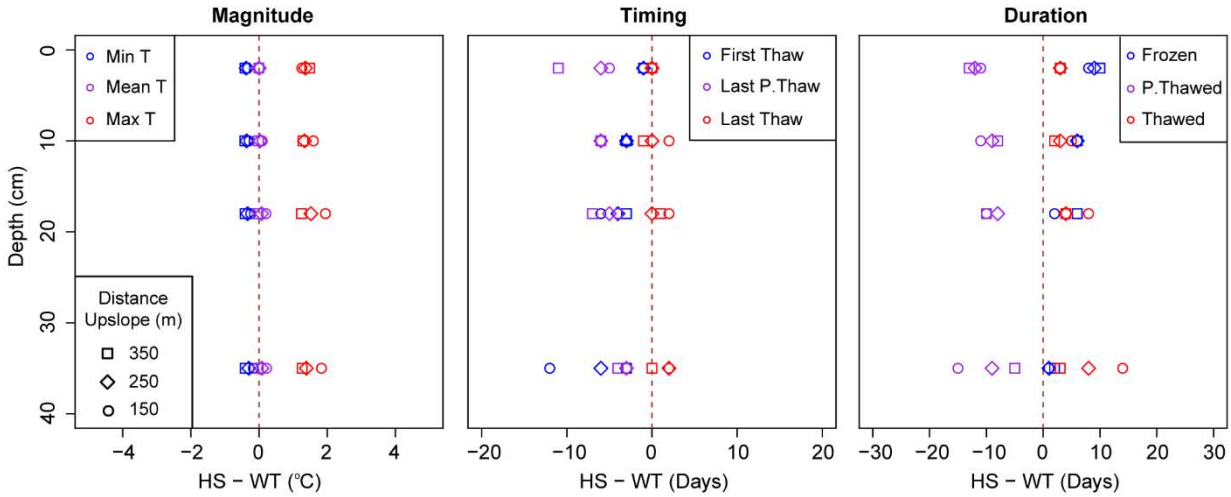

Figure 8. Differences in the three metrics of the active layer thermal regime between observation

locations with no groundwater flow on the outside "hillslope" ("HS") edge of the half-hillslope model and locations with high groundwater flow on the inside "water track" ("WT") edge (Figure 2) with depth (y-axis) and distance upslope from the model outlet face (symbol shape, bottom left inset). The left plot shows the magnitude of the difference in minimum annual temperature (blue symbols, "Min T"), mean annual temperature (purple symbols, "Mean T"), and maximum annual temperature (red symbols, "Max T"). The middle plot shows the difference in the timing of the first day of thaw (blue symbols, "First Thaw"), last day of partially frozen conditions (purple symbols, "Last P. Frozen"), and last day of thaw (red symbols, "Last Thaw"). The right plot shows the difference in the annual duration in days of frozen conditions (blue symbols, "Frozen"), partially frozen conditions (purple symbols, "P. Frozen"), and thawed conditions (red symbols, "Thawed") between hillslope and water track. The dashed line indicates the position in each plot where there is no difference between hillslope and water track locations for a particular metric, depth, and distance upslope.

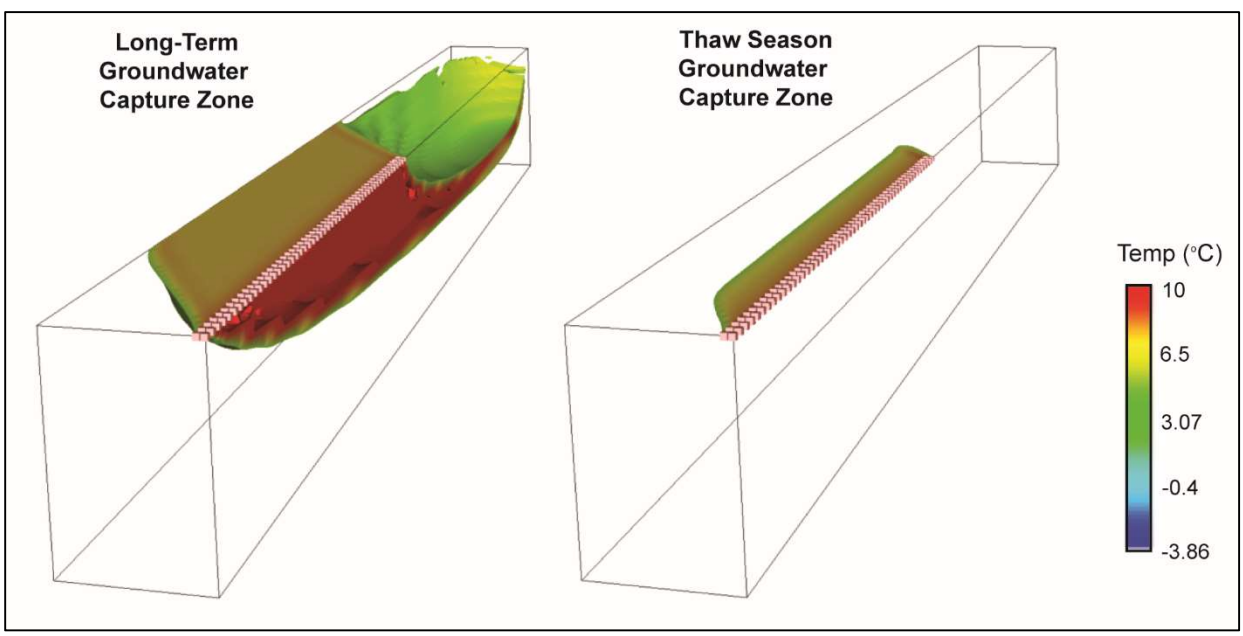

Figure 9. Shape and extent of the full (steady-state) water track capture zone (left) and of a 90-day thaw-season water track capture zone (right). Black lines outline the half-hillslope model domain and the small pink boxes at the top of the model indicate the positions of the "water track" nodes where the heat tracer was applied for both experiments (see Section 3.3.2.3 for methodological details). Note that for this reverse flow capture zone simulation, the temperature is used only as a flow-envelope tracer and does not indicate anything about the thermal regime. Regions with simulated temperatures less than 5°C are not shown to better visualize the capture zone.

Table 1. Model parameters

Parameter	Value
Freezing Function	
Type	piecewise linear
Minimum liquid saturation (unitless)	0.05
Temperature of minimum liquid saturation (°C)	-2
Temperature of maximum liquid saturation (°C)	0
Permeability of frozen regions (m^2)	$1x10^{-6}$
Ice	
Specific heat (J/kg)	2108
Thermal conductivity (J/s/m/°C)	2.18
Liquid water	
Specific heat (J/kg)	4182
Thermal conductivity (J/s/m/°C)	0.58
Upper organic layer	
Specific heat (J/kg)	1920
Thermal conductivity (J/s/m/°C)	3
Porosity (unitless)	0.9
Permeability (m^2)	$1x10^{-11}$
Lower organic layer	
Specific heat (J/kg)	1920
Thermal conductivity (J/s/m/°C)	0.25
Porosity (unitless)	0.9
Vertical permeability of peat (m^2)	$1x10^{-11}$
Mineral soil layers	
Specific heat (J/kg)	890
Thermal conductivity (J/s/m/°C)	2.77
Porosity (unitless)	0.56
Permeability (m^2)	$1x10^{-13}$

3.8 References

Atchley, A. L., Coon, E. T., Painter, S. L., Harp, D. R., & Wilson, C., (2016), Influences and interactions of inundation, peat, and snow on active layer thickness, *Geophysical Research Letters, 43(10),* 5116-6123, doi.org/10.1002/2016GL068550.

Baughman, C. A., Mann, D. H., Verbyla, D. L., & Kunz, M. L., (2015), Soil surface organic layers in Arctic Alaska: Spatial distribution, rates of formation, and microclimatic effects, *Journal of Geophysical Research: Biogeosciences, 120*, 1150-1164, doi:10.1002/2015JG002983.

Bitanja, R., & Krikken, F., (2016). Magnitude and pattern of Arctic warming governed by the seasonality of radiative forcing, *Nature, 6(38287),* doi: 10.1038/srep38287.

Bowden, W.B., Gooseff, M.N., Balser, A., Green, A., Peterson, B.J.. 2008. Sediment and nutrient delivery from thermokarst features in the foothills of the North Slope, Alaska: Potential impacts on headwater stream ecosystems. *Journal of Geophysical Research 113(G02026).* doi:10.1029/2007JG000470.

Briggs, M. A., M. A. Walvoord, J. M. McKenzie, C. I. Voss, F. D. Day-Lewis, & J. W. Lane (2014), New permafrost is forming around shrinking Arctic lakes, but will it last?, *Geophysical Research Letters, 41*, 1585–1592, doi:10.1002/2014GL059251.

Carey, S.K., & Woo, (2000). The role of soil pipe flow as a slope runoff mechanism, Subarctic Yukon, Canada. *Journal of Hydrology*, *233,* 206-222.

Dingman, S.L., (1973). Effects of permafrost on stream flow characteristics in the discontinuous permafrost zone of central Alaska. Presented at the 2nd International Conference on Permafrost, National Academy of Sciences, Yakutsk, Siberia.

Euskirchen, E. S., Bret-Harte, M. S., Scott, G. J., Edgar, C., & Shaver, G. R. (2012). Seasonal patterns of carbon dioxide and water fluxes three representative tundra ecosystems in northern Alaska. *Ecosphere, 3(1)*, 4.

Frind, E.O., Molson, J.W., Rudolph, D.L., (2006). Well vulnerability: A quantitative approach for source water protection. *Ground Water, 44(5)*, 732-742.

Fritz, M., Deshpande, B.N., Bouchard, F., Hogstrom, E., Malenfant-Lepage, J., Morgenstern, A., Nieuwendam, A., Oliva, M., Paquette, M., Rudy, A.C.A., Siewert, M.B., Sjoberg, Y., & Weedge, S., (2015). Future avenues for permafrost science from the perspective of early career researchers. *The Cryosphere, 9,* 1715-1720.

Hamilton, T. D., & Walker, D. A. (2003). Glacial geology of Toolik Lake and the Upper Kuparuk River region. In Alaska Geobotany Center, Institute of Arctic Biology (pp. 24). Fairbanks, AK: University of Alaska–Fairbanks.

Harms, T. K., & Ludwig, S. M. (2016). Retention and removal of nitrogen and phosphorus in saturated soils of arctic hillslopes. *Biogeochemistry, 127(2)*, 291–304. doi: 10.1007/s10533-016-0181-0.

Hastings, S.J., Luchessa, S.A., Oechel, W.C., & Tenhunen, J.D., (1989), Standing biomass and production in water drainages of the foothills of the Philip Smith Mountains, Alaska, *Holarctic Ecology, 12(3)*, 304-311.

Hsieh, P.A., and Winston, R.B., 2002, User's Guide To Model Viewer, A Program For Three-Dimensional Visualization of Ground-water Model Results: U.S. Geological Survey Open-File Report 02-106, 18 p.

Hinzman, L. D., Kane, D. L., Gieck, R. E., & Everett, K. R. (1991). Hydrologic and thermal properties of the active layer in the Alaskan Arctic. *Cold Regions Science and Technology, 19*, 95-110.

Hinzman, L., N. Bettez, W. Bolton, F. Chapin, M. Dyugerov, C. Fastie, B. Griffith, R. Hollister, A. Hope, H. Huntington, A. Jensen, G. Jia, T. Jorgenson, D. Kane, D. Klein, G. Kofinas, A. Lynch, A. Lloyd, A McGuire, F. Nelson, W. Oechel, T. Osterkamp, C. Racine, V. Romanovsky, R. Stone, D. Stow, M. Sturm, C. Tweedie, G. Vourlitis, M. Walker, D. Walker, P. Webber, J. Welker, K. Winker, & K. Yoshikawa (2005). Evidence and implications of recent climate change in northern Alaska and other Arctic regions. *Climate Change 72*, 251-298.

Jafarov, E.E., Nicolsky, D.J., Romanovsky, V.E., Walsh, J.E., Panda, S.K., Serreze, M.C., (2014). The effect of snow: how to better model ground surface temperatures. *Cold Regions Science and Technology, 102,* 63-77.

Jorgenson, M. T., Romanovsky, V., Harden, J., Shur, Y., O'Donnell, J., Schuur, E. A. G., Kanevskiy, M., & Marchenko, S., (2010), Resilience and vulnerability of permafrost to climate change. *Canadian Journal of Forest Resources 40*, 1219-1236.

Kane, D.L., Hinzman, L.D., Benson, C.S., & Liston, G.E., (1991). Snowhydrology of a headwater arctic basin 1. Physical measurements and process studies. *Water Resources Research, 27(6)*, 1099-1109.

Kane, D. L., Youcha, E. K., Stuefer, S. L., Myerchin-Tape, G., Lamb, E., Homan, J. W., … Toniolo, H. (2014). Hydrology and meteorology of central Alaskan Arctic: Data collection and analysis, final report, Report INE/WERC 14.05(pp. 168). Fairbanks, Alaska: University of Alaska Fairbanks, Water and Environmental Research Center.

Karra, S., Painter, S.L., & Lichtner, P.C., (2014). Three-phase numerical model for subsurface hydrology in permafrost-affected regions (PLFOTRAN-ICE v1.0). *The Cryosphere, 8*, 1935-1950. Doi: 105194/tc-8-1935/2014/.

Lewkowicz, A.G., (2008), Evaluation of miniature temperature-loggers to monitor snowpack evolution at mountain permafrost sites, Northwestern Canada, Permafrost and Periglacial Processes, 19, 323-331.

McKenzie, J. M., C. I. Voss, and D. I. Siegel (2007), Groundwater flow with energy transport and water–ice phase change: Numerical simulations, benchmarks, and application to freezing in peat bogs, *Advances in Water Resources, 30*, 966–983, doi:10.1016/j.advwatres.2006.08.008.

McKenzie, J.M., & Voss, C.I., 2013; Permafrost thaw in a nested groundwater-flow system. *Hydrogeology,* doi: 10.1007/s10040-012-0942-3.

McNamara, J. P., Kane, D. L., Hinzman, L. D., (1998). An analysis of streamflow hydrology in the Kuparuk River Basin, Arctic Alaska: a nested watershed approach. *Journal of Hydrology, 206,* 39-57.

McNamara, J. P., Kane, D. L., & Hinzman, L. D. (1999). An analysis of an arctic channel network using a digital elevation model. *Geomorphology, 29*, 339–353.

Mikan, C.J., Schimel, J.P., Doyle, A.P., (2002), Temperature controls of microbial respiration in arctic tundra soils above and below freezing. *Soil Biology & Biochemistry, 34,* 1785-1795.

Quinton, W.L., Carey, S.K., & Goeller, N.T. (2004). Snowmelt runoff from northern alpine tundra hillslopes: major processes and methods of simulation. *Hydrology and Earth System Science, 8(5),* 877-890.

Quinton, W.L, Hayashi, M., & Carey, S.K., (2008). Peat hydraulic conductivity in cold regions and its relation to pore size and geometry. *Hydrological Processes, 22,* 2829–2837. doi: 10.1002/hyp.7027.

Romanovsky, V.E., Smith, S.L., & Christianson, H.H., (2010). Permafrost thermal state in the polar Northern Hemisphere during the international polar year 2007-2009: a synthesis. *Permafrost and Periglacial Processes, 21*, 106-116, doi: 10.1002/ppp.689.

Romanovsky, V., (2017), Data & Maps. Permafrost Laboratory. URL: http://permafrost.gi.alaska.edu/content/data-and-maps. Accessed October 7, 2017.

Rushlow, C.R., & Godsey, S.E., (2017), Rainfall-runoff responses on Arctic hillslopes underlain by continuous permafrost, North Slope, Alaska, USA, *Hydrological Processes, 31,* 4092-4106. doi: 10.1002/hyp.11294.

Rushlow, C.R., Godsey, S.E., & Harms, T.K., (*in prep*), Seasonal patterns and controls on the active layer thermal regime of Arctic hillslopes.

Sjoberg, Y., Coon, E., Sannel, B.K., Pannetier, R., Harp, D., Frampton, A., Painter, S.L., & Lyon, S.W., (2016). Thermal effects of groundwater flow through subarctic fens: A case study based on field observations and numerical modeling. *Water Resources Research, 52,* 1591–1606, doi:10.1002/2015WR017571.

Stieglitz, M., Shaman, J., McNamara, J., Engel, V., Shanley, J., & Kling, G.W. (2003). An approach to understanding hydrologic connectivity on the hillslope and the implications for nutrient transport. *Global Biogeochemical Cycles, 17(4),* 1105. doi: 10.1029/2003GB002041.

Sturm, M., Schimel, J., Michaelson, G., Welker, J.M., Oberbauer, S.F., Liston, G.E., Fahnestock, J., & Romanovsky, V.E., (2005), Winter biological processes could help convert arctic tundra to shrubland, *BioScience, 55(1),* 17-26.

Voss C. I., and A. M. Provost (2010), SUTRA: A Model for Saturated-Unsaturated Variable-Density Ground-Water Flow with Solute or Energy Transport, Water Investigations Report 02-4231, U.S. Geological Survey, Reston, Virginia.

Voytek, E.B., Rushlow, C.R., Godsey, S.E., Singha, K. (2016). Identifying hydrologic flowpaths on arctic hillslopes using electrical resistivity and self potential. Geophysics 81(1): WA225–WA232.

Walker, D.A., Binnian, E., Evans, B.M., Lederer, N.D., Nordstrand, E., & Webber, P.J., (1989). Terrain, vegetation and landscape evolution of the R4D research site, Brooks Range Foothills, Alaska. *Ecography. 12,* 238–261. doi: 10.1111/j.1600-0587.1989.tb00844.x.

Walvoord, M. A., & Kurylyk, B. L. (2016). Hydrologic impacts of thawing permafrost- A review. *Vadose Zone Journal, 15(6),* doi:10.2136/vzj2016.01.0010.

Zhang, T., (2005). Influence of the seasonal snow cover on the ground thermal regime: An overview. *Reviews in Geophysics, 43,* RG4002, doi: 10.1029/2004RG000157.

Zona, D., Gioli, B., Commane, R., Lindaas, J., Wofsy, S. C., Miller, C. E., Dinardo, S. J., Dengel, S., Sweeney, C., Karion, A., Chang, R.Y.-W., Henderson, J. M., Murphy, P. C., Goodrich, J. P., Moreaux, V., Liljedahl, A., Watts, J. D., Kimball, J. S., Lipson, D. A., & Oechel, W. C., (2016). Cold season emissions dominate the Arctic tundra methane budget, *Proceedings of the National Academy of Sciences of the USA*, *113,* 40–45. doi: 10.1073/pnas.1516017113

3.9 Supplemental Figure

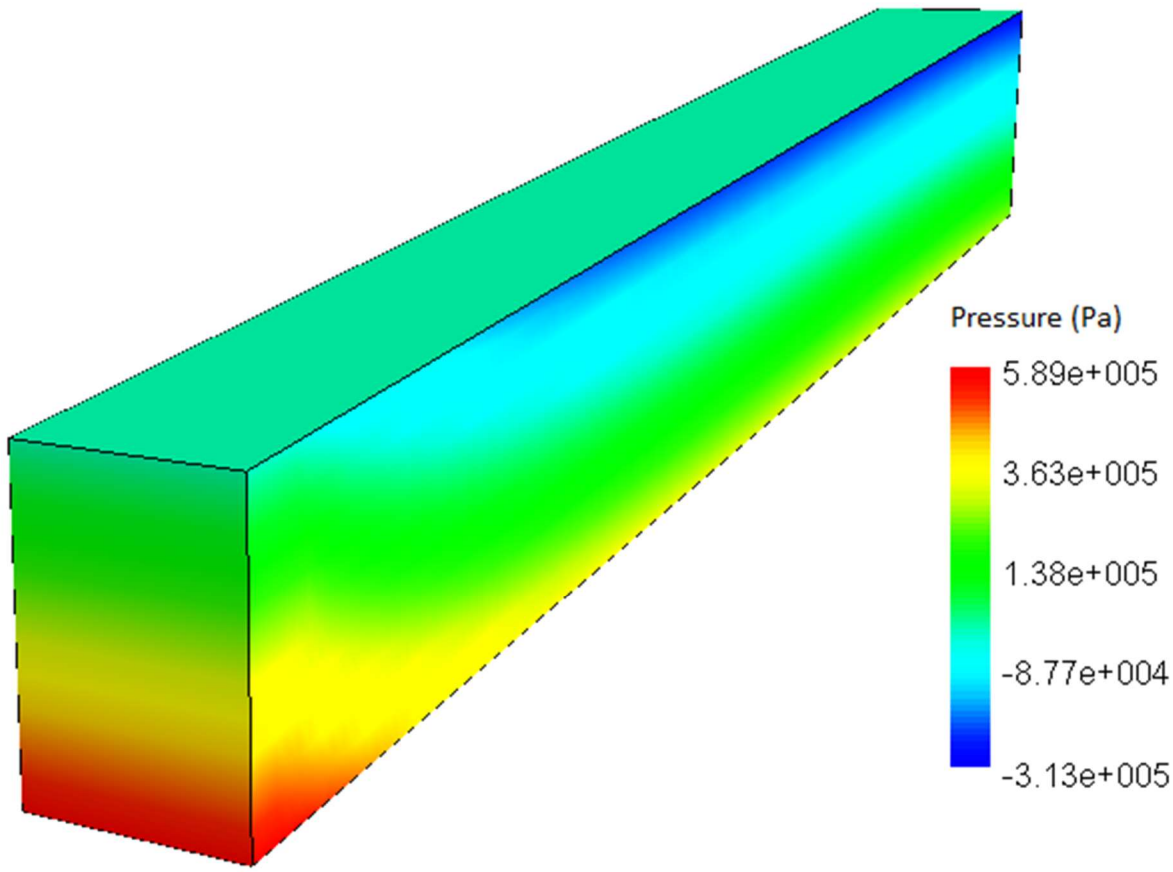

Figure S1. An example of the pressure distribution within the half-hillslope model from the simulated date of July 29th as viewed in the USGS program ModelViewer (Hsieh and Winston, 2002). Red represents zones of high pressure and blue represents zones of low pressure and pressure is in units of Pascals.

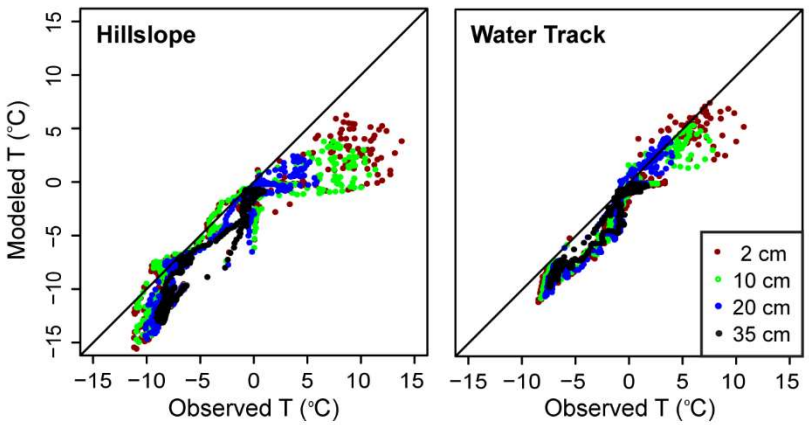

Figure S2. Correlation between observed and modeled active layer temperatures at 2 (dark red), 10 (green), 20 (blue), and 35 cm (black) below ground for the experiment using field observations as the boundary conditions for the column model.

Chapter 4: Seasonal patterns and controls on the active layer thermal regime of Arctic hillslopes

4.1 Abstract

The Arctic climate is warming most rapidly in the fall and winter, but hydrological and ecological processes are best understood in the summer. In upland Arctic watersheds, zero-order stream-like features called water tracks drain water from hillslopes to streams and lakes through the shallow soils of the active layer. Little is known about this hydrologic connection between terrestrial and aquatic ecosystems outside of the thaw season. To address this knowledge gap, we monitored the snow cover, air, and ground temperatures year-round in six tundra water track features and their adjacent hillslopes, focusing on the active layer thermal regime since the freeze and thaw of soil exerts a primary control on hydrological and biogeochemical fluxes. The active layer thermal regimes of the water tracks differed significantly from the hillslopes, and in a consistent way between sites despite variations in watershed topography and vegetation. The water track active layers were thicker, had damped diel and seasonal temperature fluctuations, and were fully frozen for much less of the year. Further, the seasonal timing of thawing and freezing was delayed by days to months, respectively, in the water tracks relative to the hillslopes. A deeper snowpack, warmer mean seasonal air temperatures, and water track features were significant predictors of the delayed freeze-up and warmer winter and spring active layer temperatures, but contrary to our expectations, feature type and air temperature had a stronger influence than snowpack thickness. These relationships support the hypothesis that the spatial and seasonal patterns in the active layer thermal regime of water tracks are strongly controlled by the latent heat effects associated with persistently high soil moisture. The observed seasonal patterns and controls on the active layer thermal regime of tundra water tracks and the hillslopes they drain suggest divergent ecological

processes and responses to future climate change between these features that are not represented in current models of upland Arctic landscapes.

4.2 Introduction

Permafrost is currently widespread in the Arctic, inhibiting groundwater flow except through the active layer: shallow soils that freeze and thaw annually (e.g., Walvoord et al., 2016). Thus, the thermal regime of the active layer, including both its temperature and freeze-thaw state, exerts a primary influence over the fluxes of water, nutrients, and carbon through terrestrial Arctic ecosystems. However, the climate of the Arctic is rapidly warming, reducing the spatial and seasonal extent of frozen ground (IPCC, 2014). Thawing this previously frozen ground will not only alter the distribution and cycling of water in Arctic landscapes (e.g., Rawlins et al., 2010), but it will also make an organic carbon reservoir more than twice that contained in the atmosphere available for microbial decomposition (Tarnocai et al., 2009). It is likely that the resulting carbon emissions will accelerate climate change globally (Schuur et al., 2008). Despite recognition of regional and global impacts, it remains challenging to predict the susceptibility of frozen ground to thaw across the Arctic landscape, because the seasonal snowpack and soil properties interact over small spatial scales to control ground heat fluxes (Hinzman and Kane, 1992; Jorgenson et al., 2009).

The seasonal snowpack mediates heat transfer between the atmosphere and the ground surface (Sturm et al., 1997). While air temperature tends to vary over large spatial scales, substantial differences in the thickness and thermal conductivity of the snowpack can naturally occur over the space of a few meters (Taras et al., 2002). The tundra snowpack lasts for six to nine months of the year and is drier than taiga or maritime snow, making it especially susceptible to wind redistribution, drifting, and accumulation in microtopographic lows (Benson and Sturm,

1993; Wainwright et al., 2017). As the snowpack thickens, it insulates the ground from the atmosphere, and winter air and ground temperature regimes can become effectively decoupled (Taras et al., 2002). Thus, interannual variations in snow cover can have as strong of an effect on ground temperatures as variation in winter temperatures, and the snowpack can either enhance or dampen the effect of a warmer winter climate on ground temperatures (Stieglitz et al., 2003). Several snowpack manipulation studies have demonstrated that when all other factors are equal, locations with a thicker, longer duration snowpack have significantly warmer winter soil temperatures (Lafreniere et al., 2012; Schimel et al., 2004; Walker et al., 1999). Expected increases in winter precipitation associated with climate warming may increase extremes in snowpack thickness and duration in the near-term (Bokhorst et al., 2016), but by the end of the century, the Arctic precipitation regime is likely to be rain-dominated (Bitanja and Andry, 2017).

A warming atmosphere and spatiotemporal variation in snow cover strongly affect the active layer thermal regime (Stieglitz et al., 2003), but it is also subject to intrinsic factors. Soils freeze and thaw at different rates depending on the thermal properties and proportions of their constituent components, which can be generalized as solid grains and interstitial ice, water, or air. For example, the thermal conductivity of peat, which typifies the upper soil profile of tundra landscapes, increases by an order of magnitude if the peat transitions from a dry, thawed state to saturated, thawed state, and then quadruples again if it freezes (French, 2013). As ground temperatures fall below freezing, interstitial ice forms and retards the flow of water through the soil. However, water near the surface of soil particles is held in tension and remains unfrozen at temperatures several degrees below freezing (Romanovsky and Osterkamp, 2000). This residual water content can account for more than half of the dry soil weight, and although the amount decreases with decreasing temperature, particle surface area, and solute content (French, 2013), its

presence allows microbial activity to continue over winter in below-freezing Arctic soils (Zimov et al., 1996; Oechel et al., 1997). The freezing of water also releases latent heat, which can cause soils to linger at "zero curtain" temperatures of 0 to -2 °C (Matsuoka and Hirakawa, 2000; French, 2013). Persistent zero curtain conditions during the fall have been linked to high methane emissions from the Arctic tundra, with higher fluxes coming from the dry uplands rather than inundated sites on the coastal plain (Zona et al., 2016). The underlying driver of this disparity is unclear, because the limited observation number of stations do not adequately capture the heterogeneity present in tundra landscapes (Euskirchen et al., 2017).

Upland tundra landscapes in northern Alaska contain a dense network of zero-order flowpath features called water tracks (Walker et al., 1989; McNamara et al., 1999). Water tracks have also been described in the polar deserts of the Canadian High Arctic (Paquette et al., 2017), the McMurdo Dry Valleys, Antarctica (Levy et al., 2011), and are comparable to recurring slope linae on Mars (Levy et al., 2014). The unifying characteristics of water tracks in the three regions are hydrological: they are zones of high soil moisture that preferentially route water downslope through groundwater flow in the active layer (Levy, 2014). Thus, water tracks function as key hydrologic flowpaths connecting terrestrial and aquatic ecosystems, yet important gaps remain in our understanding of the seasonal extent and controls on hydrologic connectivity in water tracks. In the summer, rainfall generates runoff from water tracks when the soil water storage capacity is exceeded (Rushlow and Godsey, 2017). Water tracks remain internally connected because of their high soil moisture content, but are often hydrologically disconnected from the surrounding hillslope, which dries out rapidly between storms (Stieglitz et al., 2003; Rushlow and Godsey, 2017). Nothing is known about water track active layer conditions outside of the thaw season. Higher soil water content in water tracks may delay freezing in the fall by releasing more latent

heat, which in turn would cause zero curtain conditions to persist longer, resulting in warmer winter temperatures than those of the drier soils on the hillslope, which may fully freeze more rapidly. Conversely, once water track soils are fully frozen, higher frozen water content would make them more thermally conductive, potentially resulting in colder late winter temperatures than hillslope soils. Heat transfer between soils and the atmosphere is in turn moderated by the effective thermal conductivity of the snowpack. Thicker snowpack accumulation in water tracks due to topographic depressions (McNamara et al., 1999) and emergent shrubby vegetation (Liston et al., 2002) likely buffers soils from cold winter air temperatures, but may also delay interaction between soils and warm air temperatures and solar radiation during snowmelt. The consequences of the thermal properties of water and the snowpack for the active layer thermal regime may vary from year to year, depending on the amount and pattern of precipitation, or from site to site, depending on localized watershed characteristics such as soil drainage rates and varying potential for topographic depressions or emergent vegetation to capture snow.

The aims of this study are thus to (1) characterize the active layer thermal regime in water tracks relative to the hillslopes they drain through multiple years and (2) compare the seasonal characteristics of the active layer thermal regime to potential extrinsic and intrinsic controls, including snowpack thickness, air temperature, and feature type, the latter an analog for soil moisture. Since the active layer thermal regime exerts a primary control on the rates of hydrological and biogeochemical processes in permafrost regions, describing these characteristics and relationships is critical for predicting how tundra hillslopes, water tracks, and downslope ecosystems will respond to expected changes in Arctic climate.

4.3 Study Sites

Field data were collected in the foothills region of the North Slope of Alaska. Six water tracks and their adjacent non-track hillslopes were selected for study at locations within the Upper Kuparuk River watershed (Figure 1), which is underlain by continuous permafrost and glacial deposits of the Sagavanirktok River glaciation (Hamilton and Walker, 2003). Near the watershed outlet, a meteorological station installed in 1994 has measured a mean annual air temperature of -8.8°C and rainfall of 21.7±7.5 cm (Kane et al., 2014). In the adjacent Imnavait Creek watershed, snow accounts for one third of annual precipitation, and the winter snowpack generally develops and persists from late September through mid-May, at which time it has an average depth of 43±10 cm and a snow water equivalent of 11.1±3.1 cm, according to 26 years of end-of-winter snow surveys (Kane et al., 2014). Tussock-forming sedges dominate the vegetation of the non-track hillslope at the study sites, while high densities of dwarf willow and birch grow in all the study water tracks except WT1, which primarily supports non-tussock-forming sedge and moss vegetation (Harms and Ludwig, 2016).

4.4 Methods

4.4.1 Surveying Snow and Thaw Depth

Snow and thaw depth were measured manually using depth-to-refusal frost probing. In 2014, the sampling design included one transect perpendicular to and the other along each water track to test for spatial autocorrelation inside and outside the water track. Spatial autocorrelation was assessed by fitting Gaussian models to empirical semivariograms using the R package *gstat* (Pebesma, 2004). When models exhibited pure nugget characteristics or did not converge, measurements were assumed to be spatially independent. When models converged, measurements were subsampled to points separated by at least the best-fit range. Subsampling was then repeated 1000 times to provide a bootstrapped estimate of the independent snow or thaw depth.

4.4.2. Inferring Overwinter Snow Depth Using Miniature Temperature Loggers

Over-winter snow depths were inferred from iButton miniature temperature loggers by adapting a method developed by Lewkowicz (2008). The loggers were installed every 20-50 cm starting 5 cm above the ground surface along vertical stakes placed inside each water track and on the adjacent hillslope. The loggers were installed facing north to minimize heating from direct radiation and wrapped in nitrile rubber to prevent water damage. Temperatures were recorded from mid-August through June at four-hour intervals to capture diel fluctuations in temperature. Assuming that loggers within the insulating snowpack would experience damped diel fluctuations in temperature compared to loggers exposed to the atmosphere, we differenced the temperature from one measurement time step to the next, and then smoothed the differenced temperatures using a weekly moving average. These transformed records for each logger were compared to data from higher logger locations on the same stake and the 2-m air temperature measured at the Imnavait Creek Arctic Observatory Network (AON) ridge flux tower (Euskirchen et al., 2012), adding a half-degree buffer to infer a difference between records to account for the resolution of temperature logger. The highest damped logger and the lowest undamped logger were inferred to be the minimum and maximum snowpack depth, respectively. In comparing inferred snow depth inside and outside the water track, we considered the "snow-covered season" as all times when the minimum snow depth was greater than zero in either feature. These inferred snow depths were compared with manual snow depth measurements made daily at one site (WT6) during the snow ablation period of 2013.

4.4.3 Monitoring and Analyzing Active Layer Temperatures and Freeze-Thaw State

Thermocouples were used to continuously measure active layer temperatures throughout the study period and characterize the active layer thermal regime. Thermocouple chains were

installed at each site in the water track and a few meters away on the adjacent non-track hillslope at depths of 2, 4, 6, 8, 10, 15, 20, 25, 30, and 35 cm beneath the ground surface. Installation locations were determined in the field based on observed differences in vegetation, elevation, and flow between the water tracks and non-track hillslope. Temperatures were recorded every 5 minutes from mid-May through late August and every 30 minutes from late August through mid-May beginning in mid-May 2012 when less solar energy was available to power the dataloggers. Measured 5-minute or half-hour temperatures were then averaged to hourly values.

To characterize the differences between the thermal regime of the water tracks and hillslopes, we used the active layer temperature time series to calculate mean seasonal temperatures and the annual timing and duration of freeze-thaw conditions. Time series with more than two weeks of missing data were excluded from these calculations. We defined the seasons of spring, summer, fall, and winter as March-May, June-August, September-November, and December-February, respectively, and assumed that seasonal temperatures were independent in time because of the freezing and thawing transitions in the fall and spring. For the freeze-thaw conditions, we defined "fully frozen" as temperatures less than -2°C, "thawed" as temperatures greater than 0°C, and "partially frozen" as the zero-curtain window between 0 and -2°C (French, 2013). The annual duration of each condition was calculated for the two complete years beginning on August 1, 2012. This start date facilitated inclusion of site WT1 in the analyses despite datalogger failure at that site on August 9, 2013. We used the non-parametric Wilcoxon signed-rank test to determine whether there were significant pair-wise differences in the seasonal active layer temperatures between (1) features (water tracks and adjacent hillslopes) for the same study year and (2) study years for the same feature for each measurement depth at each site. We used multiple linear regression to quantify how feature type, mean seasonal snow depth, and mean

seasonal air temperature influenced the mean active layer temperatures for each of the four seasons and the annual duration of frozen conditions. The relative importance of the three predictors for each of the five response variables was assessed using the R package *relaimpo* metric 'lmg' (Grömping, 2006).

4.5 Results

4.5.1 Deeper Snow and Thaw in Water Tracks

Across most sites, both snow and thaw depth were deeper in the water tracks than on the adjacent hillslope (Figure 2). The end-of-winter snow depth measured in the water tracks were significantly deeper than their adjacent hillslope at four of the six study sites in mid-May 2014, near the onset of spring ablation. The end-of-winter snow depth was also significantly deeper than the long-term average (Kane et al., 2014) in the water tracks at all sites but WT4, but only deeper on the hillslope at WT3. Notably, the snowpack WT4 was already partially melted at the time of measurement, apparently due to dust from the nearby highway (Figure 1). By mid-June 2014, the thaw depth was similar in the water tracks as on the adjacent hillslopes, except at WT6, where the hillslope thaw was slightly deeper, and at WT4, where thaw in the water track was significantly deeper. By the end of the thaw season, the active layer was significantly deeper in the water tracks than on the adjacent hillslopes at four of the six sites. Finally, the snow depth inferred from temperature was deeper in the water tracks than on their adjacent hillslopes throughout the majority of the snow-covered season in both 2012-2013 and 2013-2014 at all sites except WT3 (Figure 3 and S4, Table S1).

4.5.2 Muted Diel and Seasonal Active Layer Temperatures in Water Tracks

In general, the diel and seasonal amplitudes of near-surface active layer temperatures were muted in the water track relative to the adjacent hillslope across all sites and the three years of

study (Figures 4 and S1; Tables S1-S4). Mean summer temperatures were significantly warmer (Wilcoxon sign-rank test; $p < 0.05$) on the hillslopes adjacent to the water tracks, except at depths of 30 and 35 cm at WT5 and WT6, respectively, which were indistinguishable in 2014 (Figure 5 and S2). In summer, the magnitude of the difference in active layer temperatures between the hillslope and water track features was a few degrees in the shallowest soils and diminished with depth (Figure 5 and S2). There were typically large diel fluctuations in near-surface active layer temperatures in both features, although peak daily active layer temperatures were usually colder in the water tracks than on the adjacent hillslopes (Figure 4 and S1). Mean fall active layer temperatures were consistently near zero, warmer than mean fall air temperatures, and varied little from water track to hillslope, from site to site, or from year to year (Figure 5 and S2). In contrast, mean winter active layer temperatures varied the most interannually and deviated the most from air temperatures compared to other seasons (Figure 5 and S2). Winter temperatures were significantly warmer in the water track than on the hillslope (Table S4), and diel fluctuations were small or non-existent (Figure 4 and S1). Mean winter active layer temperatures were more similar with depth for the same thermocouple profile than summer active layer temperatures (Figure 5 and S2), except on the hillslope at WT3, where mean temperatures measured at the shallowest depths were several degrees colder than those measured deeper below ground (Figure S2). Finally, in spring, mean water track ground temperatures were warmer than hillslope temperatures, although the difference both between features and between active layer temperatures and air temperatures was smaller than in winter (Figure 5 and S2).

4.5.3 Duration and Timing of Thermal Conditions Offset Between Water Tracks and Hillslopes

Water tracks were consistently frozen for fewer days of the year than their adjacent hillslopes, although the difference varied substantially by site, year, and depth within the active

layer (left plot, Figure 6). The water track at WT3 (green symbols), for example, was fully frozen for 121-138 days, depending on the depth below ground, for the year beginning on August 1, 2012, while frozen conditions lasted for only 74-80 days in the subsequent year. For the same time periods at the same site, the adjacent hillslope was frozen for 171-224 days and 138-196 days, respectively, or approximately 2-3 months longer than the water track across all depths. Water tracks were typically thawed for only a few days to a few weeks longer than their adjacent hillslopes, and this difference varied little from year-to-year (right plot, Figure 6). Instead, there was significant interannual variability in the duration of zero-curtain conditions across sites, and at three of the four sites, the water tracks were partially frozen for up to three months longer than the adjacent hillslope (middle plot, Figure 6). Paired observations of the duration of frozen and partially frozen conditions were significantly negatively correlated, and the goodness of fit increased exponentially with proximity to the ground surface ($r = 0.69$ at 35-cm depth, increasing to 0.96 at 2-cm depth, $n = 18$, $p < 0.001$, Figure S3).

Not only was the duration of frozen and partially frozen conditions significantly different between water tracks and their adjacent hillslopes, but the timing of freeze-thaw conditions was also seasonally offset between the two features (Figures 7 and S4). While both hillslopes and water tracks were fully frozen on April 1 each year (lower panel, light blue), the hillslopes thawed earlier than the water tracks (green colors at all depths in spring). At WT6 in 2013, where detailed daily snow ablation measurements were made, earlier thaw on the hillslope coincided with earlier snowmelt (Figures 3 and 7). Throughout the summer, both features were typically thawed (dark blue), except in the late summer when the shallow soils of the hillslopes were more susceptible to freezing when air temperatures periodically dipped below freezing (red colors). As air temperatures consistently dropped below freezing in the fall and snow began accumulating, the

water tracks remained thawed until as late as January 10th, while the hillslopes cooled into zero curtain or fully froze (dark red and red). Finally, as the ground continued to cool into the winter, the water tracks remained at zero-curtain temperatures while the hillslopes were fully frozen until as late as March (pink), when the water tracks finally froze as well.

4.5.4 Factors Influencing Seasonal Active Layer Temperatures and Thermal Conditions

Feature type, mean seasonal air temperature, and mean seasonal snow depth were significantly correlated with the duration of frozen conditions and mean active layer temperature in each season (r = 0.63-0.93; Table 1). The variance explained by the three factors was greatest in the winter (82%) and for the duration of frozen conditions (89%) and the least in the fall (50%). Feature type (water track vs. hillslope) explained the most variance in the annual duration of frozen conditions and in mean active layer temperatures in all seasons except for the spring, when mean air temperature explained most variance. Surprisingly, snow depth explained the least variance across all metrics of the active layer thermal regime.

4.6 Discussion

4.6.1 Seasonal Patterns and Controls on Water Track and Hillslope Active Layer Thermal Regimes

Observations of thermal regimes in paired water track and adjacent hillslopes demonstrate that soil moisture exerts a dominant influence on thermal conditions within the active layer. This finding builds on previous field observations, experimental manipulation, and numerical models that identified effects of the snow depth and duration on the active layer thermal regime in tundra landscapes (e.g., Taras et al., 2002; Lafreniere et al., 2012; Rushlow et al., *in prep*). Either insulation by snow or the latent heat released during the freeze-up in the fall could cause warmer seasonal temperatures and persistent partially frozen conditions (Rushlow et al., *in prep*),

especially in the water tracks which have both higher soil water content (Rushlow et al., 2017) and deeper snow (Figure 1). However, across seasons, less of the variance in the seasonal temperatures of the active layer and the duration of freezing was explained by snow depth than feature type or air temperature, despite variation in snow depth from as little as 5 to as much as 120 cm (Figure 8). Further, the length of the thaw season varied relatively little from water track to hillslope, site to site, or year to year, while the duration of frozen and partially frozen conditions covaried strongly with all three factors (Figure 5 and S3, Table 1), suggesting an overriding role of soil moisture compared to air temperature in driving the observed patterns. The correlation between frozen and partially frozen conditions, including all sites, feature types, and years was remarkably strong, and strongest in the upper soil profile (Table 1, Figure S3), where porous and permeable peat has a higher capacity for water storage and retention, and thus latent heat release, than the deeper mineral soil (e.g., McNamara et al., 1998). The seasonal role of soil moisture in controlling the active layer thermal regime is also inferred from shifts in relative importance of air temperature and feature type. The importance of feature type diminished from winter to spring, and the importance of air temperature increased, ostensibly because both water tracks and hillslopes were fully frozen and the dominant energy transfer process shifted from latent heat exchange to vertical conduction with the reduction in liquid soil water content. At the same time, the significance of snow depth also diminished, perhaps because the snowpack structure and associated thermal conductivity were already well-developed and similar between features. In this case, the thermal gradient through the snowpack would depend more strongly on the difference between air and ground surface temperature. Hillslopes, with their colder ground temperatures, would have weaker thermal gradients through the snowpack than water tracks, with their warmer ground temperatures.

Although partially frozen conditions persisted later (Figures 7 and S4) and summer active layer temperatures were consistently colder in the water tracks than on the adjacent hillslopes (Figures 5 and S2 and Table S1-4), late summer thaw depth was significantly deeper at four of the five water tracks than their adjacent hillslopes (Figure 3). Several previous studies have also measured deeper thaw in tundra water tracks (Chapin et al., 1988; Hastings et al., 1989; Oberbauer et al., 1991; Walker et al., 1994; Kane, 2001), attributing deeper thaw to higher soil moisture and thus higher thermal conductivity in water track flowpaths relative to the drier hillslopes adjacent to them (Kane, 2001). However, the only two studies measuring water track ground temperatures observed significantly colder active layer temperatures in the water track early in the summer, but significantly warmer temperatures after periods of rainfall or coincident with high soil moisture (Hastings et al., 1989; Oberbauer et al. 1991). The fact that the water tracks in our study have significantly colder active layer temperatures throughout most of the summer season than their adjacent hillslopes, but deeper thaw could be due to higher ice content in water track soils. If the heat required for melting was met by the higher heat transferred into the wetter, more thermally conductive soils, it could thaw but not warm water track soils. Lateral water flow may also cool water track soils; for example, water track active layer temperatures were significantly colder in summer 2014, when approximately one-third more rain fell than in summer 2013 (Rushlow and Godsey, 2017). Air temperatures were also significantly colder in summer 2014 than 2013, but while feature type and near-surface active layer temperature were significantly correlated, air temperature and near-surface active layer temperature were not (Table 1). Overall, our results support the hypothesis that the high soil moisture in water tracks exerts a key control on active layer temperatures in the summer as well as in the cold seasons.

4.6.2 Implications for Ecological Processes

The active layer froze from the surface downwards and zero-curtain temperatures persisted in water tracks for several months (Figure 7 and S4), conditions that foster continued biological activity beyond the growing season. Microbial respiration in Arctic tundra soils increases exponentially with temperature both above and below freezing (Mikan et al., 2002). Thus, warmer summer ground temperatures likely support higher rates of respiration at hillslope locations in the summer growing season, and at water track locations in the cold season, unless respiration is limited by the availability of labile organic substrate or soil moisture (e.g., Oberbauer et al., 1992). Warmer soil temperatures in the water tracks may also increase plant-available nitrogen through higher rates of over-winter mineralization (Schimel et al., 2004), providing an additional explanation for higher rates of primary production during the growing season in water tracks compared to the surrounding hillslopes (Chapin et al., 1988). Net emission of CO_2 and CH_4 from tundra soils occurs when active layer soils remain unfrozen or at zero-curtain temperatures, and emissions under these conditions contribute significantly to the strength of the net annual source of CO_2 and CH_4 from Alaskan tundra to the atmosphere (Raz-Yaseef et al., 2017; Zona et al., 2016; Commane et al., 2017; Euskirchen et al., 2017). For example, cumulative CO_2 emissions from September to December are positively correlated with the number of zero-curtain days, and this correlation was strongest for wet sedge tundra, which characterizes the vegetation cover of many water tracks (Euskirchen et al., 2017).

The persistence of ground temperatures favorable to biological activity and hydrologic transport suggest that water tracks may function as hot spots of greenhouse gas emissions from autumn until freeze up, contributing significantly to regional emissions. Greater CO_2 emissions from water tracks soils than surrounding hillslopes have been observed late in the thaw season (Oberbauer et al., 1992). Such spatial contrasts may occur due to transport of dissolved CO_2 in

saturated soils of water tracks followed by evasion (Kling et al., 1991). Elevated emissions of CO_2 outside of the thaw season, combined with the broad spatial extent of water tracks, which cover between 24-34% of the central foothills region of Alaska's North Slope (McNamara et al., 1999; Trochim et al., 2016b), suggest that soil moisture-driven active layer thermal conditions in water tracks make them significant contributors to greenhouse gas budgets.

4.6.3 Climate Change and the Zero-Order Stream Network

Global climate models predict that Arctic warming will be amplified relative to lower latitudes, and that summer warming will be moderate relative to winter warming (Bitanja and Krikken, 2016). Permafrost temperatures have consistently warmed across North America and the duration of zero-curtain temperatures have increased over the past four decades (Romanovsky et al., 2010; Zona et al., 2016). We found that warmer active layer temperatures in the winter and spring were strongly correlated with warmer air temperatures, but that warming is buffered in water tracks in the summer and fall, likely due to high soil moisture and the exchange of latent heat. As the Arctic climate warms, increased evaporative demand and a shorter snow cover season may dry the tundra (Oechel et al., 2000; Hinzman et al., 2005), reducing or removing the soil moisture buffer and effectively cooling soils in the winter and spring and warming them in the summer and fall. However, those drivers may be offset by an expected increase in Arctic precipitation, particularly in the winter, because of atmospheric warming (IPCC, 2014). In either case, the interannual variability in the active layer thermal regime observed in this study will likely increase in response to climate change. Water tracks have already been associated with ground collapse ("thermokarst") due to ice wedge degradation (Gooseff et al., 2012; Trochim et al., 2016a), and the current state and controls on their ground thermal regime suggest that water tracks are particularly vulnerable to widespread permafrost degradation as winters warm. While water

tracks currently function as a part of the zero-order stream network (McNamara et al., 1999), transporting water downslope primarily through the active layer (Levy et al., 2014), thermokarst may initiate a positive feedback that leads to the stream network expansion by removing the peat-rich organic layer that currently inhibits erosion of hillslope sediment (Mann et al., 2010). Whether the thermal regime of water tracks changes gradually or abruptly in response to climate change, it is likely to have a significant impact on upland tundra carbon, nutrient, and hydrologic cycling through their function as a hydrologic connection between terrestrial and aquatic ecosystems (Stieglitz et al., 2003b; Rushlow and Godsey, 2017).

4.7 Conclusions

This was the first study to characterize the year-round active layer thermal regime of tundra water tracks, common drainage features on Arctic hillslopes. We showed that water tracks experienced more moderate thermal conditions that were temporally offset from those of surrounding hillslope. Notably, water track active layers froze from the top down and remained at partially frozen temperatures for months longer than the hillslope during the fall freeze-up period-conditions that are favorable for continued biological activity and greenhouse gas production. Localized soil properties, likely the latent heat effects of higher soil water content, were strongly correlated with the duration of partially frozen conditions and the magnitude of temperature fluctuations in the active layer across sites. Surprisingly, seasonal snow cover was a less significant predictor. Conducting similar investigations that encompass a broader range of climatic conditions would further disentangle the site-specific hierarchy of intrinsic and extrinsic controls. Our findings suggest that a better understanding of both the extent and the controls on the soil moisture status of the zero-order drainage network would be valuable for predicting active layer dynamics and associated ecological processes across the upland tundra.

4.8 Acknowledgements

Funding from the National Science Foundation's Division of Polar Programs and Division of Environmental Biology award numbers 1259930 and 1026843, the United States Geological Survey Northwest Climate Science Center, the University of Idaho College of Natural Resources McCall Outdoor Science School, and the Idaho State University Geosciences Department supported this work. Data from this study are available online in the International Arctic Research Center Data Archive (P.I. Sarah Godsey) and in the UNAVCO TLS Archive (Project U-035). Special thanks to Margit Jaeger, Melissa Barker-Tamplin, and Molly Tedesche for assistance in installing the thermocouple profiles, Logan Chance for assistance in collecting the 2013 snow ablation data, and Chris Cook for assistance in collecting and cleaning the iButton data.

4.9 Figures and Tables

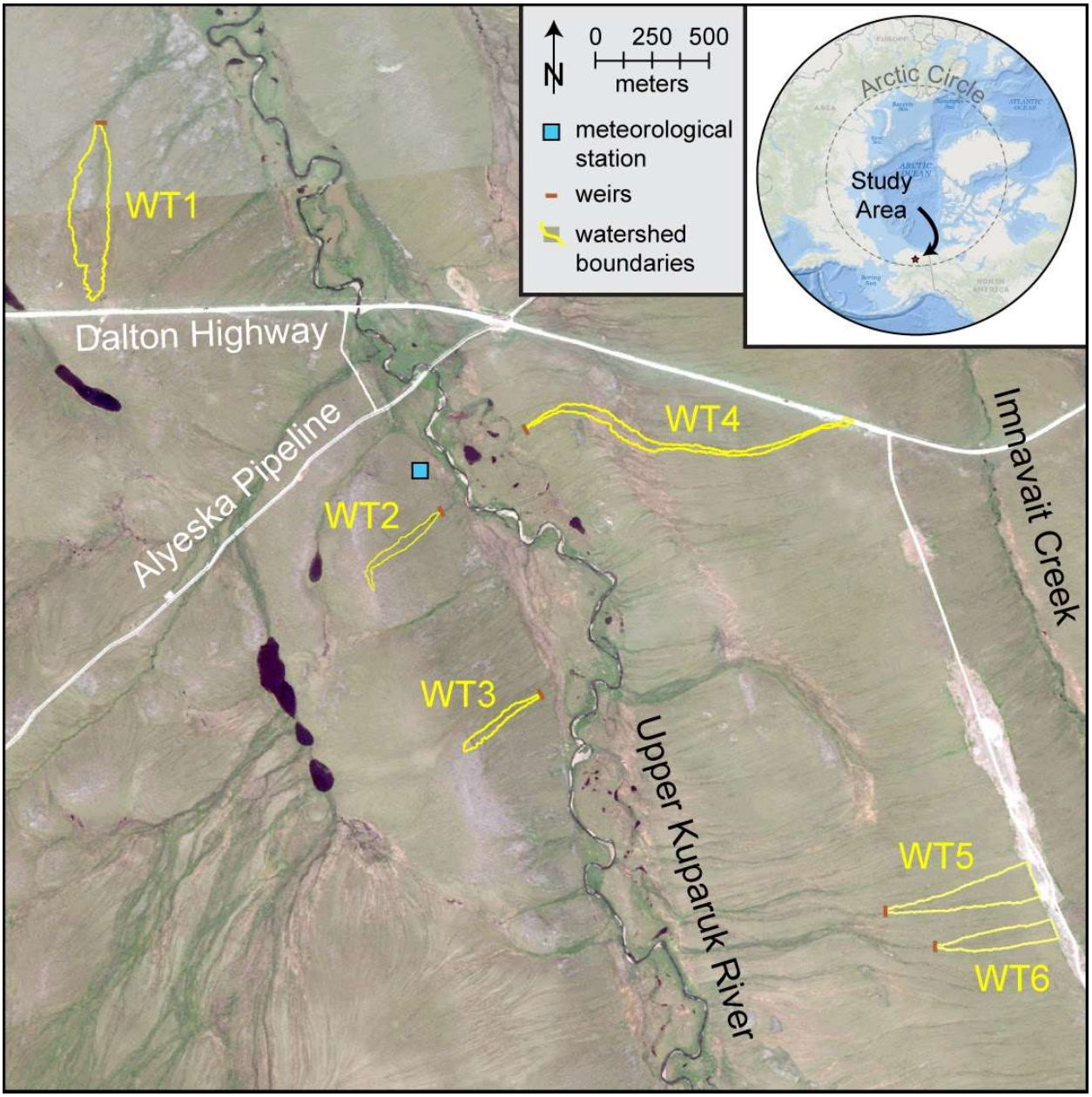

Figure 1. The study area and six water track (WT) watersheds draining the hillslopes of the Upper Kuparuk River in Arctic Alaska, USA (inset map). Numerous water tracks are visible as bands of greener vegetation that terminate at the valley bottom, while roads and pipeline stand out in white and water bodies in dark blue. The true color background image combines imagery from the Quickbird-2 satellite on July 18, 2009 (upper image) and the Worldview-2 satellite on July 10, 2011 (lower image). The border between the two images passes through WT1. Commercial

imagery (Copyright 2012, DigitalGlobe, Inc.) obtained courtesy of the Polar Geospatial Center at the University of Minnesota.

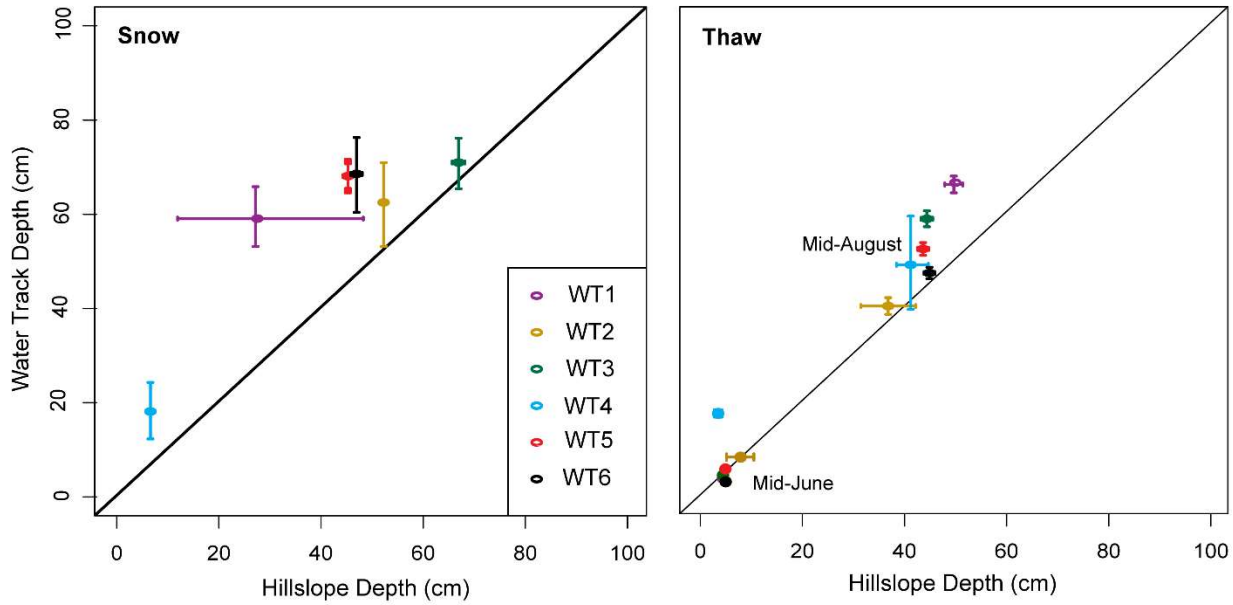

Figure 2. Mean end-of-winter snow depth (left) and early- and end-of-summer thaw depth (right) measured in the water tracks ("WT") and on their adjacent hillslopes in 2014. The 1:1 line is shown and error bars depict standard error.

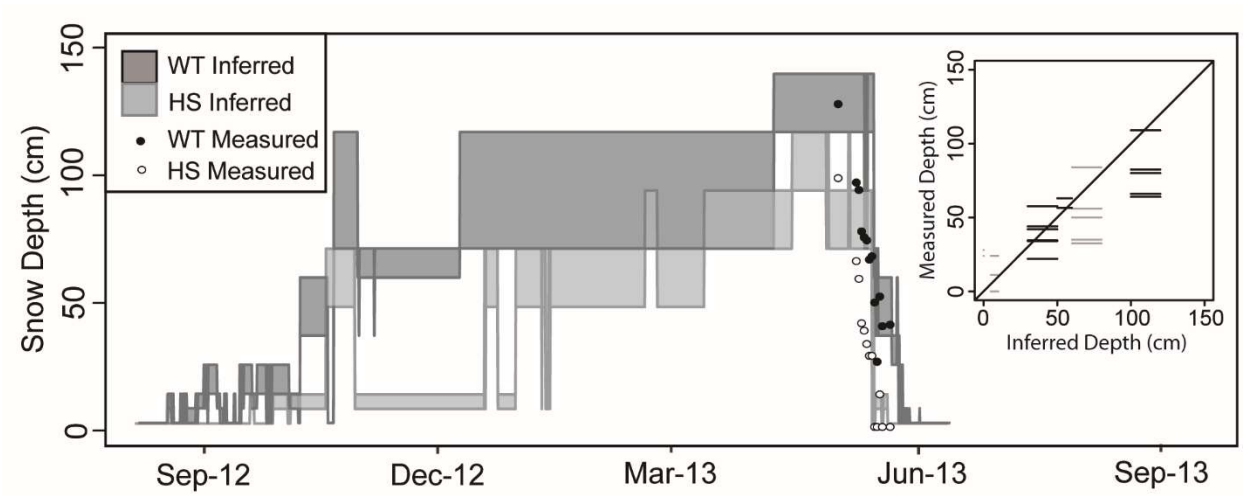

Figure 3. Inferred snow depths derived by the method described in Section 4.4.2 and field-verified measurements as described in Section 4.4.3 in the water track ("WT", dark gray) and on the

adjacent hillslope ("HS," light gray) at site WT6 from fall 2012 through spring ablation in 2013. The envelopes encompass the uncertainty in depth due to the vertical distance between the highest snow-covered logger and the lowest snow-free logger. Inset shows the relationship between inferred and measured snow depth at the hillslope and water track snow stakes for the same spring ablation period.

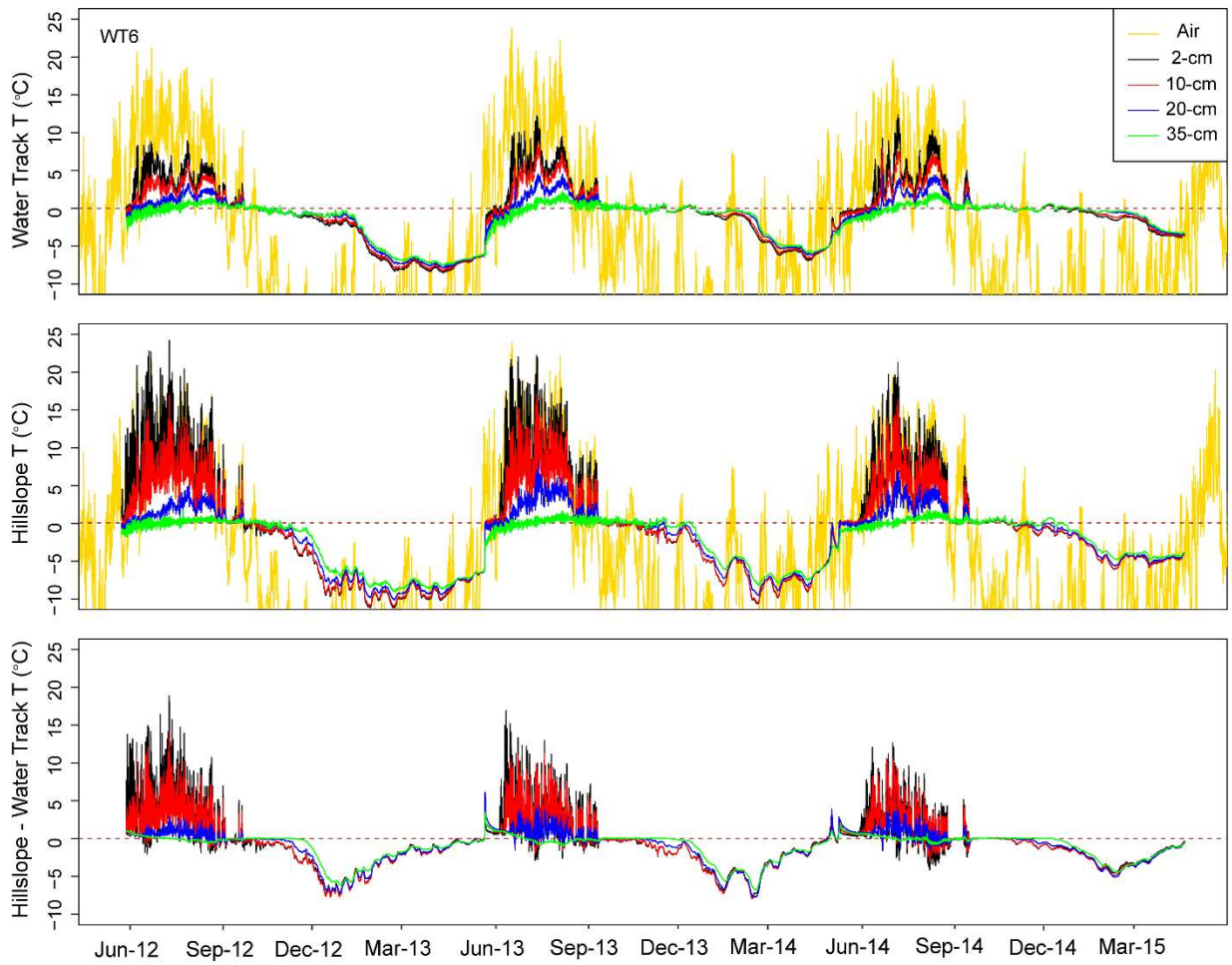

Figure 4. Hourly active layer temperatures ("T") for four depths measured at site WT6 and air temperature (yellow) measured at the AON tower over the three-year study period. The top panel shows the active layer temperatures inside the water track at 2 (black), 10 (red), 20 (blue), and 35 (green) cm depth, middle panel shows the measured active layer temperatures on the adjacent hillslope, and the bottom panel shows the difference between the active layer temperatures

measured inside the water track and on the adjacent hillslope. The horizontal brown dashed line marks 0°C in each panel.

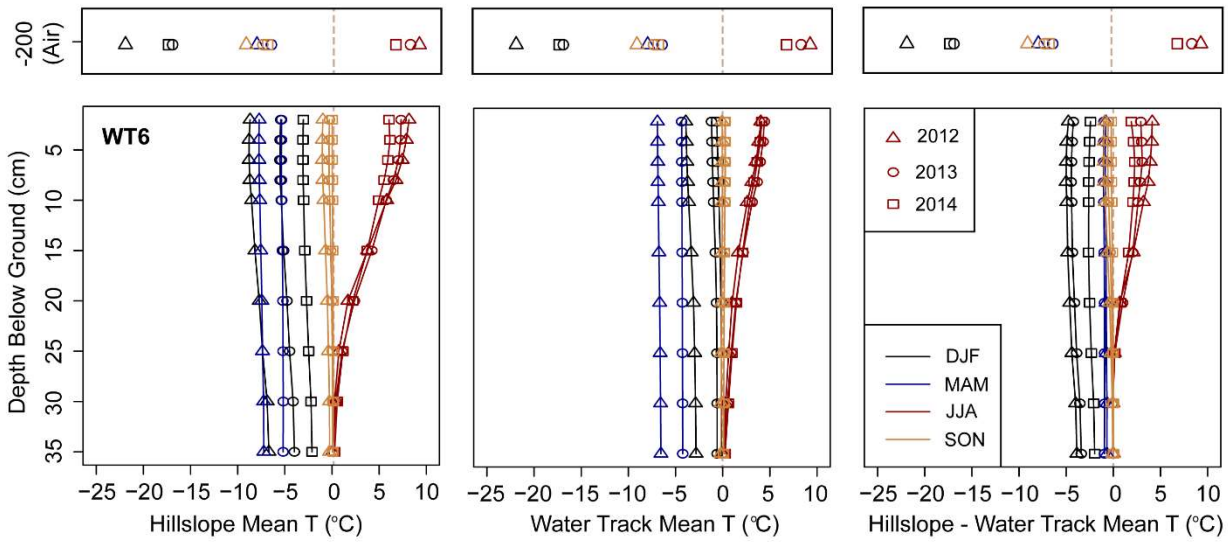

Figure 5. Mean seasonal 2-m air temperatures (top) and mean seasonal active layer temperature profiles measured at site WT6 on the hillslope (left) adjacent to the water track (middle), and the difference in mean seasonal active layer temperature between the two feature types (right) for the three study years. Study years are denoted by symbol, and seasons (winter, spring, summer, and fall) are denoted by color. The vertical brown dashed line marks 0°C.

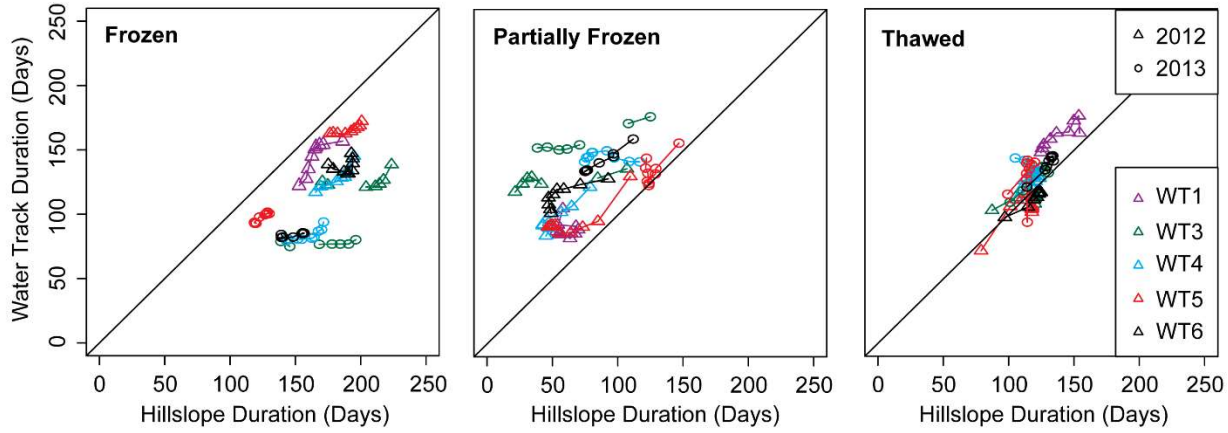

Figure 6. Duration of frozen, partially frozen, and thawed conditions for the water track ground temperature profiles compared to their adjacent hillslope profiles for a full year, beginning on

August 1, 2012 (triangles) or 2013 (circles). “Frozen” conditions are defined as colder than -2°C, “partially frozen” conditions fall between -2 and 0°C, and “thawed” conditions are above 0°C. The colors represent the five sites and match those in Figure 2; points are shown for all depths with data collection gaps of less than two weeks during a given year, and a line connects points from different depths within the same thermocouple profile. The 1:1 line is shown in each plot.

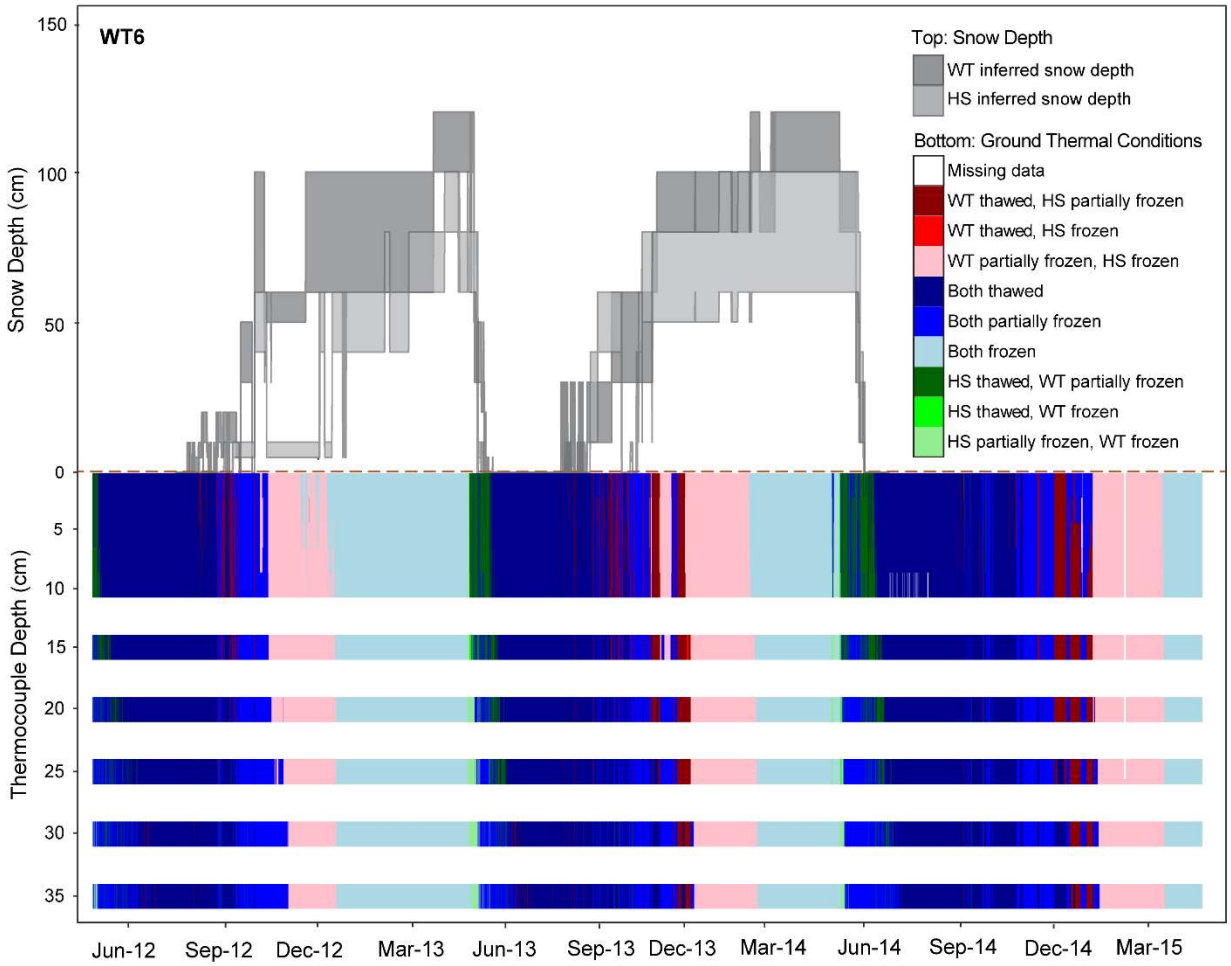

Figure 7. Inferred snow depth (upper plot) and differential ground thermal conditions (lower plot) in the water track (WT) relative to the adjacent hillslope (HS) at site WT6 over the three-year study period (May 2012–April 2015). The relative position of the ground surface is indicated with a dashed line, and there are different scales above and below ground. The upper plot shows water track snow depth with the dark gray envelope and hillslope snow depth with the gray envelope.

Envelopes are inferred from the iButton as detailed in the Section 3.4.2. The lower plot thermal conditions refer to three broad categories: green colors indicate when the hillslope was in a warmer condition than the water track, blue colors indicate when the hillslope and water track shared the same condition, and red colors indicate when the water track was in a warmer condition than the hillslope. The shades of the three colors indicate the combination of thawed, partially frozen, and frozen conditions as described in the main text and legend.

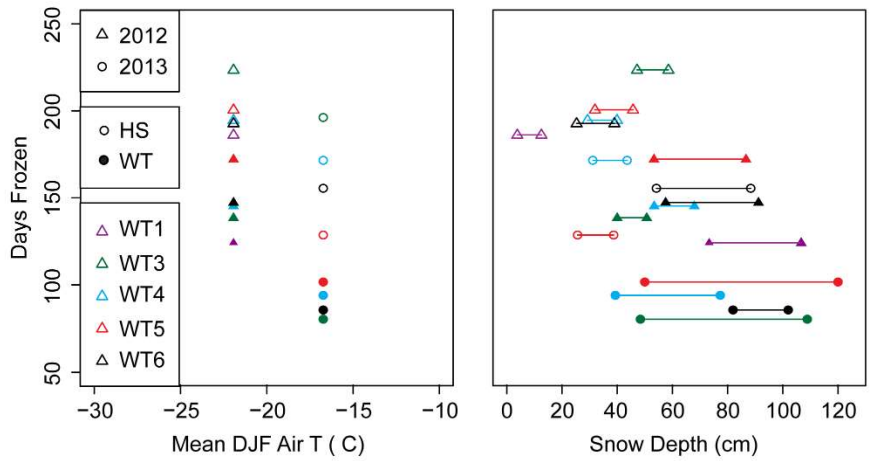

Figure 8. The relationships between the number of frozen days for the two years of record, 8/1/12-7/31/13 (triangles) and 8/1/13-7/31/14 (circles), and possible influencing factors, including mean winter air temperature, mean minimum and maximum winter snow depth, and feature type, i.e., water track (filled symbols) or hillslope (closed symbols). The five colors represent the five sites, as in Figure 6.

Table 1. Goodness-of-fit and significance levels of linear regressions

Coefficient(s)	*Days Frozen*	*Mean Summer Temperature*	*Mean Fall Temperature*	*Mean Winter Temperature*	*Mean Spring Temperature*
Loc	-0.72***	-0.78***	0.59***	0.66***	0.42*
Air	-0.50*	0.17.	0.23.	0.50**	0.71***
Snow	-0.44*	*NA*	0.41*	0.48*	0.24.
Loc + Air	-0.90***	0.78***	0.65***	0.85***	0.86***
Loc	***	***	***	***	**
Air	***	.	°	***	***
Loc + Snow	-0.67*	*NA*	0.65*	0.76***	0.49.
Loc	*	*NA*	*	**	*
Snow	.	*NA*	.	.	.
Air + Snow	-0.73*	*NA*	0.34.	0.65**	0.74**
Air	**	*NA*	.	*	***
Snow	*	*NA*	°	*	.
Loc + Air + Snow	-0.93***	*NA*	0.63°	0.88***	0.84***
Loc	***	*NA*	*	***	*
Air	***	*NA*	.	**	***
Snow	.	*NA*	.	.	.

Loc = location (water track or hillslope), air = mean seasonal air temperature (winter for Days Frozen), and snow = mean seasonal snow depth (lower estimate). Adjusted r values are shown for each model, along with the overall p-value significance level and the p-value of each coefficient.
Significance level codes: 0 '***' 0.001 '**' 0.01 '*' 0.05 '°' 0.1 '.' 1.

4.10 References

Bitanja. R., & Andry, A.O., (2017), Towards a rain-dominated Arctic, *Nature Climate Change, 7,* 263-267. doi: 10.1038/nclimate3240.

Bitanja, R., & Krikken, F., (2016). Magnitude and pattern of Arctic warming governed by the seasonality of radiative forcing, *Nature, 6(38287),* doi: 10.1038/srep38287.

Bokhorst, S., et al., (2016), Changing Arctic snow cover: A review of recent developments and assessment of future needs for observations, modelling, and impacts, *Ambio, 45(5)*, 516-537.

Chapin, F.S., Fetcher, N., Kielland, K., Everett, K.R., & Linkins, A.E., (1988). Productivity and nutrient cycling of Alaskan tundra: enhancement by flowing soil water. *Ecology 69(3)*, 693–702.

Euskirchen, E. S., Bret-Harte, M. S., Scott, G. J., Edgar, C., & Shaver, G. R. (2012). Seasonal patterns of carbon dioxide and water fluxes three representative tundra ecosystems in northern Alaska. *Ecosphere, 3(1)*, 4.

Euskirchen, E.S., Bret-Harte, M.S., Shaver, G.R., Edgar, C.W., & Romanovsky, V.E., (2017). Long-term release of carbon dioxide from arctic tundra ecosystems in Alaska, *Ecosystems, 20(5),* 960-974.

French, H.M., (2013). *The Periglacial Environment*, Somerset, UK. doi:10.1002/9781118684931.

Hamilton, T. D., & Walker, D. A. (2003). Glacial geology of Toolik Lake and the Upper Kuparuk River region. In Alaska Geobotany Center, Institute of Arctic Biology (pp. 24). Fairbanks, AK: University of Alaska–Fairbanks.

Harms, T. K., & Ludwig, S. M. (2016). Retention and removal of nitrogen and phosphorus in saturated soils of arctic hillslopes. *Biogeochemistry, 127(2)*, 291–304. doi: 10.1007/s10533-016-0181-0.

Hastings, S.J., Luchessa, S.A., Oechel, W.C., & Tenhunen, J.D., (1989), Standing biomass and production in water drainages of the foothills of the Philip Smith Mountains, Alaska, *Holarctic Ecology, 12(3)*, 304-311.

Hinzman, L. D., Kane, D. L., Gieck, R. E., & Everett, K. R. (1991). Hydrologic and thermal properties of the active layer in the Alaskan Arctic. *Cold Regions Science and Technology, 19*, 95-110.

Hinzman, L. D., & Kane, D. L., (1992), Potential response of an Arctic watershed during a period of warming, *Journal of Geophysical Research, 97(D3)*, 2811-2820.

IPCC (2013). Climate change 2013: The physical science basis. In T. F. Stocker, D. Qin, G.-K.

Plattner, M. Tignor, S. K. Allen, J. Boschung, et al. (Eds.), Contribution of working group I to the fifth assessment report of the intergovernmental panel on climate change (pp. 1535). Cambridge, United Kingdom and New York, NY, USA: Cambridge University Press. doi: 10.1017/CBO9781107415324.

Jorgenson, M. T., Romanovsky, V., Harden, J., Shur, Y., O'Donnell, J., Schuur, E. A. G., Kanevskiy, M., & Marchenko, S., (2010), Resilience and vulnerability of permafrost to climate change. *Canadian Journal of Forest Resources 40*, 1219-1236.

Kane, D. L., Youcha, E. K., Stuefer, S. L., Myerchin-Tape, G., Lamb, E., Homan, J. W., … Toniolo, H. (2014). Hydrology and meteorology of central Alaskan Arctic: Data collection and analysis, final report, Report INE/WERC 14.05(pp. 168). Fairbanks, Alaska: University of Alaska Fairbanks, Water and Environmental Research Center.

Kane, D. L., and L. D. Hinzman (2015), Climate data from the North Slope hydrology research project. University of Alaska Fairbanks, Water and Environmental Research Center. URL: http://ine.uaf.edu/werc/projects/NorthSlope/. Accessed September 8, 2016.

Lafreniere, M.J., Laurin, E., & Lamoureux, S.F., (2012), The impact of snow accumulation on the active layer thermal regime in high arctic soils, *Vadose Zone Journal,* doi:10.2136/vzj2012.0058.

Levy, J. S., Fountain, A. G., Gooseff, M. N., Welch, K. A., & Lyons, W. B. (2011). Water tracks and permafrost in Taylor Valley, Antarctica: Extensive and shallow groundwater connectivity in a cold desert ecosystem. *Geological Society of America Bulletin, 123(11/12)*, 2295-2311. doi: 10.1130/B30436.1.

Levy, J., (2014), A hydrological continuum in permafrost environments: The morphological signatures of melt-driven hydrology on Earth and Mars, *Geomorphology,* doi: 10.1016/j.geomorph.2014.02.033.

Lewkowicz, A.G., (2008), Evaluation of miniature temperature-loggers to monitor snowpack evolution at mountain permafrost sites, Northwestern Canada, *Permafrost and Periglacial Processes, 19*, 323-331.

Matsuoka, N., & Hirakawa, K., (2000), Solifluction resulting from one-sided and two-sided freezing: field data from Svalbard. *Polar Geoscience, 13*, 187-201.

McNamara, J. P., Kane, D. L., & Hinzman, L. D. (1999). An analysis of an arctic channel network using a digital elevation model. *Geomorphology, 29*, 339–353.

Mikan, C.J., Schimel, J.P., Doyle, A.P., (2002), Temperature controls of microbial respiration in arctic tundra soils above and below freezing. *Soil Biology & Biochemistry, 34,* 1785-1795.

Oechel, W.C., Vourlitis, G., Hastings, S.J., 1997. Cold season CO2 emission from arctic soils. *Global Biogeochemical Cycles, 11*, 163–172.

Paquette, M., Fortier, D., & Vincent, W. F. (2017), Water track in the High Arctic: A hydrological network dominated by rapid subsurface flow through patterned ground, *Arctic Science, 3*, 334-353. dx.doi.org/10.1139/as-2016-0014.

Pebesma, E. J. (2004), Multivariable geostatistics in S: the gstat package. *Computers and Geosciences, 30,* 683-691.

Raz-Yaseef, N., Torn, M.S., Wu, Y., Billesbach, D.P., Liljedahl, A.K., Kneafsey, T.J., Romanovsky, V.E., Cook, D.R., & Wullschleger, S.D., (2017), Large CO_2 and CH_4 emissions from polygonal tundra during spring thaw in northern Alaska, *Geophysical Research Letters, 44,* 504-513, doi: 10.1002/2016/GL071220.

Romanovsky, V.E., Osterkamp, T.E., (2000). Effects of unfrozen water on heat and mass transport processes in the active layer and permafrost. *Permafrost and Periglacial Processes 11,* 219–239.

Romanovsky, V.E., Smith, S.L., & Christianson, H.H., (2010). Permafrost thermal state in the polar Northern Hemisphere during the international polar year 2007-2009: a synthesis. *Permafrost and Periglacial Processes, 21*, 106-116, doi: 10.1002/ppp.689.

Rushlow, C.R., & Godsey, S.E., (2017), Rainfall-runoff responses on Arctic hillslopes underlain by continuous permafrost, North Slope, Alaska, USA, *Hydrological Processes, 31,* 4092-4106. doi: 10.1002/hyp.11294.

Rushlow, C.R., Sawyer, A.S., Voss, C.I., Godsey, S.E. (*in prep*), The influence of snow cover, air temperature, and groundwater flow on the active layer thermal regime of Arctic hillslopes drained by water tracks.

Schimel, J.P., Bilbrough, C., Welker, J.A., (2004). Increased snow depth affects microbial activity and nitrogen mineralization in two Arctic tundra communities. *Soil Biology & Biogeochemistry, 36(2)*, 217–227.

Shaver, G.R., Johnson, L.C., Cades, D.H., Murray, G., Laundre, J.A., Rastetter, E.B., Nadelhoffer, K.J., & Giblin, A.E., (1998). Biomass and CO2 flux in wet sedge tundras: responses to nutrients, temperature, and light. *Ecolological Monographs, 68(1)*, 75–97.

Schuur, E. A. G., Bockheim, J., Canadell, J. G., Euskirchen, E., Field, C. B., Goryachkin, S. V., Hagemann, S., Kuhry, P., LaFleur, P. M., Lee, H., Mazhitova, G., Nelson, F. E., Rinke, A., Romanovsky, V. E., Shiklomanov, N. Tarnocai, C., Venevsky, S., Vogel, J. G. & Zimov, S. A. (2008). Vulnerability of permafrost carbon to climate change: Implication for the global carbon cycle. *BioScience, 58(8),* 701-714.

Stieglitz, M., Dery, S.J., Romanovsky, V.E., & Osterkamp, T.E., (2003a), The role of snow cover in the warming of arctic permafrost, *Geophysical Research Letters, 30(13)*, 1721. doi: 10.1029/2003GL017337.

Stieglitz, M., Shaman, J., McNamara, J., Engel, V., Shanley, J., & Kling, G. W. (2003b). An approach to understanding hydrologic connectivity on the hillslope and the implications for nutrient transport. *Global Biogeochemical Cycles, 17(4),* 1105. doi: 10.1029/2003GB002041.

Sturm, M., Homgren, J., Konig, M., & Morris, K. (1997). The thermal conductivity of seasonal snow. *Journal of Glaciology, 43(143)*, 26-41.

Sturm, M., Schimel, J., Michaelson, G., Welker, J.M., Oberbauer, S.F., Liston, G.E., Fahnestock, J., & Romanovsky, V.E., (2005), Winter biological processes could help convert arctic tundra to shrubland, *BioScience, 55(1),* 17-26.

Taras, B., Sturm, M., & Liston, G. E. (2002). Snow-ground interface temperatures in the Kuparuk River Basin, Arctic Alaska: Measurements and model. *Journal of Hydrometeorology, 3*, 377-394.

Tarnocai, C., Canadell, J. G., Schuur, E. A. G., Kuhry, P., Mazhitova, G., & Zimov, S. (2009). Soil organic carbon pools in the northern circumpolar permafrost region. *Global Biogeochemical Cycles, 23(GB2023)*, doi:10.1029/2008GB003327.

Trochim, E. D., Jorgenson, M. T., Prakash, A., & Kane, D. L. (2016a). Geomorphic and biophysical factors affecting water tracks in northern Alaska. *Earth and Space Science, 3.* doi: 10.1002/2015EA000111.

Trochim, E. D., Prakash, A., Kane, D. L., & Romanovsky, V. E. (2016b). Remote sensing of water tracks. *Earth and Space Science, 3*. doi: 10.1002/2015EA000112.

Wainwright, H.M., Liljedahl, A.K., Dafllon, B., Ulrich, C., Peterson, J.E., Gusmeroli, A., & Hubbard, S.S., (2017), Mapping snow depth within a tundra ecosystem using multiscale observations and Bayesian methods, *The Cryosphere, 11*, 857-875.

Walker, D.A., Binnian, E., Evans, B.M., Lederer, N.D., Nordstrand, E., & Webber, P.J., (1989). Terrain, vegetation and landscape evolution of the R4D research site, Brooks Range Foothills, Alaska. *Ecography. 12,* 238–261. doi: 10.1111/j.1600-0587.1989.tb00844.x.

Walker, M.D., Walker, D.A., & Auerbach, N.A., (1994), Plant communities of a tussock tundra landscape in the Brooks Range Foothills, Alaska, *Journal of Vegetation Science, 5,* 843-866.

Walker, M.D., Walker, D.A., Welker, J.M., Arft, A.M., Bardsley, T., Brooks, P.D., Fahnestock, J.T., Jones, M.H., Losleben, M., Parson, A.N., Seasteadt, T.R., & Turner, P.L., (1999).

Long-term experimental manipulation of winter snow regime and summer temperature in arctic and alpine tundra. *Hydrological Processes, 13*, 2315-2330.

Walvoord, M. A., & Kurylyk, B. L. (2016). Hydrologic impacts of thawing permafrost- A review. *Vadose Zone Journal, 15(6)*, doi:10.2136/vzj2016.01.0010.

Yano, Y., Shaver, G. R., Giblin, A. E., Rastetter, E. B., & Nadelhoffer, K. J. (2010). Nitrogen dynamics in a small arctic watershed: Retention and downhill movement of 15N. *Ecological Monographs, 80(2),* 331–351.

Zimov, S.A., Davidov, S.P., Prosiannikov, Y.V., Semiletov, I.P., Chapin, M.C., & Chapin, F.S., (1996). Siberian CO_2 efflux in winter as a CO_2 source and cause of seasonality in atmospheric CO_2. *Climatic Change 33,* 111–120.

Zona, D., Gioli, B., Commane, R., Lindaas, J., Wofsy, S. C., Miller, C. E., Dinardo, S. J., Dengel, S., Sweeney, C., Karion, A., Chang, R.Y.-W., Henderson, J. M., Murphy, P. C., Goodrich, J. P., Moreaux, V., Liljedahl, A., Watts, J. D., Kimball, J. S., Lipson, D. A., & Oechel, W. C., (2016). Cold season emissions dominate the Arctic tundra methane budget, *Proceedings of the National Academy of Sciences of the USA*, *113,* 40–45. doi: 10.1073/pnas.1516017113.

4.11 Supplemental Information

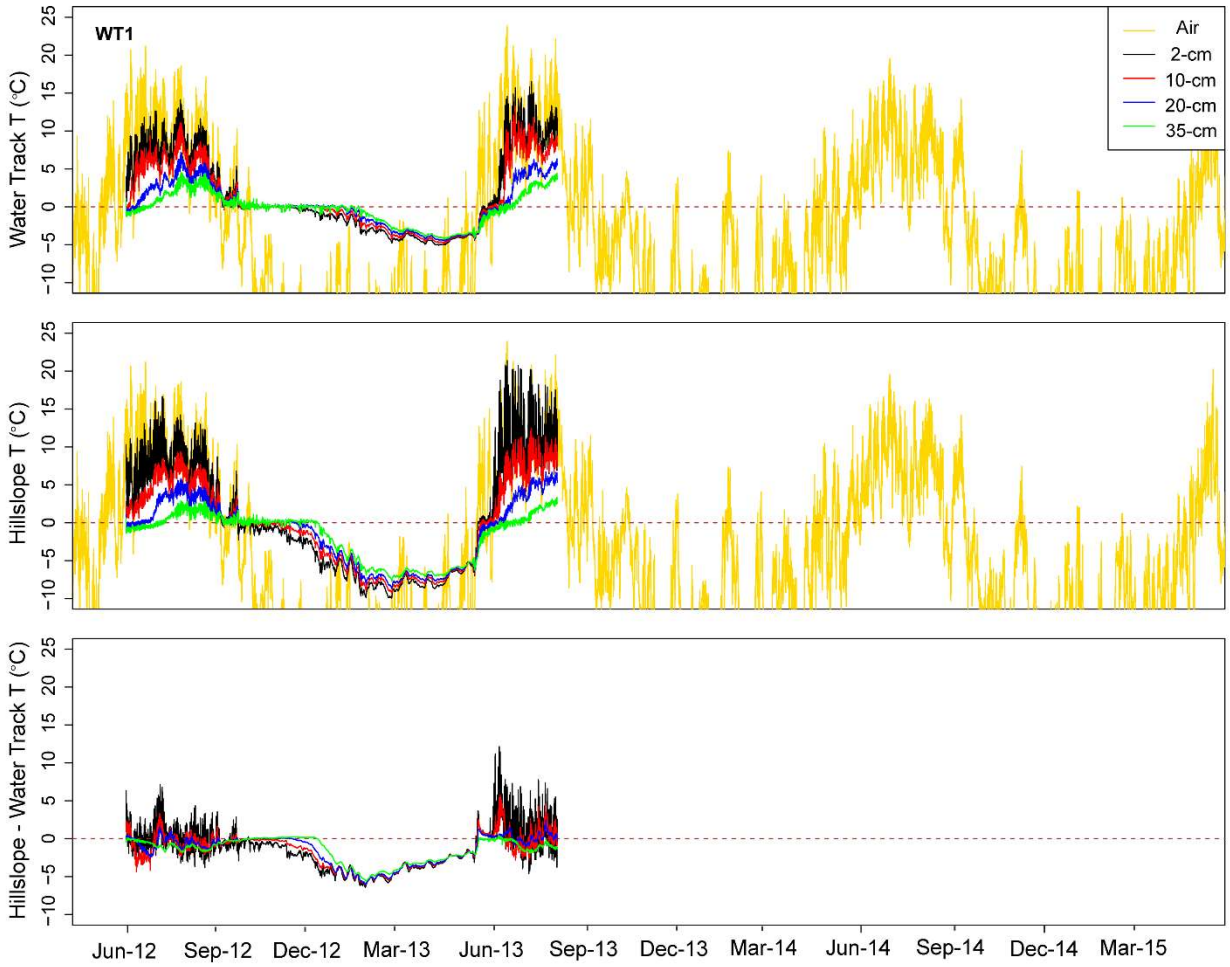

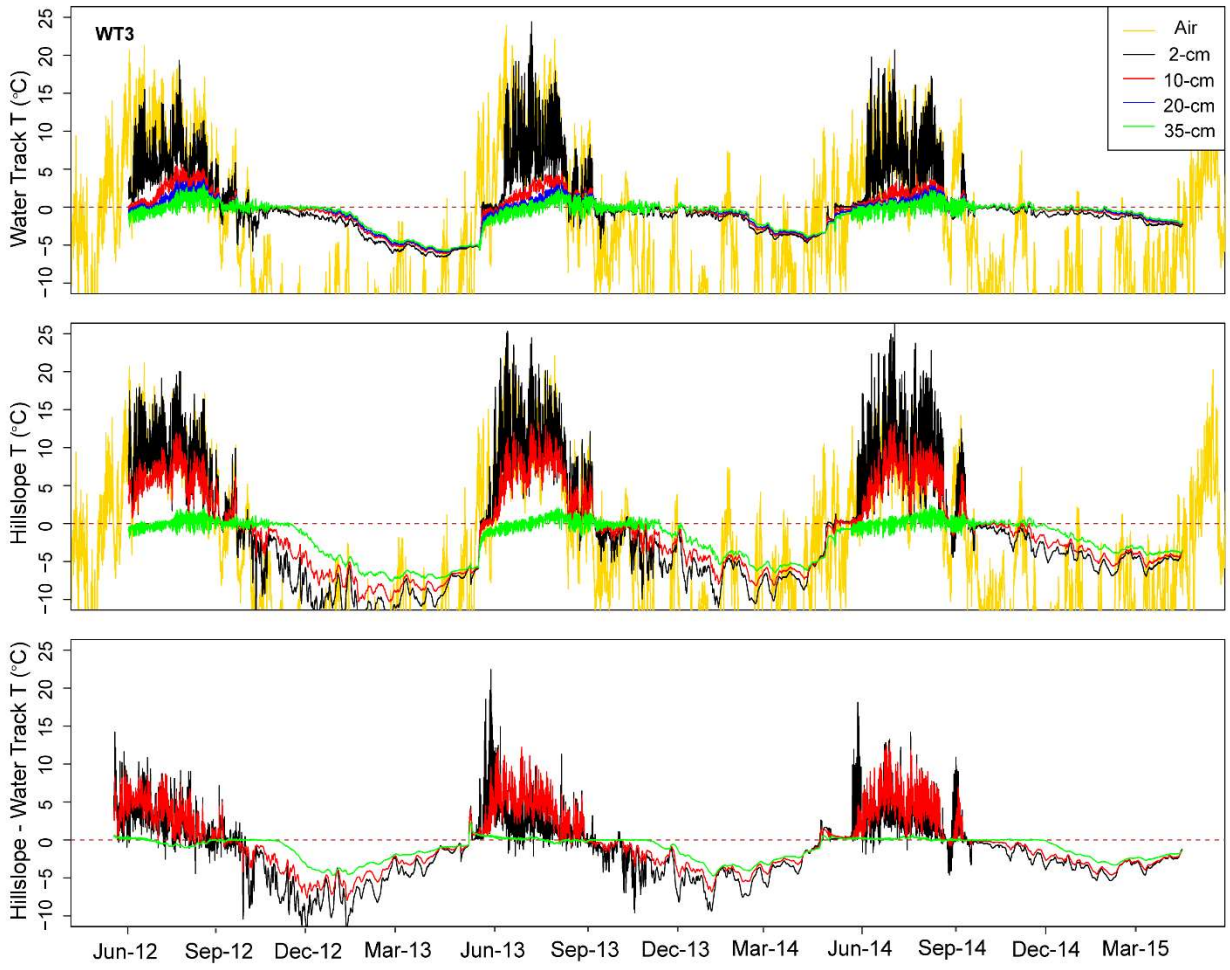
WT3
Air
2-cm
10-cm
20-cm
35-cm
Water Track T (°C)
Hillslope T (°C)
Hillslope - Water Track T (°C)
Jun-12
Sep-12
Dec-12
Mar-13
Jun-13
Sep-13
Dec-13
Mar-14
Jun-14
Sep-14
Dec-14
Mar-15

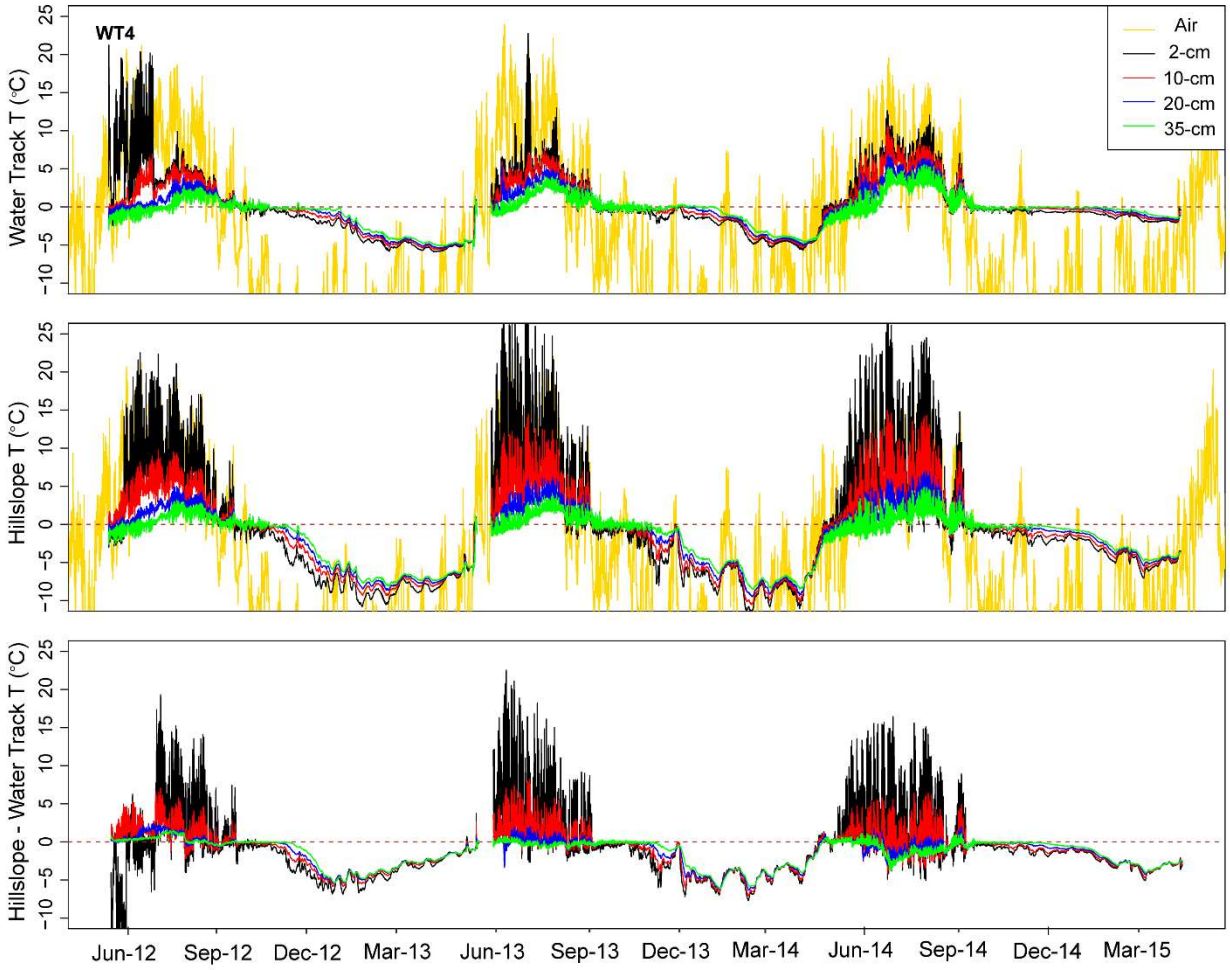
WT4
Air
2-cm
10-cm
20-cm
35-cm
Water Track T (°C)
Hillslope T (°C)
Hillslope - Water Track T (°C)
25
20
15
10
5
0
−5
−10
Jun-12
Sep-12
Dec-12
Mar-13
Jun-13
Sep-13
Dec-13
Mar-14
Jun-14
Sep-14
Dec-14
Mar-15

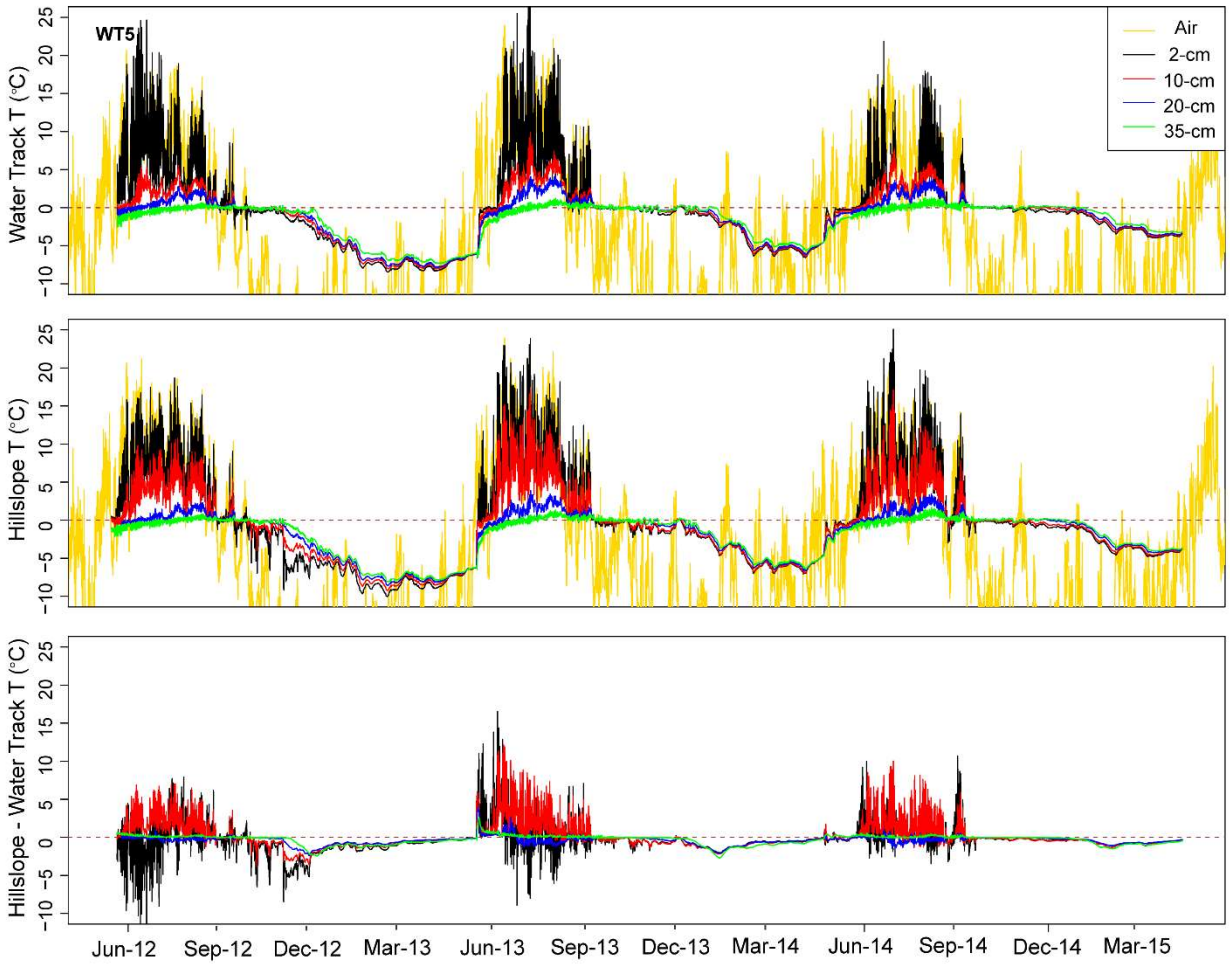

Figure S1. Air temperature (yellow) measured at the AON tower and hourly ground temperatures ("T") for four depths measured for the four sites not shown in the main text over the three-year study period. The top graph shows the ground temperatures inside the water track at 2 (black), 10 (red), 20 (blue), and 35 (green) cm depth, middle graph shows the measured ground temperatures on the adjacent hillslope, and the bottom panel shows the difference between the ground temperatures measured inside the water track (top panel) and on the adjacent hillslope (middle panel).

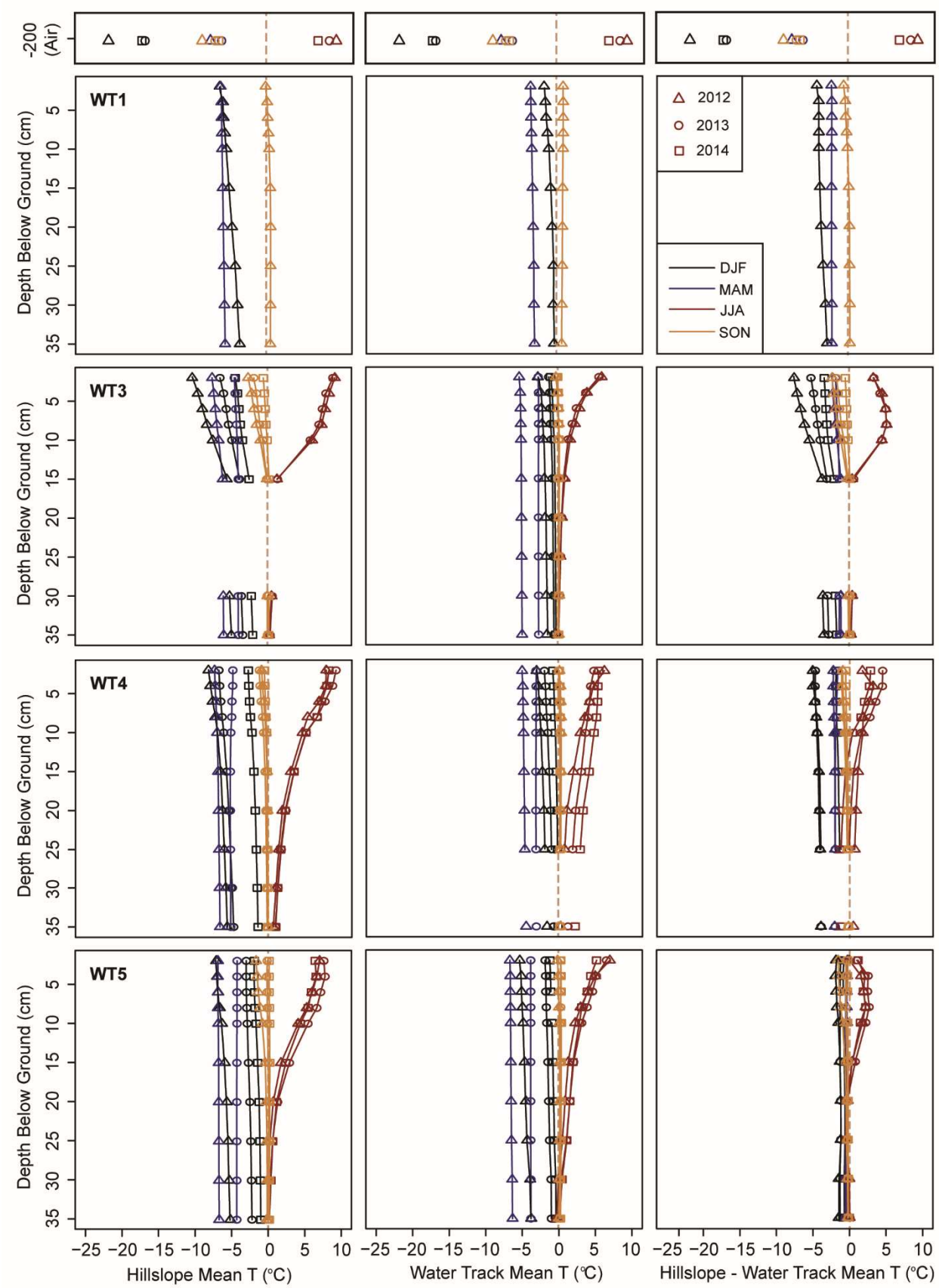
-200 (Air)
WT1
WT3
WT4
WT5
Depth Below Ground (cm)
2012
2013
2014
DJF
MAM
JJA
SON
Hillslope Mean T (°C)
Water Track Mean T (°C)
Hillslope - Water Track Mean T (°C)

Figure S2. Mean seasonal air temperatures measured at the AON ridge eddy flux tower and mean seasonal ground temperature profiles measured in the water track (WT, middle), on the adjacent hillslope (HS, left), and the difference in mean seasonal ground temperature between the two feature types (HS – WT, right) for the three study years. The three study years are denoted with the three different symbols and the four seasons (winter, spring, summer, and fall) are denoted with the four different colors. The vertical brown dashed line marks 0°C in each plot.

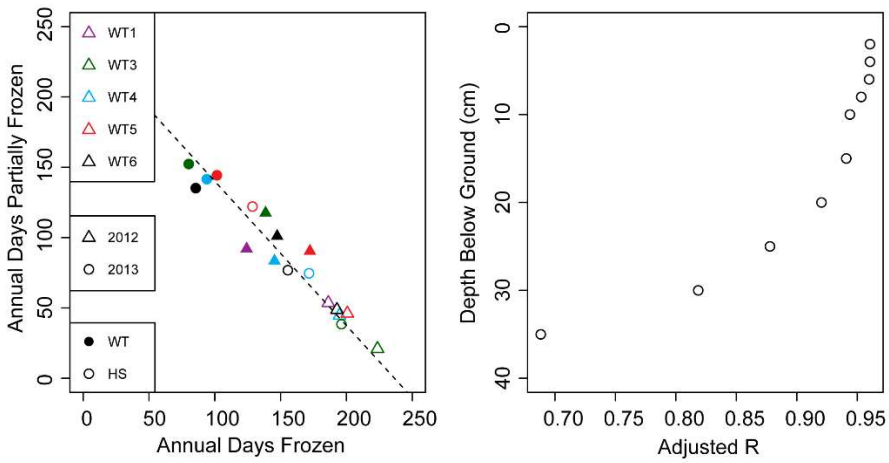

Figure S3. Left plot: Paired observations of the number of days frozen and partially frozen at 2 cm below ground for the two full years of data beginning on 8/1/12 (triangles) and 8/1/13 (circles), respectively. The five sites are shown with five different colors and water track and hillslope features are shown with closed and open symbols, respectively. The dashed line is the best-fit linear regression line (r = 0.96). Right plot: Decline in the goodness-of-fit between days frozen and partially frozen with depth.

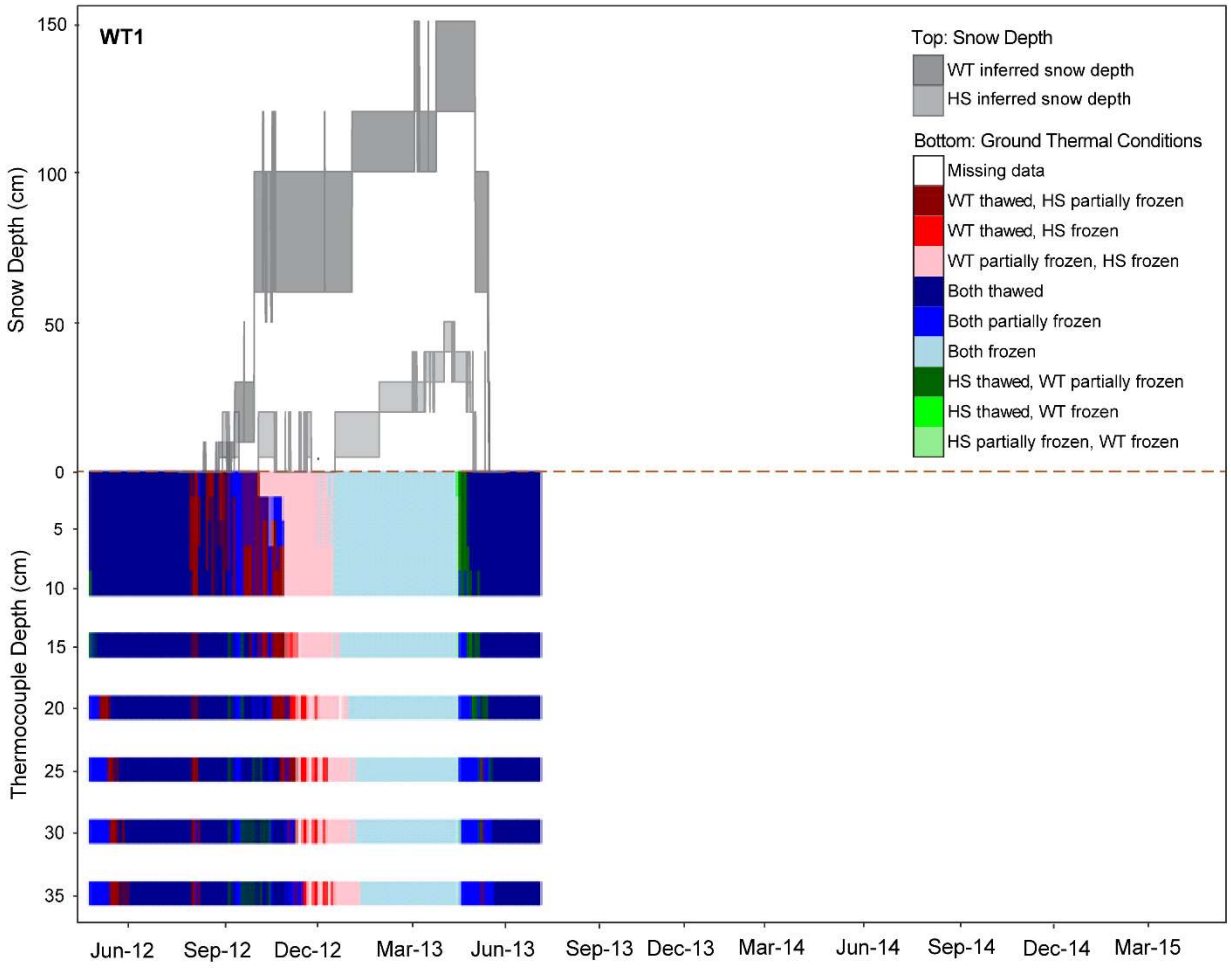
WT1
Top: Snow Depth
WT inferred snow depth
HS inferred snow depth
Bottom: Ground Thermal Conditions
Missing data
WT thawed, HS partially frozen
WT thawed, HS frozen
WT partially frozen, HS frozen
Both thawed
Both partially frozen
Both frozen
HS thawed, WT partially frozen
HS thawed, WT frozen
HS partially frozen, WT frozen
Snow Depth (cm)
150
100
50
0
Thermocouple Depth (cm)
5
10
15
20
25
30
35
Jun-12
Sep-12
Dec-12
Mar-13
Jun-13
Sep-13
Dec-13
Mar-14
Jun-14
Sep-14
Dec-14
Mar-15

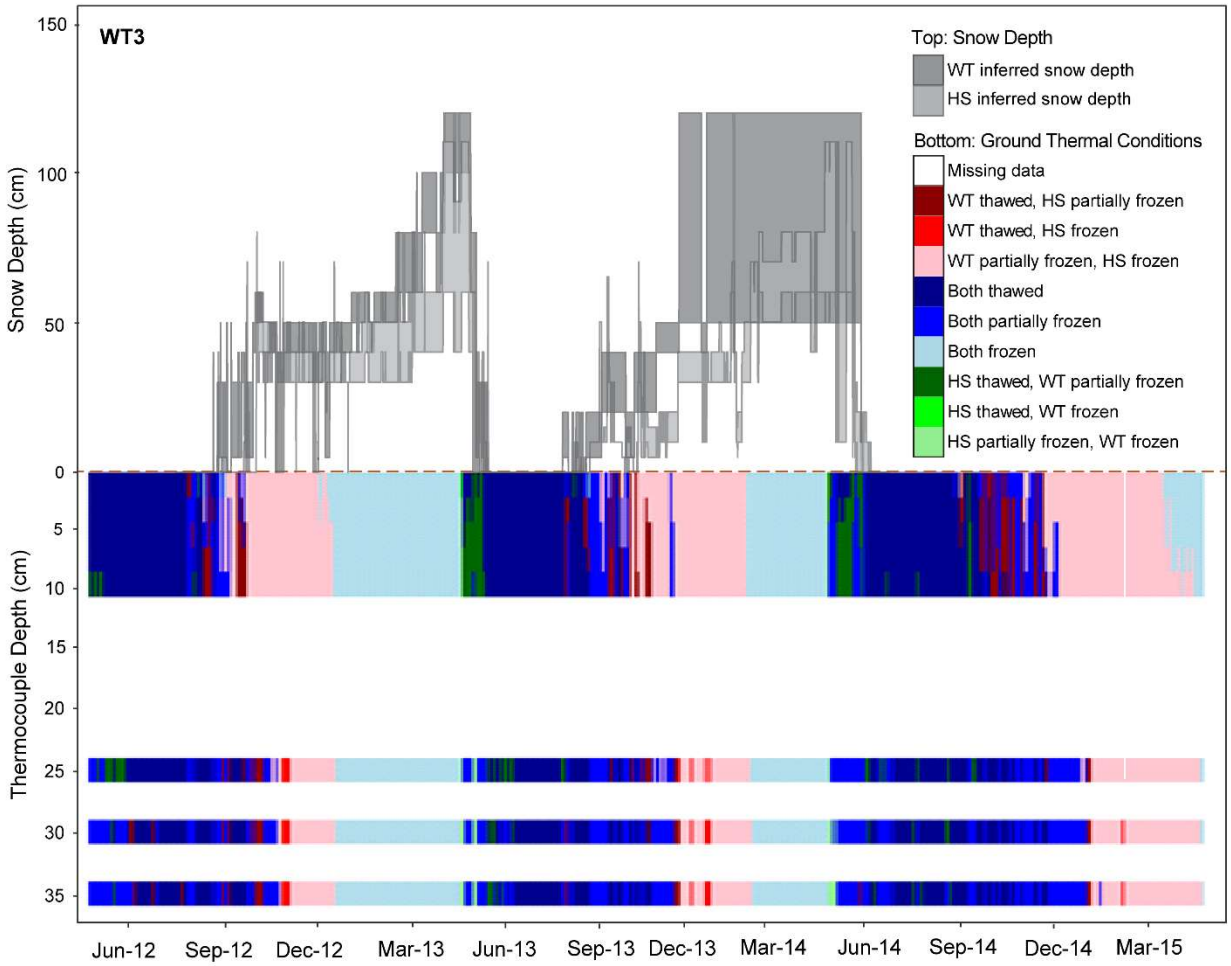
WT3
Top: Snow Depth
WT inferred snow depth
HS inferred snow depth
Bottom: Ground Thermal Conditions
Missing data
WT thawed, HS partially frozen
WT thawed, HS frozen
WT partially frozen, HS frozen
Both thawed
Both partially frozen
Both frozen
HS thawed, WT partially frozen
HS thawed, WT frozen
HS partially frozen, WT frozen
Snow Depth (cm)
150
100
50
0
Thermocouple Depth (cm)
5
10
15
20
25
30
35
Jun-12
Sep-12
Dec-12
Mar-13
Jun-13
Sep-13
Dec-13
Mar-14
Jun-14
Sep-14
Dec-14
Mar-15

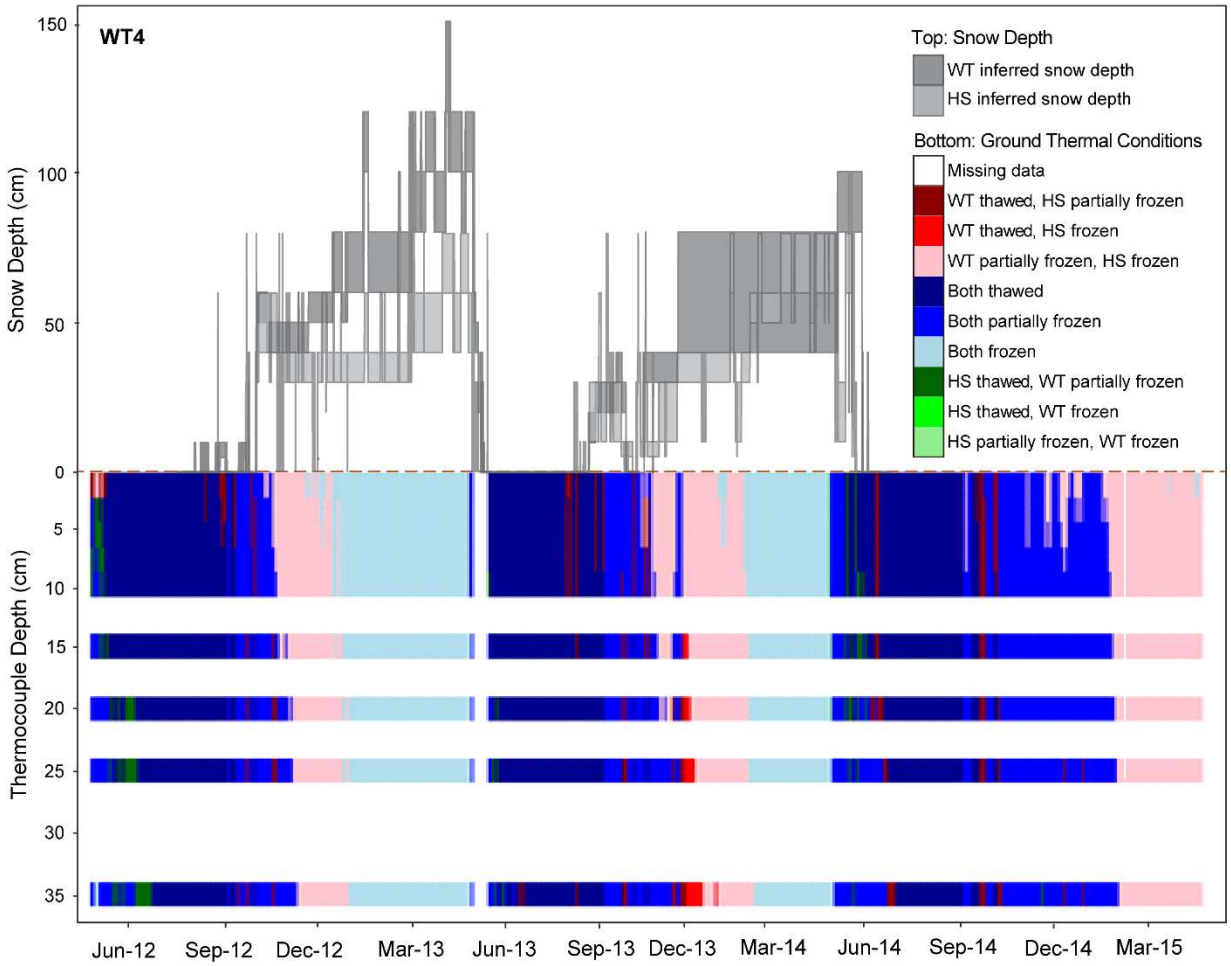
WT4
Top: Snow Depth
WT inferred snow depth
HS inferred snow depth
Bottom: Ground Thermal Conditions
Missing data
WT thawed, HS partially frozen
WT thawed, HS frozen
WT partially frozen, HS frozen
Both thawed
Both partially frozen
Both frozen
HS thawed, WT partially frozen
HS thawed, WT frozen
HS partially frozen, WT frozen
Snow Depth (cm)
150
100
50
0
Thermocouple Depth (cm)
5
10
15
20
25
30
35
Jun-12
Sep-12
Dec-12
Mar-13
Jun-13
Sep-13
Dec-13
Mar-14
Jun-14
Sep-14
Dec-14
Mar-15

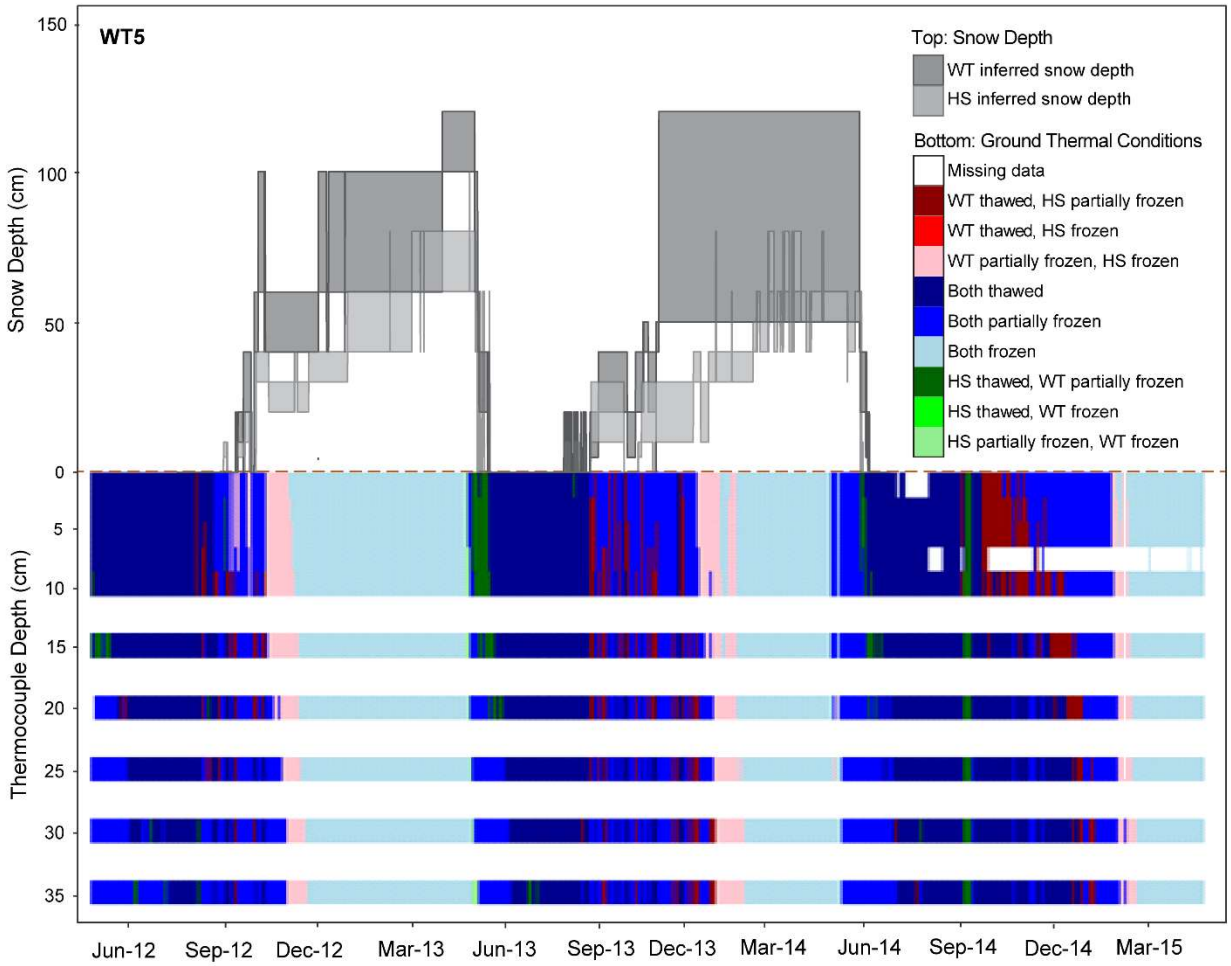

Figure S4. Inferred snow depth and thermal conditions through time for the four sites not shown in the main text.

Table S1. Percentage of each snow-covered season with deeper snow in the water track than on the hillslope

Site	*2012-2013 Season (%)*	*2012-2013 Season Duration (days)*	*2013-2014 Season (%)*	*2013-2014 Season Duration (days)*
WT1	96.1	260	96.2	279
WT3	15.4	253	19	315
WT4	87.1	238	51.1	261
WT5	84	244	56.9	276.3
WT6	85.4	272	60.5	278.5

Table S1. Significance levels of the Wilcoxon signed rank tests at WT3

Depth (cm)	HS vs. WT '12	HS vs. WT '13	HS vs. WT '14	WT '12 vs. '13	HS '12 vs. '13	WT '13 vs. '14	HS '13 vs. '14
				Summer			
2	NA	0	0	NA	NA	0	0.0063
4	NA	0	0	NA	NA	0.0349	0
6	NA	0	0	NA	NA	0	0
8	NA	0	0	NA	NA	0	0
10	NA	0	0	NA	NA	0	0
15	NA	NA	NA	NA	NA	0	NA
20	NA	NA	NA	NA	NA	0.3735	NA
25	NA	0	0	NA	NA	0.0107	0.0254
30	NA	0	0	NA	NA	0	0
35	NA	0	0	NA	NA	0	0
				Fall			
2	0	0	0	0	0	0	0
4	0	0	0	0	0	0	0
6	0	0	0	0.1358	0	0	0
8	0	0	0	0.1660	0	0	0
10	0	0	0	0	0	0	0
15	NA	NA	NA	0	NA	0	NA
20	NA	NA	NA	0	NA	0	NA
25	0	0	0	0	0.5507	0	0
30	0	0	0	0	0.0197	0	0
35	0	0	0	0	0.0092	0	0
				Winter			
2	0	0	0	0	0	0	0
4	0	0	0	0	0	0	0
6	0	0	0	0	0	0	0
8	0	0	0	0	0	0	0
10	0	0	0	0	0	0	0
15	NA	NA	NA	0	NA	0	NA
20	NA	NA	NA	0	NA	0	NA
25	0	0	0	0	0	0	0
30	0	0	0	0	0	0	0
35	0	0	0	0	0	0	0
				Spring			
2	NA	0	0	NA	NA	0	0
4	NA	0	0	NA	NA	0	0
6	NA	0	0	NA	NA	0	0
8	NA	0	0	NA	NA	0	0
10	NA	0	0	NA	NA	0	0
15	NA	NA	NA	NA	NA	0	NA
20	NA	NA	NA	NA	NA	0	NA
25	NA	0	0	NA	NA	0	0
30	NA	0	0	NA	NA	0	0
35	NA	0	0	NA	NA	0	0

"HS" refers to hillslope locations and "WT" refers to water track locations.

Table S2. Significance levels of the Wilcoxon signed rank tests at WT4

Depth (cm)	HS vs. WT '12	HS vs. WT '13	HS vs. WT '14	WT '12 vs. '13	HS '12 vs. '13	WT '13 vs. '14	HS '13 vs. '14
				Summer			
2	0	0	0	0	0.0001	0	0
4	0	0	0	0	0	0	0
6	0	0	0	0	0	0	0.0175
8	0	0	0	0.0239	0	0	0.0511
10	0	0	0	0	0.0051	0	0.0240
15	0	0	0	0	0	0	0.0003
20	0	0	0	0	0	0	0.2670
25	0	0	0	0	0	0	0.2695
30	NA	NA	NA	NA	0	NA	0.0900
35	0	0	0	0	0	0	0
				Fall			
2	0	0	0	0	0	0	0
4	0	0	0	0	0	0	0
6	0	0	0	0	0	0	0
8	0	0	0	0	0	0.0003	0
10	0	0	0	0	0	0.0236	0
15	0	0	0	0	0	0.6899	0
20	0	0	0	0	0	0.4392	0
25	0	0	0	0	0	0.8049	0
30	NA	NA	NA	NA	0	NA	0
35	0	0	0	0	0	0.5994	0
				Winter			
2	0	0	0	0	0	0	0
4	0	0	0	0	0	0	0
6	0	0	0	0	0	0	0
8	0	0	0	0	0	0	0
10	0	0	0	0	0	0	0
15	0	0	0	0	0	0	0
20	0	0	0	0	0	0	0
25	0	0	0	0	0	0	0
30	NA	NA	NA	NA	0	NA	0
35	0	0	0	0	0	0	0
				Spring			
2	NA	0	0	NA	NA	0	0
4	NA	0	0	NA	NA	0	0
6	NA	0	0	NA	NA	0	0
8	NA	0	0	NA	NA	0	0
10	NA	0	0	NA	NA	0	0
15	NA	0	0	NA	NA	0	0
20	NA	0	0	NA	NA	0	0
25	NA	0	0	NA	NA	0	0
30	NA	NA	NA	NA	NA	NA	0
35	NA	0	0	NA	NA	0	0

"HS" refers to hillslope locations and "WT" refers to water track locations.

Table S3. Significance levels of the Wilcoxon signed rank tests at WT5

Depth (cm)	HS vs. WT '12	HS vs. WT '13	HS vs. WT '14	WT '12 vs. '13	HS '12 vs. '13	WT '13 vs. '14	HS '13 vs. '14
				Summer			
2	0	0	0	0	0	0.1211	0
4	0	0	0	0.9490	0	0	0
6	0	0	0	0	0	0	0
8	0	0	0	0	0	0	0
10	0	0	0	0	0	0	0
15	0	0	0	0	0	0	0
20	0	0	0	0	0	0.6716	0
25	0	0	0	0	0	0.0039	0.0873
30	0	0	0.2056	0	0	0	0
35	0	0	0	0	0	0	0
				Fall			
2	0	0	0	0	0	0	0
4	0	0	0	0	0	0	0
6	0	0	0	0	0	0	0
8	0	0	0	0	0	0.0045	0
10	0	0	0	0	0	0	0
15	0	0	0	0	0	0	0
20	0	0	0	0	0	0	0
25	0	0	0	0	0	0	0
30	0	0	0	0	0	0	0
35	0	0	0	0	0	0	0
				Winter			
2	0	0	0	0	0	0	0
4	0	0	0	0	0	0	0
6	0	0	0	0	0	0	0
8	0	0	0	0	0	0	0
10	0	0	0	0	0	0	0
15	0	0	0	0	0	0	0
20	0	0	0	0	0	0	0
25	0	0	0	0	0	0	0
30	0	0	0	0	0	0	0
35	0	0	0	0	0	0	0
				Spring			
2	NA	0	0	NA	NA	0	0
4	NA	0	0	NA	NA	0	0
6	NA	0	0	NA	NA	0	0
8	NA	0	0	NA	NA	0	0
10	NA	0	0	NA	NA	0	0
15	NA	0	0	NA	NA	0	0
20	NA	0	0	NA	NA	0	0
25	NA	0	0	NA	NA	0	0
30	NA	0	0	NA	NA	0	0
35	NA	0	0	NA	NA	0	0

"HS" refers to hillslope locations and "WT" refers to water track locations.

Table S4. Significance levels of the Wilcoxon signed rank tests at WT6

Depth (cm)	HS vs. WT '12	HS vs. WT '13	HS vs. WT '14	WT '12 vs. '13	HS '12 vs. '13	WT '13 vs. '14	HS '13 vs. '14
				Summer			
2	0	0	0	0	0	0	0
4	0	0	0	0	0	0	0
6	0	0	0	0	0	0	0
8	0	0	0	0	0.0013	0	0
10	0	0	0	0	0.5744	0	0
15	0	0	0	0	0	0.0016	0
20	0	0	0	0	0	0.1790	0
25	0	0	0	0	0	0	0
30	0	0	0	0	0	0	0
35	0.0143	0	0.1712	0	0	0	0
				Fall			
2	0	0	0	0	0	0.0790	0
4	0	0	0	0	0	0.0930	0
6	0	0	0	0	0	0.0872	0
8	0	0	0	0	0	0.0846	0
10	0	0	0	0	0	0.1022	0
15	0	0	0	0	0	0.0456	0
20	0	0	0	0	0	0.0171	0
25	0	0	0	0	0	0.0062	0
30	0	0	0	0	0	0.0028	0
35	0	0.4673	0	0	0	0.0014	0
				Winter			
2	0	0	0	0	0	0	0
4	0	0	0	0	0	0	0
6	0	0	0	0	0	0	0
8	0	0	0	0	0	0	0
10	0	0	0	0	0	0	0
15	0	0	0	0	0	0	0
20	0	0	0	0	0	0	0
25	0	0	0	0	0	0	0
30	0	0	0	0	0	0	0
35	0	0	0	0	0	0	0
				Spring			
2	NA	0	0	NA	NA	0	0
4	NA	0	0	NA	NA	0	0
6	NA	0	0	NA	NA	0	0
8	NA	0	0	NA	NA	0	0
10	NA	0	0	NA	NA	0	0
15	NA	0	0	NA	NA	0	0
20	NA	0	0	NA	NA	0	0
25	NA	0	0	NA	NA	0	0
30	NA	0	0	NA	NA	0	0
35	NA	0	0	NA	NA	0	0

"HS" refers to hillslope locations and "WT" refers to water track locations.

Chapter 5: Conclusions

This work investigated the hydrological and thermal dynamics of tundra hillslopes and the water tracks draining them. In Chapter 2, my co-authors and I found that water tracks exhibited a delayed runoff response to rainfall compared to nearby headwater streams, although the overall response timing was similar. The threshold for water track runoff generation depended on the amount of rainfall and antecedent soil water storage, although the dependence on the latter varied from site to site, likely because of distinct patterns in hydrologic connectivity throughout the respective hillslope watersheds. In Chapter 3, my co-authors and I assessed the role of seasonal air temperatures, snow depth, and groundwater flow in active layer thermal dynamics. We found that the contrasting winter active layer dynamics in a water track and its adjacent hillslope can be simulated with the same substrates but upper boundary conditions dictated by the snow cover regime at each location. An exploration of spatial and interannual variations in the current microclimate at the study sites revealed dramatic differences in seasonal active layer temperatures and the timing and duration of frozen conditions, where the scenarios with the warmest mean annual temperatures and deepest snow cover formed taliks. When we fully coupled groundwater flow and heat transport, we found that the advection of heat by flowing water has a significant moderating effect on the active layer thermal regime at the scale of a small hillslope watershed. In Chapter 4, my co-authors and I found that the active layer thermal regime of water tracks and the adjacent non-track hillslope contrasted strongly and consistently between sites and study years. The active layers of water tracks were thicker, had damped diel and seasonal temperature fluctuations, were frozen for less of the year, and the freeze-thaw conditions were temporally offset compared to their adjacent hillslopes. Along with warmer seasonal air temperatures and deeper snow, water track locations were significant predictors of warmer active layer temperatures and

much shorter periods of freezing, likely because of latent heat effects associated with higher soil moisture.

The contributions in this work improved our understanding of the role of water tracks in Arctic landscapes and their potential responses to climate change, but important knowledge gaps remain. Chapters 2 and 4 required intensive field work to develop relatively simple mechanistic relationships between water track function and their extrinsic and intrinsic characteristics at a small number of sites within the watershed of the same second-order stream. The predictive ability and assumptions of these models should be tested for the full range of water tracks, which first requires better identification of that range. Much like zero-order streams at lower latitudes (e.g., Downing et al., 2012), the pan-Arctic abundance, distribution and biophysical characteristics of water tracks are mostly unknown. Only three studies have estimated water track density on the landscape: two in the central upland tundra of the Brooks Range, Alaska (McNamara et al., 1999; Trochim et al., 2016b) and one in eastern Siberia (Curasi et al., 2016), areas representing less than one millionth of a percent of the upland Arctic (CAVM team, 2003). Other studies have shown that water tracks are also present in the High Arctic of northern Canada (Paquette et al., 2017) and the McMurdo Dry Valleys, Antarctica (Levy et al., 2011). Pan-Arctic satellite imagery and derived digital elevation models are now available at resolutions finer than the scale of water tracks (Morin et al., 2016; see also Dai et al., 2018), making accurate mapping of these features based on their topographic and spectral characteristics (e.g., Curasi et al., 2016) a feasible prospect across the Arctic. Once mapped, predictor datasets on the extrinsic and intrinsic properties of the water tracks, specifically soil properties and climate information including seasonal air temperatures, rainfall, and snow cover, which are used for the models in chapters 2-4, should be measured, estimated, or compiled wherever possible. Chapter 3 required a difficult-to-use and computationally expensive

model to identify controls on the spatiotemporal dynamics of the hillslope active layer thermal regime, but all simulations assumed fully saturated conditions within the hillslope, and the groundwater flow model used an idealized and spatially homogeneous hillslope structure. Testing these assumptions with variably saturated, heterogeneous model with realistic topography should provide a better understanding of the role of hillslope structure in controlling soil saturation, hydrologic connectivity, and thus water track runoff response, as identified in Chapter 2. Emergent responses from a range of model structures could allow for statistically based, and computationally less expensive, upscaling of these findings across the diversity of upland hillslope watersheds.

References:

Dai, C., Durand, M., Howat, I. M., Altenau, E. H., & Pavelsky, T. M. (2018). Estimating river surface elevation from ArcticDEM. *Geophysical Research Letters, 45,* 3107-3114. https://doi.org/10.1002/2018GL077379.

Curasi, S. R., Loranty, M. M., & Natali, S. M. (2016). Water track distribution and effects on carbon dioxide flux in an eastern Siberian upland tundra landscape, *Environmental Research Letter, 11*, doi:10.1088/1748-9326/11/4/045002.

Downing, J. A., J. J. Cole, C. M. Duarte, J. J. Middelburg, J. M. Melack, Y. T. Prairie, P. Kortelainen, R. G. Striegl, W. H. McDowell, & Tranvi, L. J. (2012). Global abundance and size distribution of streams and rivers, *Inland Waters, 2(4)*, 229–236, doi:10.5268/IW-2.4.502.

Levy, J. S., Fountain, A. G., Gooseff, M. N., Welch, K. A., & Lyons, W. B. (2011). Water tracks and permafrost in Taylor Valley, Antarctica: Extensive and shallow groundwater connectivity in a cold desert ecosystem. *Geological Society of America Bulletin, 123(*11/12), 2295-2311. doi: 10.1130/B30436.1.

McNamara, J. P., Kane, D. L., & Hinzman, L. D. (1999). An analysis of an arctic channel network using a digital elevation model. *Geomorphology, 29,* 339–353.

Morin, P., Porter, C., Cloutier, M., Howat, I., Noh, M-J., Willis, M., Bates, B., Williamson, C., & Peterman, K. (2016). ArcticDEM; A publicly available, high resolution elevation model of the Arctic. *EGU General Assembly Conference Abstracts, 18*, 8396.

Paquette, M., Fortier, D., & Vincent, W. F. (2017), Water track in the High Arctic: A hydrological network dominated by rapid subsurface flow through patterned ground, *Arctic Science, 3*, 334-353. dx.doi.org/10.1139/as-2016-0014.

Trochim, E. D., Jorgenson, M. T., Prakash, A., & Kane, D. L. (2016a). Geomorphic and biophysical factors affecting water tracks in northern Alaska, *Earth and Space Science, 3,* doi:10.1002/2015EA000111.

Trochim, E. D., Prakash, A., Kane, D. L., & Romanovsky, V. E. (2016b). Remote sensing of water tracks. *Earth and Space Science, 3*, doi:10.1002/2015EA000112.